AN ABSTRACT OF THE THESIS OF

John Russell Duncan, Jr. (Name of student) for the Ph. D. (Degree)

in Oceanography (Major) presented on April 3, 1968 (Date)

Title: LATE PLEISTOCENE AND POSTGLACIAL SEDIMENTATION AND STRATIGRAPHY OF DEEP-SEA ENVIRONMENTS OFF OREGON

Abstract approved: Redacted for Privacy

LaVerne Duane Kulm

Sediments deposited during the last 35, 000 or 40, 000 years BP (Before the Present) were analyzed in 53 piston cores from deep-sea environments within southern Cascadia Basin and the adjoining Blanco Fracture Zone off Oregon. The analyses reveal that mechanisms of sediment transport, proximity to sediment sources, and influx of debris from different sources has influenced the sedimentation regime. However, sedimentation during the time interval under study has been controlled most notably by paleoclimatic conditions, eustatic sea level fluctuations, and submarine physiography.

Changes in paleoclimatic conditions can be detected from the relative abundances of radiolarians and planktonic foraminiferans produced in the surface marine waters and subsequently deposited

in the deep-sea sediments. Greater productivity of planktonic foraminiferans compared to radiolarians seems to have occurred during glacial advances, while radiolarians are relatively more abundant during times of glacial retreat. Radiocarbon age determinations verify that an abrupt change in the faunal stratigraphy, from an older planktonic foraminiferan-dominant interval to a younger radiolarian-dominant interval, occurred about 12,500 years BP. The stratigraphic position of the abrupt change is believed to be the boundary between late Pleistocene and postglacial deep-sea sedimentation.

The overall marine sedimentation rate in the late Pleistocene interval is approximately six times higher than that of postglacial time. In addition, proportionately less coarse sediment reached the deep-sea area during the postglacial interval.

More illite is present in the clay fractions (<2 microns) of the late Pleistocene lutites, on a comparative basis with chlorite and montmorillonite, than is present in those of the postglacial lutites. The stratigraphic change in clay mineral composition is abrupt and, therefore, not thought to be caused by marine diagenesis. Instead, this stratigraphic change may be the result of climatically controlled variations in the weathering and erosion processes affecting the Columbia River drainage area, which supplies most of the clays found in the marine environments studied.

The organic carbon content of the postglacial lutites is up to five times higher than that of the late Pleistocene lutites. It appears that the higher influx of sediments in the late Pleistocene masks the organic carbon content in these older sediments.

In eastern Cascadia Basin, an abrupt change in the color of the lutites is evident at the late Pleistocene-postglacial boundary. The lutites of the late Pleistocene section are gray, while those of the postglacial interval are generally olive gray or light olive gray. The color difference is mostly a function of organic carbon content: gray lutite has the lowest organic carbon content, light olive gray lutite has an intermediate content, while olive gray lutite has the highest content.

Four heavy mineral provinces (A, B, C, and D) are evident in the deep-sea area off Oregon. Province A is located in the Blanco Fracture Zone-Gorda Ridge transition area; the textural and mineralogical compositions of the deposits suggest local submarine volcanism. Province B is restricted to the late Pleistocene sediments of Vancouver Valley and of western Cascadia Abyssal Plain; the probable sediment source is Vancouver Island. Province C (postglacial and late Pleistocene deposits) occurs in southeastern Cascadia Basin and in Cascadia Channel. Sediments in this province are derived from the Columbia River drainage basin. During postglacial time, the supply of coarse-grained detritals from the

Columbia River diminished due to restricted offshore transport accompanying the last rise of sea level. At this time sediments derived locally from the Klamath Mountains were deposited at the base of the continental slope (Blanco Valley) off southern Oregon and northern California (Province D), overriding the influence of Columbia River sedimentation.

Some of the deep-sea deposits in the Blanco Fracture Zone reflect the influence of tectonic activity in the Zone which presumably is related to sea-floor spreading along the Gorda Ridge and the Juan de Fuca Ridge. Angular greenstone fragments were found in one of the Blanco Fracture Zone troughs; these fragments imply both submarine regional metamorphism of submarine basalt flows and subsequent vertical displacement permitting the exposure of the metamorphosed rocks. A core from the top of a submarine hill north of Cascadia Gap in the Blanco Fracture Zone has several turbidite sequences in its lower portion, while the upper section of this same core contains only hemipelagic deposits. This stratigraphic section implies gradual uplift of the hill on the order of 250 fathoms (460 m) over the last 25,000 or 30,000 years BP. A 70-fathom (128-m) structural depression appears to have developed in Cascadia Channel just west of Cascadia Gap during the last 6600 years BP (post Mt. Mazama eruption). As a result, the bottom transport of sediment through Cascadia Channel out onto Tufts Abyssal Plain has temporarily been cut off while the depression is being filled.

Late Pleistocene and Postglacial Sedimentation and Stratigraphy of Deep-Sea Environments off Oregon

by

John Russell Duncan, Jr.

A THESIS

submitted to

Oregon State University

in partial fulfillment of
the requirements for the
degree of

Doctor of Philosophy

June 1968

APPROVED:

Redacted for Privacy

Assistant Professor of Oceanography
in charge of major

Redacted for Privacy

Chairman, Department of Oceanography

Redacted for Privacy

Dean of Graduate School

Date thesis is presented April 3, 1968

Typed by Opal Grossnicklaus for John Russell Duncan, Jr.

ACKNOWLEDGMENTS

I wish to express sincere gratitude to my major professor, Dr. LaVerne D. Kulm, for giving so freely of his time and knowledge during the entire course of this study and for critically reviewing the manuscript. Special thanks are due Dr. John V. Byrne for guiding me in the initial stages of research and for later making helpful suggestions that improved the manuscript.

The generic and specific identifications of benthic foraminiferans made by Dr. Gerald A. Fowler are greatly appreciated. I am indebted to Dr. William G. Melson of the Smithsonian Institution for the petrographic analysis of six rock samples believed to be greenstones. Appreciation is extended to Eric Crecelius for running organic carbon and carbonate analyses and to Daniel R. McKeel and John Michael King for drafting assistance. Editing by Diane Merten considerably refined the final manuscript.

I am grateful to Dr. Kenneth S. Deffeyes for numerous enlightening discussions. Informal discussions with fellow students also proved quite beneficial; thanks go especially to Dr. Paul R. Carlson, Dr. C. Hans Nelson, Gary B. Griggs, Richard Couch, Kenneth L. Russell, David W. Allen, Richard S. Boettcher, and David M. Chambers.

To the staff members and the students of the Department of

Oceanography, Oregon State University, and to the personnel of the R/V YAQUINA who helped with the collection of the data at sea a hardy thank you is extended.

I am very grateful to my wife, Suzanne, for assisting with many tedious tasks and for being so patient with me during the course of the study. I also wish to extend gratitude to my parents for their constant encouragement throughout the many years of my formal education, the culmination of which is represented in this thesis.

Research pertaining to this study was made possible through the financial support of the National Science Foundation (Grants GP-5076, GA-1246, GP-3556, and GA-738) and the Office of Naval Research (Contract Nonr 1286(10)) and through the use of laboratory and shipboard facilities of the Department of Oceanography, Oregon State University. Personal financial support for three years (1964-1967) was also supplied by the National Science Foundation through its Graduate Fellowship program.

TABLE OF CONTENTS

TABLE OF CONTENTS (CONTINUED)

TABLE OF CONTENTS (CONTINUED)

LIST OF FIGURES

LIST OF FIGURES (CONTINUED)

LIST OF FIGURES (CONTINUED)

LIST OF FIGURES (CONTINUED)

PLATE

LIST OF TABLES

LATE PLEISTOCENE AND POSTGLACIAL SEDIMENTATION AND STRATIGRAPHY OF DEEP-SEA ENVIRONMENTS OFF OREGON

I. INTRODUCTION

The improvement of deep-sea coring techniques in recent years has enabled the marine geologist to begin constructing not only a present-day areal view of ocean basin sedimentation but also a historical one. Studies of deep-sea stratigraphic sections are now bringing to light accounts of physical and biological phenomena that that have been written and preserved in these muddy pages of nature's manuscript for her abyssal biography. As scientists, we are essentially reporters, editors, and translators of this extensive and comprehensive story. The manuscript, of course, is too vast for complete mastery by any single individual. It must be studied in parts by numerous workers. Slowly, the story is being compiled. This writer chose to work on that part of the story dealing with the type and the significance of temporal and areal variations in sediments of the deep-sea environments off Oregon (Figure 1; Plate 1, back cover pocket). Particular emphasis is focused on the environments within southern Cascadia Basin and the adjoining Blanco Fracture Zone.

The study area, which mainly encompasses southern Cascadia Basin and the eastern part of the Blanco Fracture Zone, is of

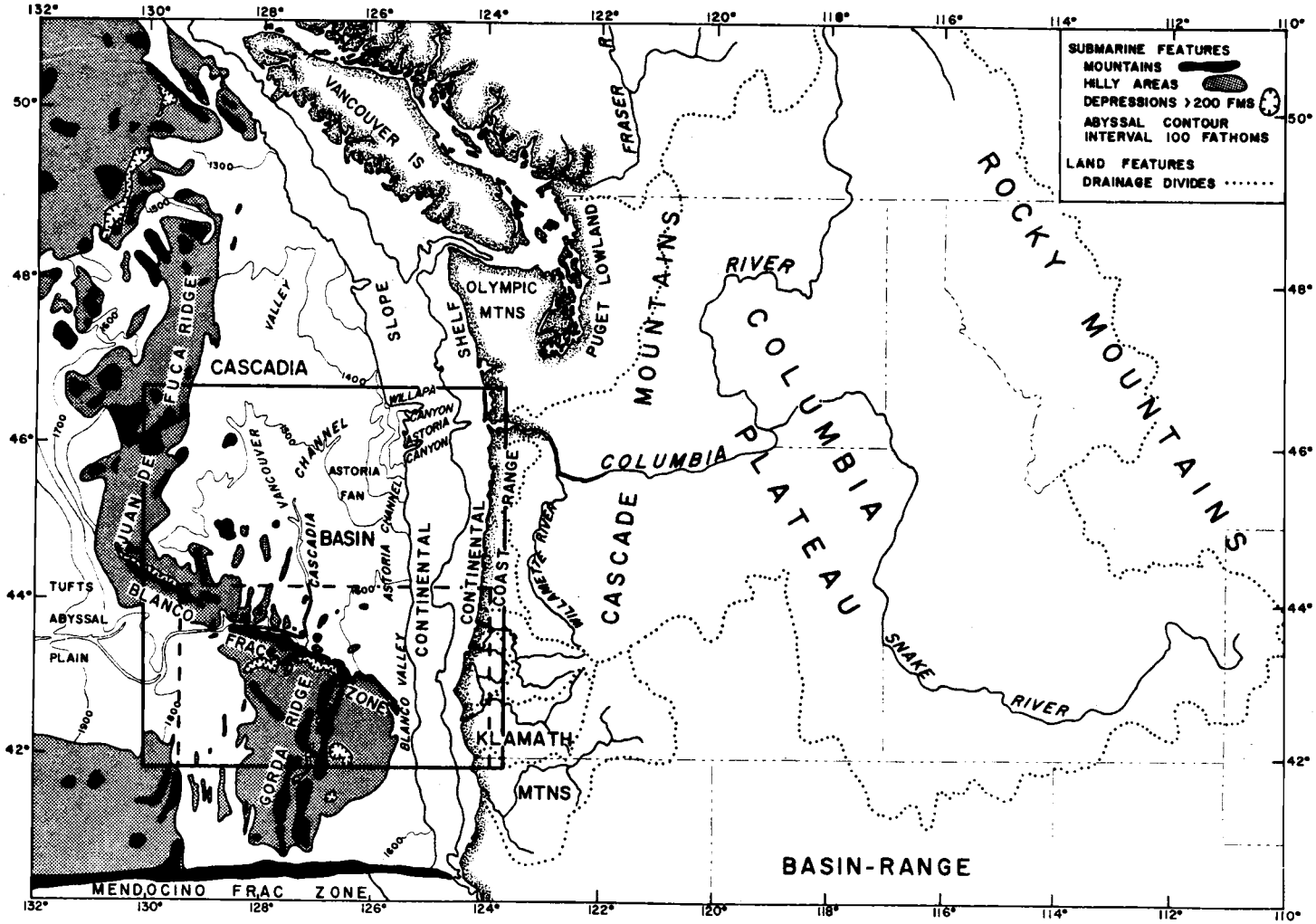

Figure 1. Submarine and continental physiography in the vicinity of the study area in the northeastern Pacific Ocean. Boundaries are outlined for general study area off Oregon (solid), enlarged in Plate 1, and for detailed bathymetric chart (dashed), given in Figure 3.

considerable size (70,000 nautical miles,^{2} 240,000 km^2) and is receiving substantial amounts of sediment from several continental sources. It also is characterized by a system of deep-sea channels and valleys which are believed to be avenues of submarine sediment dispersal. These avenues play an important role in the development of sediment-filled areas far removed from the continental sources.

Samples used for analysis were mainly obtained with a piston corer, and it will be demonstrated that these cores are composed of debris which was deposited in the ocean within the last 35,000 to 40,000 years. One objective of this study is to establish key stratigraphic horizons within this time interval and to correlate these horizons from one area to another. During the time interval under consideration, climatic conditions changed profoundly. Numerous transformations occurred over the entire world as it emerged from a period of widespread continental glaciation. A considerable portion of this study is devoted to establishing differences in sediment characteristics in the deep-sea stratigraphic column that are indicative of, and related to, the direct and the indirect effects of the climatic change.

Other objectives of this investigation are to determine which source areas are contributing substantial quantities of sediment to the marine environment and to define the routes by which sediments are dispersed in the deep-sea region off Oregon. Particular

emphasis is given to Cascadia Channel, the most extensive deep-sea channel known in the northeastern Pacific Ocean. This channel may have played a significant role in the development of Tufts Abyssal Plain to the west of the study area.

Several different physiographic features are present within the southern Cascadia Basin-Blanco Fracture Zone area; the topographic relief varies considerably from smooth plains to rugged mountains with gorges. An endeavor is made to describe the depositional facies in some of these physiographic environments and to interpret their significance.

The mineralogical and the textural characteristics of sediments often are good indicators of tectonic or volcanic activity. Using sedimentary as well as bathymetric data, the writer made attempts to detect and locate areas of such activities, particularly in the Blanco Fracture Zone.

Several important studies have recently been completed dealing with the submarine physiography, structure, and tectonics in the northeastern Pacific Ocean (Gibson, 1960; Hurley, 1960; McManus, 1964, 1965, 1967; Menard, 1964; Raff and Mason, 1961; Vine, 1966; Vine and Wilson, 1965; Wilson, 1965). The general surface sediment distribution in the northeastern Pacific has been outlined briefly by Menard (1953) and by Nayudu and Enbysk (1964), and the relationships between topography and sedimentation processes have

been discussed by Menard (1955) and by Hamilton (1967).

Within the area studied off Oregon, comprehensive investigations concerning the sediments of Astoria Canyon (Carlson, 1968) and of Astoria Fan (Nelson, 1968) have recently been completed. Several other published and unpublished studies have touched on certain aspects of sedimentation in the general area under investigation; reference to these studies is made in subsequent discussions.

No comprehensive studies have previously been made that specifically focus attention on the stratigraphy, sediment dispersal system, and sources of sediments in the southern Cascadia Basin-Blanco Fracture Zone area. It is hoped that this study will enhance our knowledge of deep-sea sedimentation off Oregon and also provide a solid foundation for future detailed investigations of adjacent areas having related sedimentational histories.

II. SUBMARINE PHYSIOGRAPHY

Much of the northeastern Pacific Ocean has been divided into physiographic provinces on the basis of regional depth, number of seamounts and submarine hills, the presence of fault blocks, and the character of the microtopography (Hurley, 1960). Echograms of the bottom have provided the means for studying the nature of the microtopography and for determining whether it is irregular like a volcanic or tectonic terrane or smooth like a sedimentary plain. These echograms indicate that the northeastern Pacific Ocean has the most extensive system of abyssal plains in the entire Pacific Ocean basin (Hurley, 1960). Subbottom acoustic reflection profiles have revealed an undulating topography, which is believed to be of volcanic origin, beneath the smooth sediment-filled surface of these abyssal plains (Hamilton, 1967).

The nature of much of the minor topography in the northeastern Pacific Ocean basin is correlated with the accessibility of a given area to deposition from turbidity currents (Menard, 1955; Hamilton, 1967). Pre-existing barriers, such as seamounts and ridges, tend to trap, and to cause the accumulation of, bottom-transported sediments spreading outward from the continent. Until the resulting traps are filled to overflowing with sediments, relatively little debris reaches the oceanic side of the topographic high, except those

materials that are in suspension or that trickle around or through the barriers by way of deep-sea channels and other low features.

A brief discussion of the submarine physiography off the coast of Oregon is therefore necessary to more fully understand the nature of the deep-sea sediments and their routes and mechanisms of dispersal. The deep-sea bathymetry shown in Figure 1 and in Plate 1 is primarily based on published charts by Hurley (1960) and by McManus (1964, 1965) as well as on sounding data recently collected by the Department of Oceanography, Oregon State University.

General Features

The transition between the continent and the ocean basin off Oregon has been described by Byrne (1962; 1963a, b; 1966) as consisting of a generally convex surface 35 to 60 nautical miles (65 to 110 km) wide (Plate 1). The continental shelf, which forms the upper part of this surface, ranges irregularly in width from 9 to 35 miles (18 to 65 km) and slopes seaward less than one degree (1:57). The shelf edge is in 70 to 120 fathoms (128 to 220 m) of water. The continental slope forms the lower part of the convex surface and has slope angles of two to three degrees (1:29 to 1:19) in the upper part increasing to 8 to 15 degrees (1:7 to 1:4) along a continuous basal escarpment. The base of the slope deepens away from the apex of Astoria Fan from approximately 1100 fathoms

(2000 m) in the north to 1650 fathoms (3000 m) in the south.

Structural features typify the continental slope. Off southern Oregon a number of benches and minor escarpments are evident. Along the central slope irregular groups of hills are common; to the north, parallel and subparallel ridges and troughs modify the slope.

Several submarine valleys and canyons transect the continental slope at various places in the study area, but only two, Astoria Canyon and Willapa Canyon, are of considerable size. Astoria Canyon originates nine miles (16 km) west of the Columbia River at a depth of 55 fathoms (100 m), cuts across the continental shelf and slope for a distance of 65 miles (120 km) and emerges at the base of the slope at a depth of 1140 fathoms (208 m) (Carlson, 1968). At this depth the Canyon hooks sharply to the left and connects with Astoria Channel on Astoria Fan. Willapa Canyon, which lies approximately 15 miles (28 km) north of Astoria Canyon, heads 17 miles (31 km) off the southern Washington coast in the vicinity of 46°30'N at 100 fathoms (183 m); it extends westward about 60 miles (110 km) and then swings southward to merge into Willapa Channel (a tributary of Cascadia Channel) at approximately 1000 fathoms (1826 m) (Royse, 1964).

A trough- or basin-like feature with a remarkably smooth floor takes up a large portion of the deep-sea area under study (Figure 1). It lies adjacent to the continental slope off Oregon,

Washington, and Vancouver Island, and is bordered by the submarine hills, ridges, and seamounts of the Juan de Fuca Ridge on the west and by the Blanco Fracture Zone on the south. Both of these features act as barriers to the seaward flow of bottom-transported sediment. The trough- or basin-like feature has an area of approximately 50,000 square miles (170,000 km^2) (McManus, 1964). It was originally called the Great Trough by Menard (1955) and was included as part of the Ridge and Trough Province (Menard and Dietz, 1951) in the northeastern Pacific Ocean. Hurley (1960) renamed the feature Cascadia Abyssal Plain after being impressed by the very smooth nature of portions of its sediment-filled bottom. Although much of the bottom is smooth and the overall gradient is fairly low (1:700), this entire region cannot be strictly classified as an abyssal plain. More recently, in an attempt to formalize the descriptive terminology, McManus (1964) named it Cascadia Basin. McManus (1967) has subsequently attempted a genetic classification in which he divided the same area into a continental rise on the east and the flank of an oceanic rise on the west.

Sufficient criteria are still lacking to determine the genetic relationship of the above variously named feature to its surroundings. Thus, Cascadia Basin will be used herein as the designation for the region in its entirety. In subsequent discussions it will be necessary to call attention to specific abyssal environments on the

floor of southern Cascadia Basin. For this purpose, the name Cascadia Abyssal Plain will be used to refer to the relatively smooth, low gradient (1:000) areas lying east and west of Cascadia Channel (Plate 1).

The floor of Cascadia Basin has a consistent slope to the south, parallel to the continental slope rather than perpendicular to it in the usual manner. Depths generally increase from 1300 fathoms (2400 m) in the north to 1600 fathoms (2900 m) in the south.

The depth of the sea floor in the eastern half of Cascadia Basin rises to about 1100 fathoms (2000 m), largely as a consequence of the two large submarine fans at the foot of the continental slope off Washington and Oregon. One of them, Astoria Fan, has its apex at the mouth of Astoria Canyon and forms a prominent feature in the study area covering approximately 6000 square miles (20, 000 km^2). Nelson (1968) has divided Astoria Fan into upper, middle, and lower portions (Plate 1) on the basis of progressive downslope decrease in gradient and relief. Willapa Channel and Cascadia Channel form the northern and the western extremities of Astoria Fan, and its southern border is arbitrarily drawn at the 1550-fathom (2840-m) contour.

Two main deep-sea channel systems are present in Cascadia Basin (McManus, 1964). The smaller of the two systems is mainly represented by Astoria Channel which heads near the mouth of Astoria Canyon and which has a general southward course down

the flank of Astoria Fan. The larger system consists of Cascadia and its tributaries, Willapa Channel and Vancouver Valley. Willapa Channel is somewhat poorly-defined at the mouth of Willapa Canyon, but it extends westerly for 60 nautical miles (110 km) as a prominent feature to join Cascadia Channel at 46°15'N, 126°30'W. Vancouver Valley generally trends southward from the base of the continental slope off Vancouver Island for 325 miles (600 km) until it joins Cascadia Channel at 45°N.

Cascadia Channel is the most prominent and most extensive deep-sea channel known in the northeastern Pacific Ocean. This channel generally trends southward in southern Cascadia Basin until it enters a large structurally controlled gorge where it makes a right-angle turn westward (43°30'N, 127°12'W). At Cascadia Gap Plate 1) the Channel passes through the submarine hills and mountains of the Blanco Fracture Zone and eventually emerges onto Tufts Abyssal Plain to the west. There, its course is less well known. The total length of Cascadia Channel is believed to be about 1200 miles (2200 km) (Hurley, 1960).

The rugged submarine topography which characterizes a considerable portion of the study area can generally be grouped into three distinct but related provinces: 1) the west-northwest trending Blanco Fracture Zone, 2) the north-northeast trending Gorda Ridge, and 3) the north-northeast trending Juan de Fuca Ridge.

Menard (1962) originally recognized that the Blanco Fracture

Zone is a major zone of fracturing, but the Zone was formally named later when studied in more detail by McManus (1965). The Blanco Fracture Zone joins the northern end of Gorda Ridge with the southern extremity of Juan de Fuca Ridge to the west (Plate 1; Figure 1). It is about 250 miles (460 km) long and consists of a series of individual parallel and subparallel ridges and troughs with many of the ridges rising to water depths of 1300 to 1200 fathoms (2380 to 2200 m). The troughs extend to depths of as much as 2800 fathoms (5060 m) forming relief of up to 1500 fathoms (2750 m) with the crests of adjacent ridges. The crest to trough relief is generally on the order of 400 to 600 fathoms (730 to 1100 m).

A prominent but somewhat discontinuous ridge in the Blanco Fracture Zone essentially defines much of the southern border of Cascadia Basin and acts as a barrier to the southward flow of bottom-transported sediment through the Fracture Zone (Plate 1; Figure 1). This prominent ridge in most places rises at least 200 fathoms (365 m) above the 1600- to 1650-fathom (2940- to 3030-m) depth of the floor of Cascadia Basin and can be traced eastward to a point 15 miles (28 km) west of the foot of the continental slope off Cape Blanco, Oregon.

The Gorda Ridge (named by Wilson, 1965) is separated from Cascadia Basin by the Blanco Fracture Zone into which it merges. The crest of the Ridge has an average relief of 300 to 400 fathoms

(550 to 730 m) and an average depth of about 1200 fathoms (2200 m), although a few peaks rise to depths of less than 1000 fathoms (1830 m). The Ridge has a well-defined median valley which has an average depth of 1800 fathoms (3300 m) and a relief of 200 to 1000 fathoms (365 to 1830 m).

The Juan de Fuca Ridge (named by Wilson, 1965) forms the western margin of Cascadia Basin and does not have a crest or a median valley as pronounced as those of Gorda Ridge. Instead, the relief is more subdued and less distinctive. The crest of the Juan de Fuca Ridge is at a depth of about 1400 fathoms (2600 m), although numerous seamounts have summits at much shallower depths (McManus, 1967).

New Bathymetric Data

The bathymetric surveys conducted during this study were project oriented and were limited to specific physiographic features of particular interest. These surveys centered largely around the eastern half of the Blanco Fracture Zone, the course of Cascadia Channel through the Blanco Fracture Zone, and the abyssal region adjacent to the continental slope off southern Oregon. The main objective of the surveys was to determine if and where it was topographically feasible for sediments from Cascadia Basin to be transported along the bottom through the complex ridges and troughs or

around the east end of the Blanco Fracture Zone toward the Mendocino Fracture Zone. Another objective was to more specifically locate the structurally controlled course of Cascadia Channel through the Blanco Fracture Zone.

New bathymetric data obtained in the above outlined areas consist of more than 2500 nautical miles (4600 km) of Precision Depth Recorder (PDR, Times Facsimile Corporation Mark V) sounding tracks (fathograms) made during Oregon State University cruises in 1965 and in 1966 (Figure 2). An additional 1100 miles (2000 km) of previously unreported Oregon State University sounding tracks (run in 1963), obtained with an Edo recorder (UQN-1), also are included in the bathymetric investigation. Positioning for all track lines was accomplished by using Loran A fixes at intervals of two to three miles. These new sounding data were incorporated with previously published data (Hurley, 1960; McManus, 1964, 1965; Byrne, 1962, 1963b) to construct an improved bathymetric chart of the eastern portion of the Blanco Fracture Zone off southern Oregon (Figure 3).

Blanco Valley

On the basis of limited echo soundings, McManus (1964) inferred that a saddle (Blanco Saddle) was present in the area between the steep continental slope off Cape Blanco on the east and the

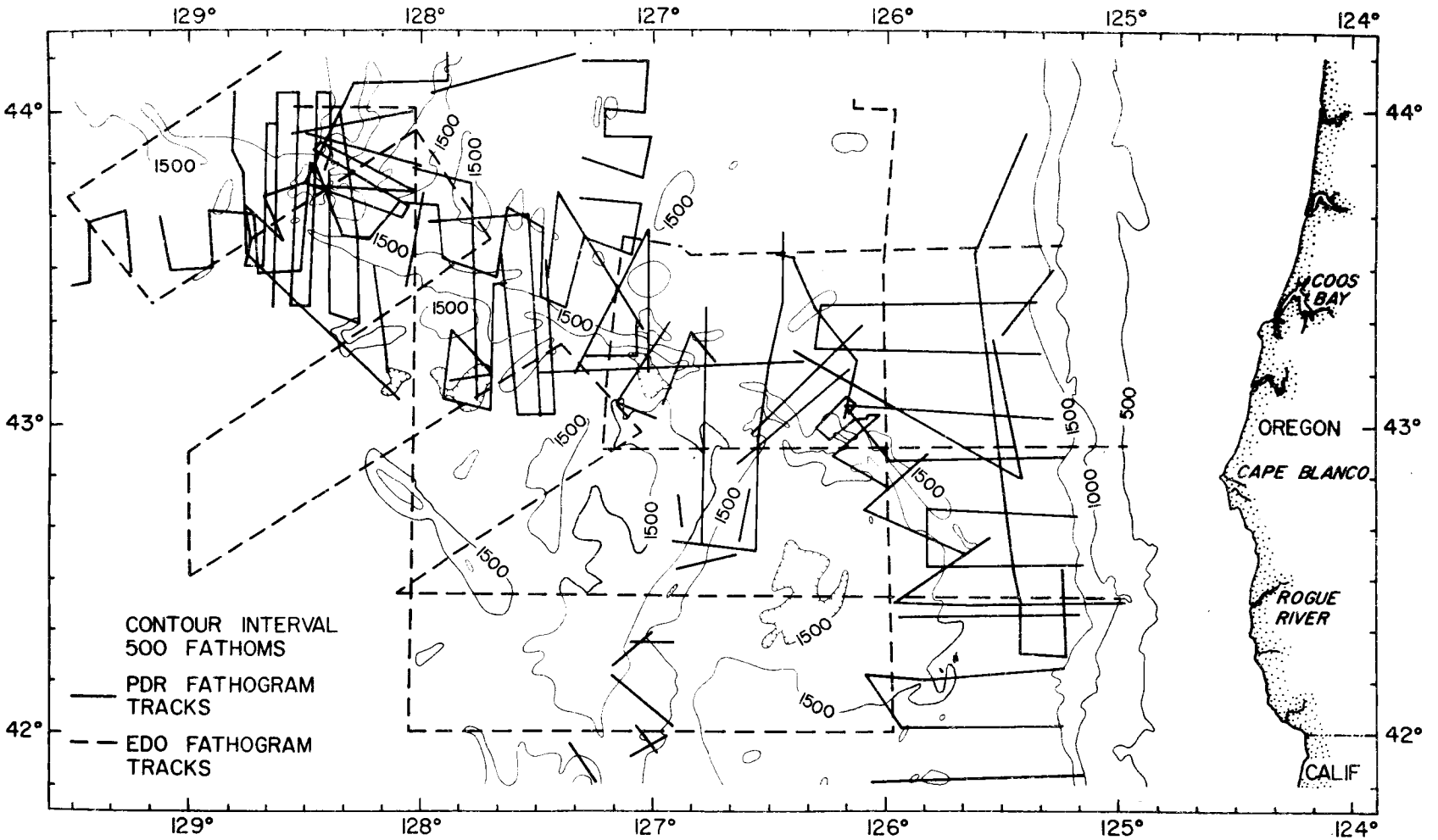

Figure 2. Track map of echo soundings (fathograms) of the eastern part of Blanco Fracture Zone and vicinity.

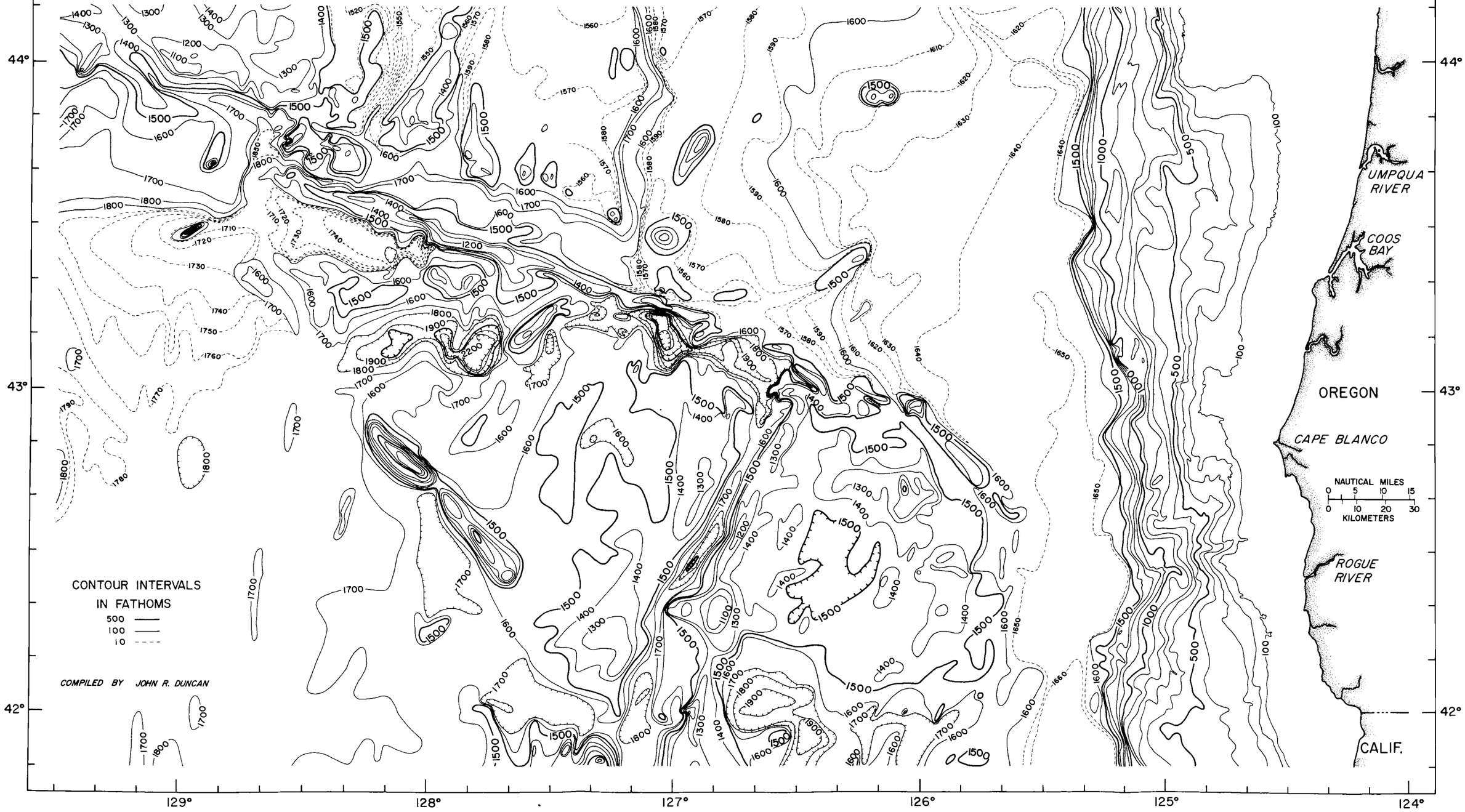

Figure 3. Bathymetry of the eastern part of Blanco Fracture Zone and vicinity.

submarine mountains and hills on the west. Presumably, he thought that this area represented a low point in the main ridge of the Blanco Fracture Zone, and that from this point the slope gently descended in opposite directions (north and south). Results from north-south and east-west echo sounding tracks (Figures 2, 4) over this feature indicate no such slope reversal. Instead, a low but continuous southward gradient (1:5700) is evident. It is suggested that the feature is valley-like, and hence the name Blanco Valley seems more appropriate.

The new sounding data also indicate that it is feasible for sediments to be transported southward out of Cascadia Basin through Blanco Valley. The Valley appears to be a continuation of the southward-trending Astoria Channel. It is inferred that these two features join at 44°N where Astoria Channel turns eastward to the foot of the continental slope. The extent of Blanco Valley south of the area surveyed is unknown.

Cascadia Channel

A new course has been mapped for Cascadia Channel in the vicinity of Cascadia Gap which is located in the Blanco Fracture Zone (Figure 5). The course is different from the one proposed by McManus (1964) and somewhat similar to that suggested by Hurley (1960). West of the Gap the Channel abruptly turns south along a zone of structural weakness and continues in a southerly direction

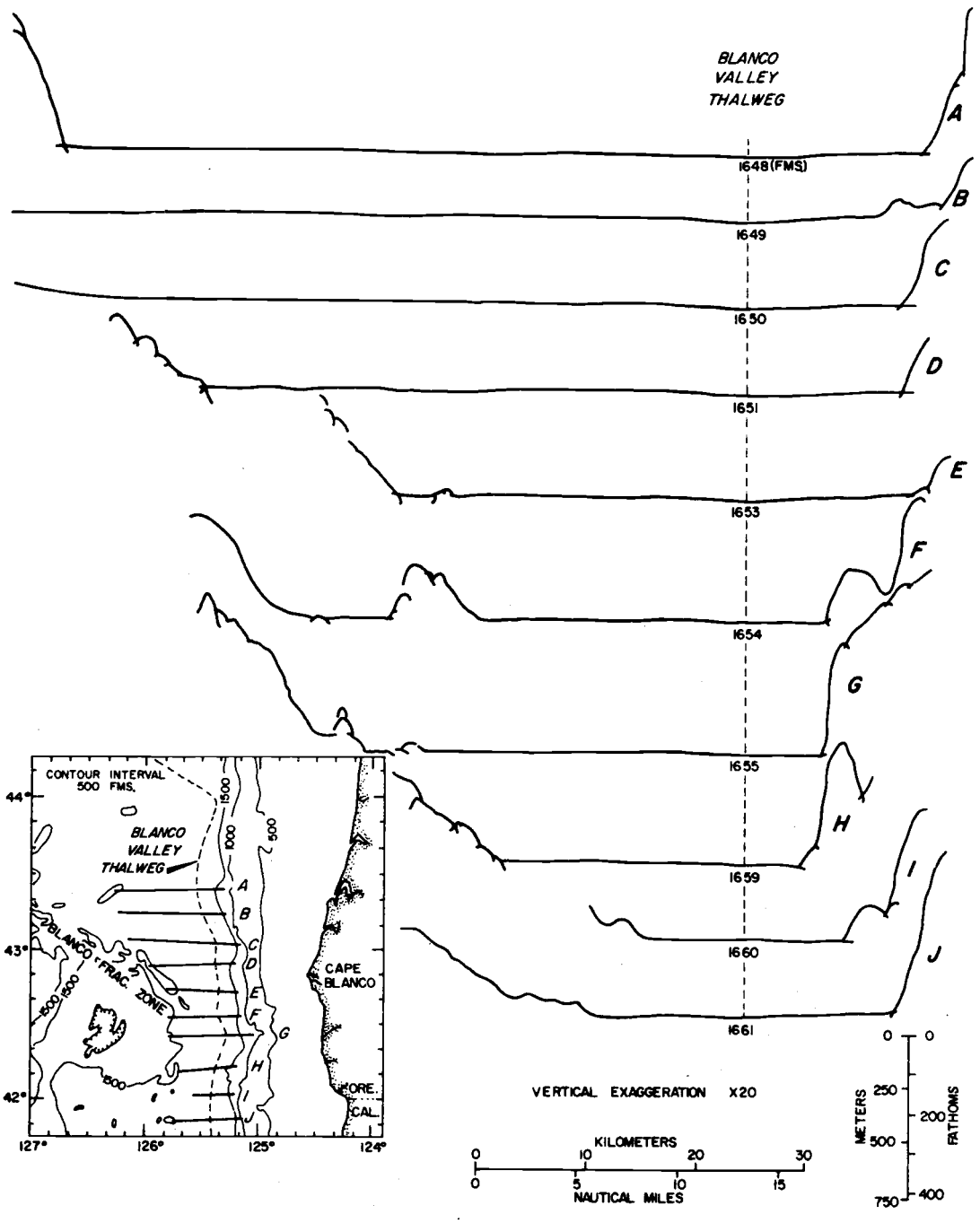

Figure 4. Transverse PDR profiles of Blanco Valley.

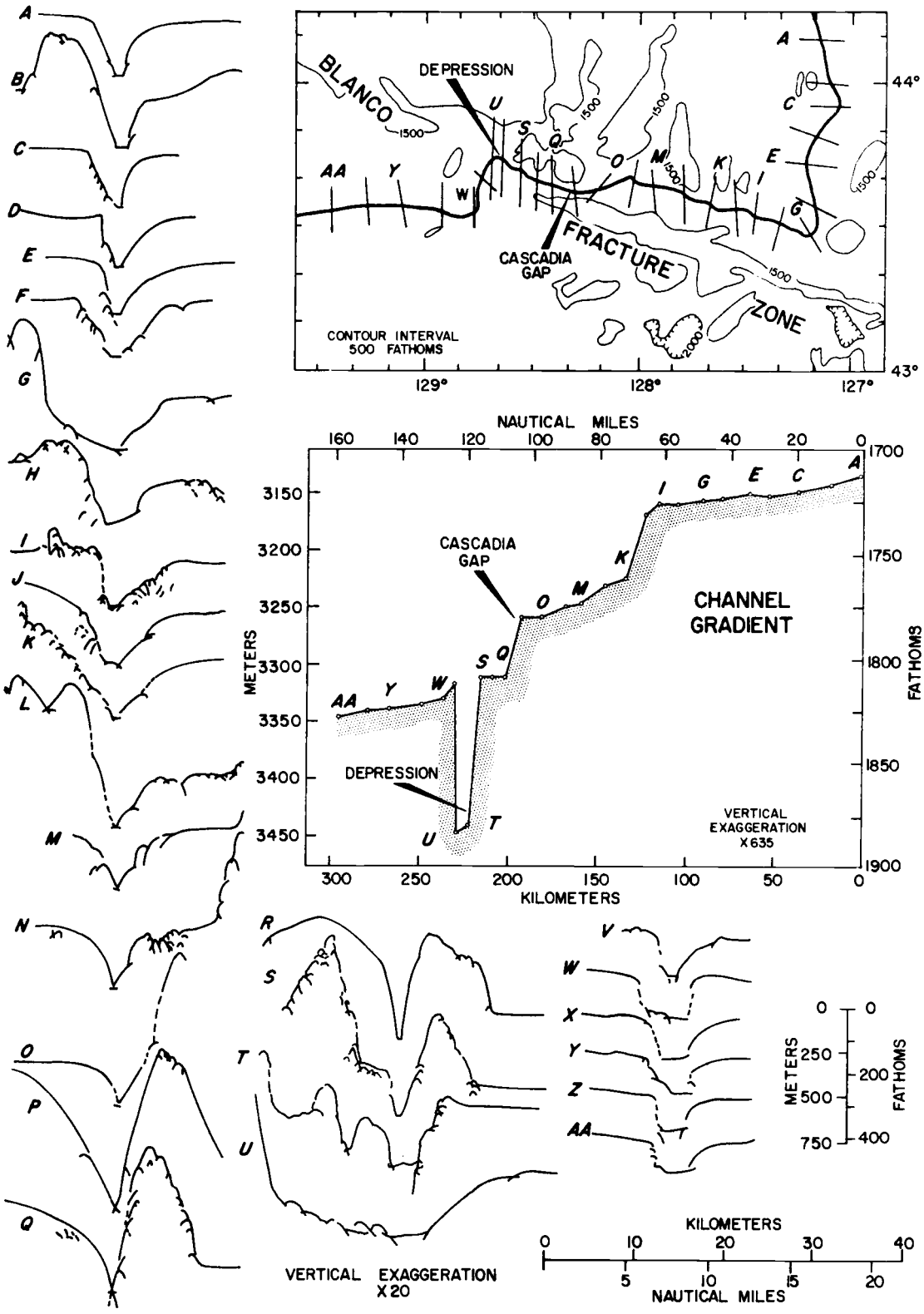

Figure 5. Transverse PDR profiles and longitudinal gradient of Cascadia Channel through the Blanco Fracture Zone.

for 12 miles (22 km) before resuming a western course. In the northern part of this south-trending segment, a roughly linear depression, with about 70 fathoms (120 m) relief, occurs along the axis of Cascadia Channel. The influence of this axial depression on the bottom transport of sediment through the Channel is discussed in Chapter XI.

Blanco Fracture Zone

The submarine mountains and ridges of the Blanco Fracture Zone, between Cascadia Gap and Blanco Valley, appear to be very effective barriers to the southern transport of sediment from Cascadia Basin (Figures 3, 6). The troughs south of the main north-northwest trending ridge are frequently rough-bottomed and much deeper than the general depth of Cascadia Basin, suggesting that there are few gaps in the submarine ridges and mountains through which sediments can pass and fill the troughs. However, one trough, south of Cascadia Gap (profiles C, D, E, F of Figure 6; see also Figure 3), has a smooth, relatively shallow floor, which does suggest appreciable sediment fill. Heavy mineral data, presented in Chapter VII, indicate that this fill may have been derived chiefly from occasional sediment overflows of turbidity currents that passed through Cascadia Channel; these overflows presumably occurred at the point where the Channel is sharply deflected to the right in the

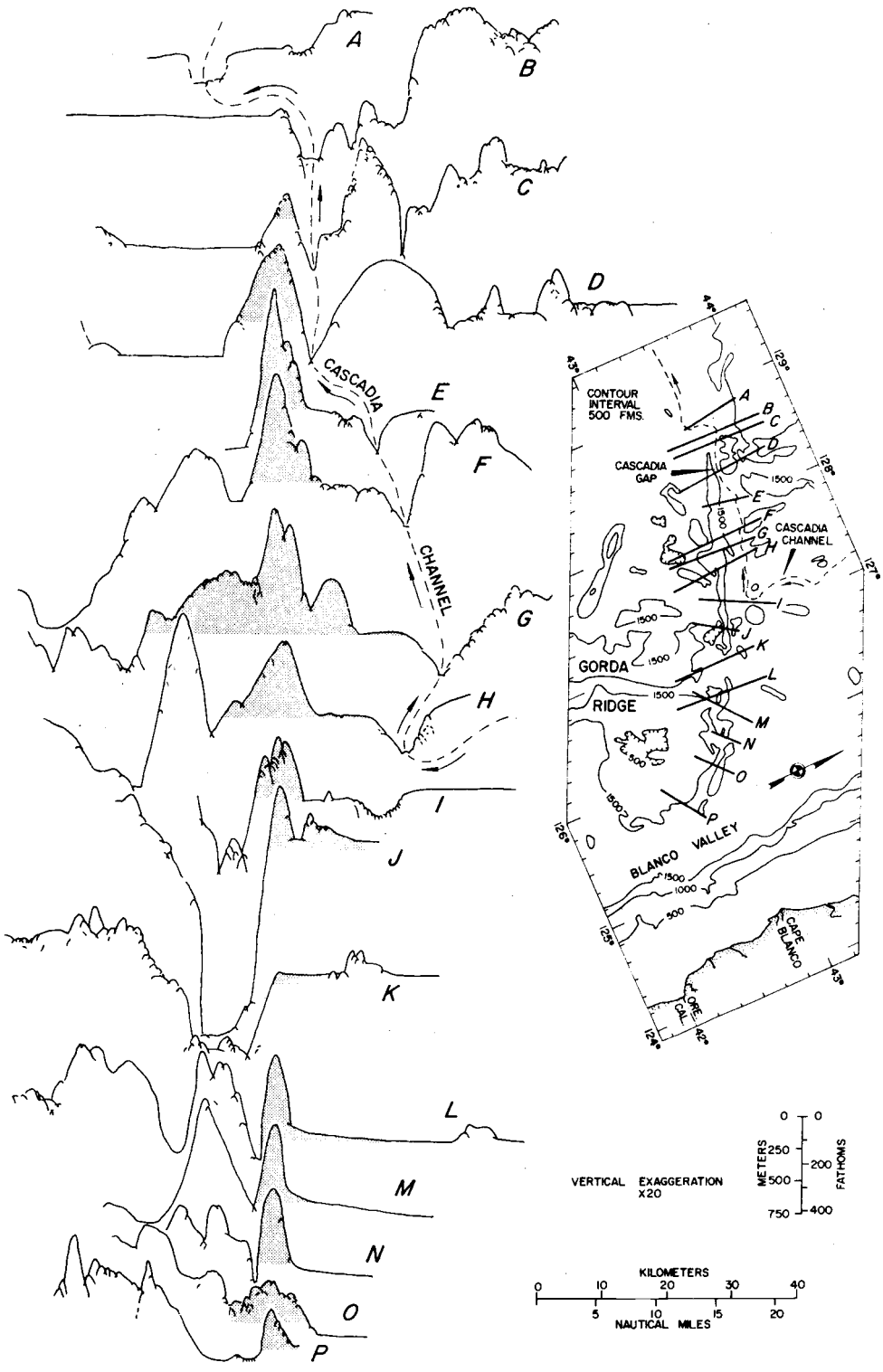

Figure 6. Transverse PDR profiles of the eastern part of the Blanco Fracture Zone. The prominent ridge which forms much of the southern margin of Cascadia Basin is shaded to a water depth of 1600 fathoms (2930 m).

area west of Cascadia Gap (43°35'N, 128°45'W).

The continuity of the ridge and trough system of the Blanco Fracture Zone, in the vicinity where the crest and the axial valley of Gorda Ridge merge with the Fracture Zone (Figure 3; 43°N, 126°30'W), is more disrupted than previously depicted by former surveys (Hurley, 1960; McManus, 1964, 1965). Also, a low point is evident in the ridge that forms the margin of Cascadia Basin in this transition area between the crestal zone of Gorda Ridge and the Blanco Fracture Zone; in profile K (Figure 6), the ridge rises less than ten fathoms (18 m) above the sediment-filled floor of Cascadia Basin on the north. However, the roughness and the depth of the adjacent trough on the south of the low ridge suggest that little material has entered from the north.

III. SEDIMENT SAMPLES AND LABORATORY METHODS

Sampling Devices and Locations

The deep-sea sediment samples used in this investigation were collected during several cruises of the R/V ACONA and the R/V YAQUINA from 1962 to 1966. Station locations were selected to give as wide a representation as possible of specific features and environments (Plate 1; Appendix 1).

Sampling was mainly done with a modified Ewing piston corer; the cores range in length from 30 to 1055 centimeters. Surface sediment was sampled with a multiple corer (Fowler and Kulm, 1966) or a phleger corer as a trip weight at each piston core station. No piston cores were recovered at five coring stations, but the short trip-weight cores were retrieved and used for analysis (see Appendix 1). In all, cores from 55 stations are included in this study. In addition, sediments in one pipe-dredge haul from Astoria Canyon and seven grab samples from the Columbia and Rogue Rivers were taken for analysis.

Core Processing

The cores were collected in plastic liners and kept under refrigeration until processed to prevent deterioration. The core

processing procedure consisted of cutting the plastic liner open with a circular saw, sectioning the core lengthwise with a thin wire, photographing the sectioned core, and describing the sediment characteristics with the aid of a binocular microscope and the Rock Color Chart (Geological Society of America, 1963).

Because the variations in sediment color are significant, care was taken to accurately describe the sediment color in a consistent manner. The colors were recorded immediately after opening a core while it was still moist and before oxidation set in.

The piston cores from Astoria Canyon and from Astoria Fan were originally processed and analyzed by Carlson (1968) and by Nelson (1968), respectively. Griggs (1968) is currently conducting a detailed study of sediments in Vancouver Valley, northern Cascadia Channel, and Willapa Channel, and he was kind enough to supply samples and general descriptions of the cores from Vancouver Valley (6610-2) and from Willapa Channel (6508-K1) used by the writer. All these workers processed the cores in an identical manner to that outlined above.

The upper few centimeters in the piston cores were frequently lost or badly distrubed during the coring operation. Hence, trip-weight cores were used to supplement the study of the surface sediments and to replace the upper stratigraphic sequence when lost in a piston core.

Grain Size and Coarse Fraction Analyses

Two hundred and twenty samples, selected to represent the different sediment types, age units (postglacial and late Pleistocene), and deep-sea environments, were analyzed for coarse fraction (Shepard and Moore, 1960) and for grain size compositions. For these analyses, samples up to 10 cm in length were taken from the cores. The length of the sample interval depended upon the thickness of the lithologic unit; units that were less than 10 cm thick were sampled in their entirety.

A simplified grain size analysis was performed on each sample; only the percents of sand (> 62 microns), silt (62 to 4 microns), and clay (<4 microns) were determined. A representative sample split of approximately 25 grams (dry weight) was used. The sediment was dispersed in a 0.2 percent solution of Calgon (sodium hexametaphosphate) after the seawater was removed with millipore filters. The silt and the clay content were then analyzed by the pipette method (Krumbein and Pettijohn, 1938, p. 166-170), and the sand content was determined by weighing the dried sand-size constituents retained on a 62-micron screen after wet sieving.

A coarse fraction count was made of the constituents greater than 62 microns. At least 300 grains, in a representative split of each sample, were identified with the aid of a binocular dissecting

microscope and the use of a grid for unbiased grain selection.

Approximately 1500 samples, 1 to 2 cm thick, were taken from 40 of the cores at intervals of about 10 cm to determine the relative abundances of planktonic foraminiferans and radiolarians. These samples were wet sieved on a 62-micron screen without any previous dis-aggregation treatments to preserve the fragile tests. A combination of at least 100 planktonic foraminiferans and radiolarians per sample were identified and counted. The compositions of the remaining constituents were only noted semi-quantitatively.

Petrographic Analysis of Sand-Size Sediments

Where possible, layers best representing the different sedimentational environments and established age intervals and containing an abundance of sand-size grains were selected for examination of regional and temporal variations in both the light and the heavy mineral suites of the sands. Seventy-three deep-sea samples were chosen from those previously analyzed for grain size composition. The heavy mineral assemblages of four additional samples from the Columbia River were also analyzed.

Many of the sandy units analyzed were graded; hence, to minimize the effect of selective sorting due to depositional processes and to insure proper representation of the overall mineral assemblage, the writer sampled the graded units *in toto* and analyzed splits from

these composite samples to obtain average mineral compositions. All sand samples were treated with 30 percent hydrogen peroxide and 2 N hydrochloric acid to remove organic and carbonate materials. Particles finer than 62 microns were removed by wet sieving. The sand-size material was separated by means of tetrabromoethane (sp. gr. = 2.96) into light and heavy mineral fractions.

The light mineral fraction was stained to differentiate potash feldspar from plagioclase feldspar (Bailey and Stevens, 1960). The light mineral composition of each sample was then determined with the aid of a binocular dissecting microscope; at least 300 grains were counted from a grid pattern.

The heavy mineral fractions were mounted in Aroclor (R.I. = 1.65), and 300 or more grains per sample were identified by using a mechanical stage and polarizing microscope. Only heavy mineral grains in the 62- to 125-micron size fraction were included in each count; the upper limit of this size interval was determined with an eyepiece micrometer graticule.

Clay Mineral Analysis by X-ray Diffraction

X-ray analyses were performed on 76 selected sediment samples to determine their clay mineral compositions. The samples were processed according to the technique outlined by Russell (1967) for detecting montmorillonite, illite, chlorite, and kaolinite in

marine sediments. All organic matter and calcium carbonate were removed from the samples with hydrogen peroxide and a buffered weak-acid solution consisting of sodium acetate and acetic acid (pH= 5.0). All clay mineral identifications were made from X-ray traces of magnesium ion-saturated, ethylene-glycol-treated clays in the less than two-micron size fraction. The X-ray work was done on a Norelco diffractometer with a Geiger-Müller counting tube. Data were recorded on a linear scale, strip chart recorder at one degree per inch per minute. No pulse height analyzer was used. Other machine settings were as follows: time constant four seconds, current 35 ma, voltage 50 KV, 1° scatter and receiving slits, 0.006-inch divergence slit. Nickel-filtered copper radiation (lambda=1.54Å) was used for all samples. Samples were scanned from 3° to 14° 2θ with the rate meter at 1000 counts per second as full scale and from 24° to 26° 2θ with the rate meter turned down to 500 counts per second as full scale.

For samples processed in the manner outlined above, montmorillonite is identified on X-ray traces by a basal spacing of 16.8Å; no differentiation of montmorillonite into its several members is made. The 001 peak for illite occurs at 9.95Å and is quite sharp. Biscaye's technique (1964a) was used to differentiate between kaolinite and chlorite. Using this technique, the writer found kaolinite to be absent in all samples studied; thus, the maximum inflection at

7.05Å designates the 002 peak of chlorite.

To detect the regional and temporal variations in the clay mineral composition of the deep-sea sediments, the writer used the semi-quantitative technique suggested by Biscaye (1964b, 1965). The percentages of montmorillonite, illite, and chlorite were calculated from their respective peak areas multiplied by scale factors. These scale factors are used to compensate for differences in diffraction intensities inherent in each mineral and thus to approximate real percentages more closely. The assumption is made that the identified clay minerals on each trace total to 100 percent. Factors and areas suggested by Biscaye (1965) and used herein are one times the 17Å montmorillonite peak, four times the 10Å illite peak, and twice the 7Å peak divided between kaolinite and chlorite. Since no kaolinite is present, the 7Å peak is assumed to represent only chlorite.

Organic Carbon and Calcium Carbonate Analyses

The percents of organic carbon and of calcium carbonate were analyzed in 74 selected samples with a Leco induction furnace, coupled with a Leco gasometric carbon analyzer. To determine the calcium carbonate content in the sediments, the writer treated 1-to 2-gram samples of finely ground, unwashed, dried sediment with hydrochloric acid and measured the evolved carbon dioxide in the manner described by Curl (1962). Two sub-samples were run

for each sediment sample, and the results were averaged and calculated in terms of percent by weight calcium carbonate.

The organic carbon content was estimated by measuring the average total carbon content of two sub-samples of dried sediment (1 to 2 grams) and subtracting from it the carbonate carbon recovered as carbon dioxide. Total carbon content was determined by combusting a sample heated in the Leco induction furnace. The carbon dioxide released by combustion of carbon compounds and by decomposition of carbonate was collected and measured gasometrically.

Measurement of Oxidation-Reduction Potentials

Oxidation-reduction potentials (Eh) were measured in sediments of trip-weight cores at three stations (6609-13, -16, -19) with a Beckman pH meter coupled with a platinum electrode and a calomel electrode. Immediately after the cores were brought aboard ship the measurements were taken by inserting the electrodes directly into the freshly exposed sediments.

IV. GENERAL SEDIMENT TYPES AND THEIR DISTRIBUTION

In this chapter, only a very generalized description of the sedimentary regime is set forth. Discussions center on results obtained from preliminary sediment core examinations with a binocular microscope and the Rock Color Chart (Geological Society of America, 1963). Subsequent chapters relate sediment characteristics and trends noted in more sophisticated analyses. However, some of the results, which were obtained from these more sophisticated analyses, are interjected here to clarify and to substantiate certain aspects of the sediment classification presented in this chapter. To some extent, the interrelationships and regional distributions of the different sediment types are herein briefly discussed; the main purpose of this brief discussion is to give the reader an overall preview of the sediment regime in the deep-sea area under investigation.

Description of Sediment Types

Ten sediment types are distinguished in the deep-sea environments off Oregon (Table 1). These sediment types are defined on the basis of megascopic differences in texture, structure, color, and biologic or lithologic content of the sediments. An attempt is made to describe the sediments as objectively as possible but not necessarily to classify them according to origin or mode of

Table 1. General sediment types in the deep-sea environments off Oregon.

SEDIMENT TYPE	DIAGNOSTIC CHARACTERISTICS
LUTITE GROUP	Homogeneous, poorly sorted sediments; composed mostly of silt and clay but may contain some coarser debris
BROWN LUTITE	Color (10YR4/2 to 10YR2/2) *
OLIVE GRAY LUTITE	Color (5Y3/2)
GRAY LUTITE	Color (5Y4/1, 5GY 4/1 and N4)
LIGHT OLIVE GRAY LUTITE	Color (5Y 4/2)
FORAMINIFERAL LUTITE	Composed of more than 30% planktonic foraminiferans
GREENSTONE LUTITE	Angular greenstone fragments present in coarse fraction (> 62 microns)
BASALTIC GLASS LUTITE	Basaltic glass shards (dark brown) present in coarse fraction
BASALTIC RUBBLE OR SAND LAYER	Mainly composed of angular basaltic rock fragments
TERRIGENOUS SAND-SILT LAYER	Stratified, fine sands to coarse silts of continental origin
GRAVEL	Mainly composed of rounded to sub-rounded pebble-size rock fragments

*Geological Society of America Rock Color Chart (1963) color code.

deposition, although changes in these factors frequently result in noticeable differences in sediment character.

Lutite Group

The term "lutite" is gaining popularity among marine scientists (Ericson et al., 1961; Heezen, Hollister and Ruddiman, 1966; Conolly and Ewing, 1967). This term is used to describe sediments which are predominantly composed of clay- and silt-size particles but cannot be classified into specific grain size categories by megascopic examination.

Approximately 80 percent of the sediments cored fall into the lutite group. This group is subdivided into seven different lutites. Four of these lutites (brown, olive gray, light olive gray and gray lutites) are homogeneous-looking sediments typically composed of sand-, silt-, and clay-size mixtures which are classified by Shepard (1954) as silty clays though in some instances the mixtures are classified as clays or clayey silts (Figure 7). These four lutites are distinguished from each other mainly on the basis of color. The three other lutites--foraminiferal lutite, basaltic glass lutite (Figure 7), and greenstone lutite--contain a biologic or lithologic component which readily differentiates them from the other lutites.

Brown lutite. Lutites which are dark yellowish brown (10YR 4/2) to dusky yellowish brown (10YR 2/2) have been lumped together

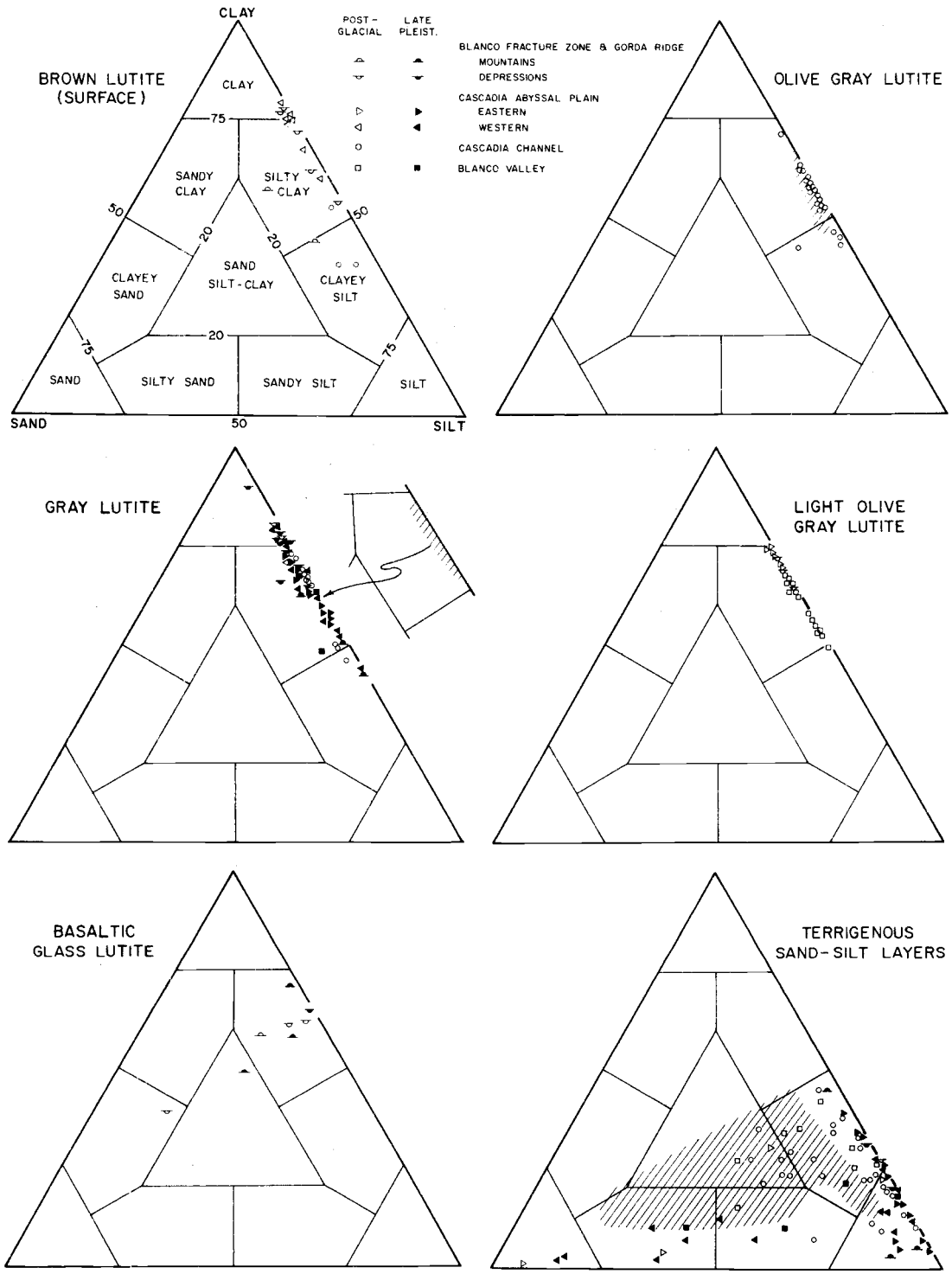

Figure 7. Percent sand-silt-clay distribution diagrams for sediment types from late Pleistocene and postglacial stratigraphic intervals in the deep-sea environments off Oregon. Criteria for recognition of time intervals are given in Chapter V. Hachured areas show range of values for Astoria Canyon sediments (from Carlson, 1968).

and classified as brown lutite. The brown lutite is only found at the surface and is quite gelatinous. This lutite is composed of clay, silty clay, and clayey silt size mixtures, and in all cases, it is coarser grained than the very fine grained pelagic "brown clays" or "red clays" (Shepard, 1963, p. 402-404) found in abyssal environments far from continental sources of sediment.

Olive gray lutite. This sediment is olive gray (5Y3/2) and has a high organic content. A strong odor of decaying organic matter as well as the presence of abundant plant fibers, which are visible under a binocular microscope, are evidences of the high organic content. The olive gray lutite is poorly consolidated, has a relatively high moisture content, and is composed usually of silty clay and occasionally of clayey silt size mixtures.

Gray lutite. Although called "gray" and definitely restricted to use for lutites with grayer tones, the actual colors included in the gray lutite category are olive gray (5Y4/1), dark greenish gray (5GY4/1), and medium dark gray (N4). The gray lutite is quite cohesive and considerably more consolidated than the olive gray or brown lutites. The sediment size mixture is variable (clay, silty clay, and clayey silt), but the finest clay-size material in the area is included in this category.

Light olive gray lutite. This lutite, which is light olive gray (5Y4/2), appears to be transitional between the olive gray and the

gray lutites. Although this lutite is best classified as light olive gray, the color is somewhat variable; in certain instances, it approaches a shade designated for gray lutite. Conversely, some of the light olive gray lutites tend towards the color characteristics of olive gray lutite. The grain size composition includes clay, silty clay, and clayey silt.

Foraminiferal lutite. Silty clay deposits containing more than 30 percent planktonic foraminiferans (mainly Globigerina bulloides and Globigerina pachyderma) are classified as foraminiferal lutite. This lutite varies from yellowish gray (5Y6/2) to light olive gray (5Y5/2). It generally is firmer and apparently contains less moisture than other fine-grained deposits in the area studied. Carbonate analyses were run on two samples, and both contained 42 percent calcium carbonate by weight.

Greenstone lutite. The sediment in core 6604-6 from one of the troughs in the Blanco Fracture Zone (Plate 1), is characterized by unstratified angular sand- to pebble-size greenstone fragments set in a matrix of dusky yellow (5Y6/4) silty clay. The rock fragments constitute 20 to 30 percent of the sediment, and hence, the designation, greenstone lutite, is appropriate. A petrographic analysis of six rock fragments, carefully selected to represent the various macroscopic varieties collected, was kindly performed by Dr. William G. Melson of the Smithsonian Institution (1967). His

petrographic descriptions are given in Appendix 2, and a discussion of the tectonic implications of the greenstones is presented in Chapter XI.

Basaltic glass lutite. Certain lutite deposits vary from olive gray (5Y4/1) to dark greenish gray (5GY4/1) or light olive gray (5Y5/2) and contain a noticeable amount of dark brown, sand-size volcanic glass shards. The dark brown glass fragments constitute up to 15 percent of the sediment. Even when present in small quantities (one or two percent), the fragments are readily observed in a core section with a binocular microscope. The shards are somewhat randomly distributed within the clay and silt matrix. They have undergone little or no alteration and have indices of refraction ranging from 1.59 to 1.60. This range of indices indicates that the shards are composed of a glass that contains only 48 to 49 percent silica; hence, the shards are derived from a basic magma (Mathews, 1951). According to George (1924), volcanic glass which has a basic composition is "basaltic glass;" therefore, the term "basaltic glass lutite" will be used as the designation for the whole sediment. The textural composition of the basaltic glass lutite is quite variable; samples plot in the silty clay, sand-silt-clay, and clayey silt categories (Figure 7).

Basaltic Rubble or Sand Layers

Sediment layers consisting almost entirely of pebble- to sand-size basalt and basaltic glass fragments are called basaltic rubble or sand layers, depending upon whether the dominant constituent is rubble or sand, respectively. Individual basalt and basaltic glass fragments generally show little or no alteration.

Terrigenous Sand-Silt Layer

Many of the cores contain distinct layers of sediment in which terrigenous sand- to coarse silt-size feldspar, quartz, and ferromagnesian minerals predominate. On Shepard's (1954) triangular diagram, these layers fall into the sand, silty sand, sandy silt, silt, clayey silt, and sand-silt-clay categories (Figure 7). However, it is not considered important in this study to separate these textural categories; any sediment unit that is distinctly layered and has an abundance of sand or coarse silt of terrestrial origin is referred to as a terrigenous sand-silt layer.

The terrigenous sand-silt units range in thickness from a few millimeters to more than 150 cm. In general they appear to have the characteristics of turbidity current deposits, although some may have been reworked by ocean-bottom currents (Hubert, 1964). Included with the detrital constituents are displaced benthic

foraminiferans, which are known to be indigenous to the continental shelf and slope environments (Duncan, 1966; Griggs, 1966; Carlson, 1968; Nelson, 1968). Most of these sandy layers are visibly coarser grained and better sorted than the lutite units, but, still, they usually contain more than ten percent clay-size particles. The terrigenous sand-silt layers are generally graded, though non-graded layers occur. When present, the grading is frequently irregular and consists of a number of individually graded layers of varying thickness grouped together in one unit that displays an overall decrease in sediment size from the bottom to the top of the unit. A clean, moderately sorted silt or sand layer, several centimeters in thickness, frequently occurs between very poorly sorted silt layers within an irregularly graded terrigenous sand-silt unit.

Gravel

A few graded layers of gravel were cored which are composed of subrounded to rounded pebbles up to 30 mm in diameter. These layers contain a mixed assemblage of igneous (acid to basic), metamorphic, and sedimentary rock types, with finely crystallized basic igneous rocks being most common.

Distribution and Interrelationship of Sediment Types

Surface Sediments

The surface of the cores are frequently capped with a poorly consolidated or gelatinous brown lutite. This brown lutite cover varies in thickness from a mere film (less than 1 mm) up to 20 cm. The basal contact consists of a mottled or gradational color tone transformation downward into a lutite of another color. When present, the brown lutite only occurs as a surface unit.

The variations in thickness of the brown lutite surface unit show a definite regional trend (Figure 8; thicknesses determined from trip-weight cores taken simultaneously with the piston cores). As a rule, the thickness of the brown lutite unit increases with increased distance offshore. In Astoria Canyon (Carlson, 1968) and on upper Astoria Fan (Nelson, 1968), brown lutite is absent, and olive gray lutite occurs at the surface. However, farther seaward on the middle and the lower portions of Astoria Fan, the brown layer is present and generally thickens (up to 4 cm) in an offshore direction (Nelson, 1968).

The surface sediments of Cascadia Channel appear to be an exception to the thickening offshore trend of brown lutite. When compared to immediately adjacent environments, the brown lutite

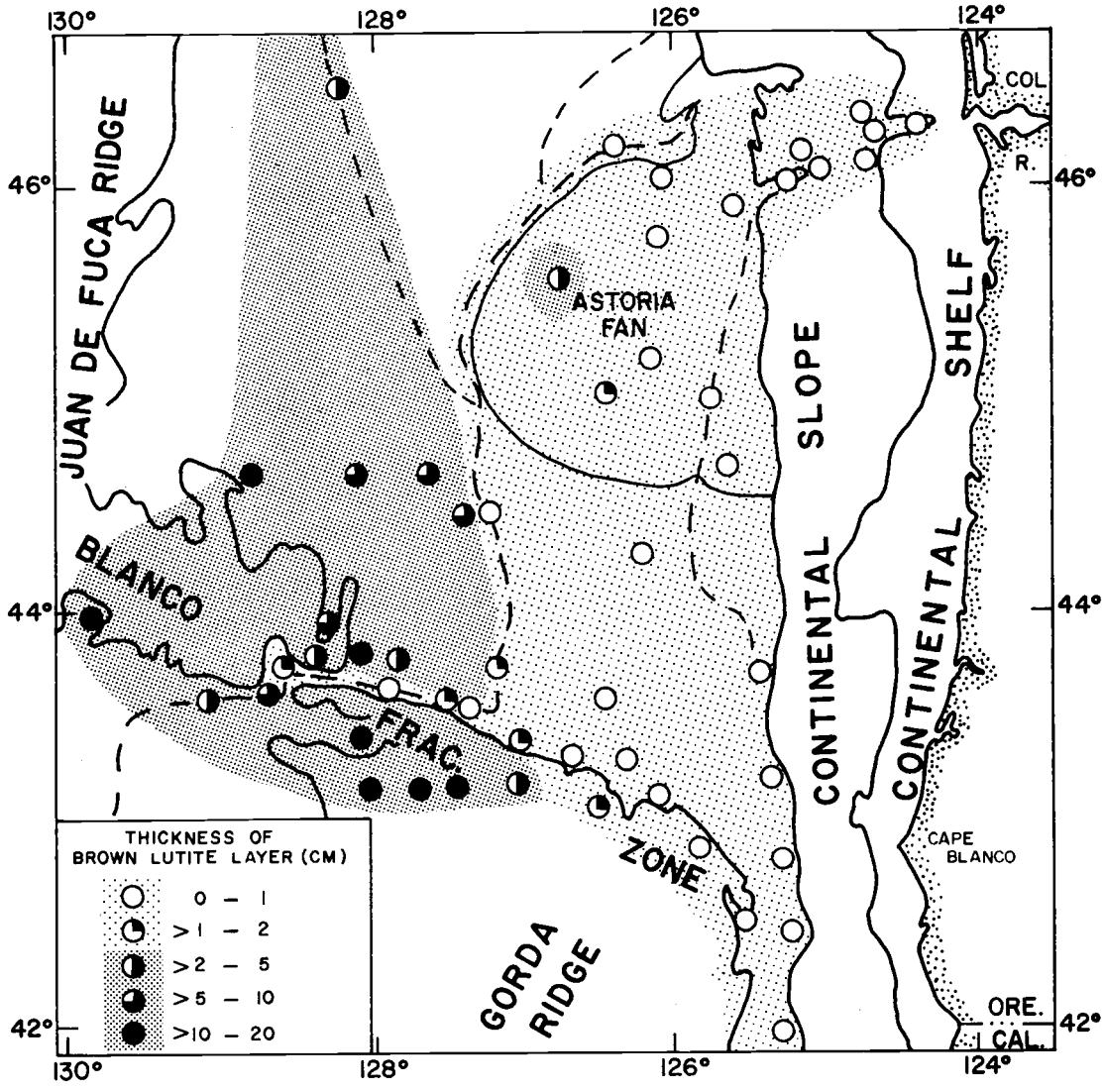

Figure 8. Areal variations in thickness of brown lutite surface covering in southern Cascadia Basin and vicinity.

covering in the Channel sediments is always thinner. However, in the west-trending portion of the Channel course, the thickness appears to increase in an offshore direction, though not as much as in the depositional environments to the north and the south.

Subsurface Sediments

Throughout much of the area studied, relatively thin layers of terrigenous sand-silt are intercalated in olive gray, light olive gray, and gray lutites (Plate 1). These terrigenous layers are even present in Cascadia Channel west of Cascadia Gap (cores 6609-19, 6604-1, 6509-25A) as well as on the eastern part of Tufts Abyssal Plain (core 6509-21A). In sharp contrast, terrigenous sand-silt layers are usually absent in the Blanco Fracture Zone troughs and the axial valley of Gorda Ridge. However, a few terrigenous sand-silt layers are present in the shallow Fracture Zone trough south of Cascadia Gap (core 6604-3), and one layer is evident in core 6609-3 taken in a valley near the eastern extremity of the Fracture Zone adjacent to Cascadia Basin.

Graded layers of gravel have been cored in a few places in the abyssal environments off Oregon. Nelson (1968) penetrated a few such layers on upper Astoria Fan, and Griggs (1968) has observed them in three cores taken in Cascadia Channel, just north of the Channel's union with the southeast-trending Vancouver Valley.

Only one gravel layer (more than 30 cm thick) was uncovered in the present study; it is located in Cascadia Channel west of both Cascadia Gap and the depression in the Channel axis (core 6604-1).

Basaltic glass lutite and basaltic rubble and sand layers are restricted to the transition area between the Blanco Fracture Zone and the crest of the Gorda Ridge. Layers of basaltic rubble (up to 7 cm thick) and basaltic sand (1 to 2 cm thick) separated by basaltic glass lutite units are present in a 70 cm-long core (6609-8) from a deep trough in the Blanco Fracture Zone. Core 6601-1 (560 cm long), taken on a submarine mountain-slope is composed of lutite containing basaltic glass, as is the short core (6609-6) from the axial valley of the Gorda Ridge.

Regional and vertical trends are evident in the lutite color characteristics (Plate 1). With the exception of the relatively thin capping of brown lutite, the lutites of the environments in the western half of the region under study are generally gray. These environments include western Cascadia Abyssal Plain, eastern Tufts Abyssal Plain and the Blanco Fracture Zone troughs west of the Gorda Ridge crestal zone. Gray lutites are also present in eastern Cascadia Basin, but most of them are restricted to a lower sedimentary unit of unknown thickness which occurs in many of the cores.

The upper sedimentary unit in the cores from eastern Cascadia Basin varies in thickness and is characterized by either light olive

gray or olive gray lutite. Within this upper unit there is a tendency for the lutites to become lighter in color, grading from olive gray to light olive gray, away from the continent. Although the upper lutite units of both eastern Cascadia Abyssal Plain and Blanco Valley are classified as light olive gray (Plate 1), there is a slight shift from the darker to the lighter tones of this color category in a seaward direction. A south to north color transition from light olive gray to olive gray is also evident; the lutites change from light olive gray in the Blanco Valley-eastern Cascadia Abyssal Plain area to a decidedly olive gray tone in the region of Astoria Fan and Astoria Canyon.

As in the case of the surface brown lutite, Cascadia Channel subsurface sediments are an exception to the above color trends. Olive gray lutite is the most abundant sediment type throughout the entire length of channel studied. The Channel sediments have a characteristic sedimentary sequence consisting of cyclic units of relatively thin basal terrigenous sand-silt layers (up to 35 cm thick) grading upward into thick olive gray lutite layers (generally 40 to 80 cm, but varying from a few to 420 cm) which are capped with thin gray lutites (1 to 10 cm). On the average, the cyclic units in Cascadia Channel consist of 12 percent terrigenous sand-silt layers, 85 percent olive gray lutite, and 3 percent gray lutite. The upper contacts of the thin gray lutite layers with the overlying terrigenous sand-silt layers are always sharp; whereas, their basal contacts

with the underlying olive gray lutites are usually mottled and somewhat difficult to locate. Mottles and burrows of gray lutite extend downward 5 to 40 cm into the underlying olive gray lutite (Griggs, Kulm and Carey, 1968).

Foraminiferal lutite is present in only one core (6609-20) which was taken from a submarine hilltop north of Cascadia Gap. This lutite is present in the upper sections of the core, while the lower portions consist of alternating units of terrigenous sand-silt and gray lutite layers similar to those of the western portion of Cascadia Abyssal Plain.

V. SEDIMENT AGES AND STRATIGRAPHIC CORRELATION

Accurate reconstruction of the sedimentational histories of different but related depositional environments requires that comparisons be made between temporally equivalent environmental facies. Any deviation from exact time equivalence of the facies compared is likely to cause some inaccuracy in interpretations. Thus, to help prevent erroneous interpretations and to understand more fully the distribution of sediment types in the deep-sea cores, it is now necessary to establish correlative time horizons from core to core in the various environments. Once established, these time horizons are later used as guidelines for grouping the sediments and for interpreting subtle similarities and differences that are of important temporal or environmental significance.

Criteria used to establish correlative time horizons and stratigraphic sections are 1) radiocarbon age determinations of certain core intervals; 2) vertical changes in the relative abundance of radiolarians compared to planktonic foraminiferans in the sediments; 3) lutite color changes in the stratigraphic section; and 4) presence of absence of ash from the Mount Mazama eruption 6600 years ago.

Radiocarbon Age Determinations

The radiocarbon age determination method was used primarily to establish the absolute ages of events recorded in terms of biological or lithological changes in the core sections and to verify the correlation of these events from core to core. For these purposes, radiocarbon analyses were run for 24 samples from various key intervals in 12 cores (Figure 9; Appendix 3). The sample intervals were chosen as close as possible to the boundaries of significant lithologic or biologic units. However, in many instances the amount or quality of datable material at the preferred interval was insufficient to obtain a reliable date. As a result, an interval some distance from the boundary had to be chosen, or else a long section (up to 85 cm) was sampled to supply sufficient carbon. In the latter case, a composite age was obtained which is assumed to be centered at the midpoint of the sample.

Radiocarbon ages were determined for most of the samples by measurement of only the carbonate carbon content of the sediment. However, in a few samples, the amount of carbonate carbon present was insufficient to establish a reliable date. In these instances the total carbon (organic carbon plus carbonate carbon) was used. The validity of direct comparison of the results of total carbon versus carbonate carbon analysis was checked. In three cores, radiocarbon dates

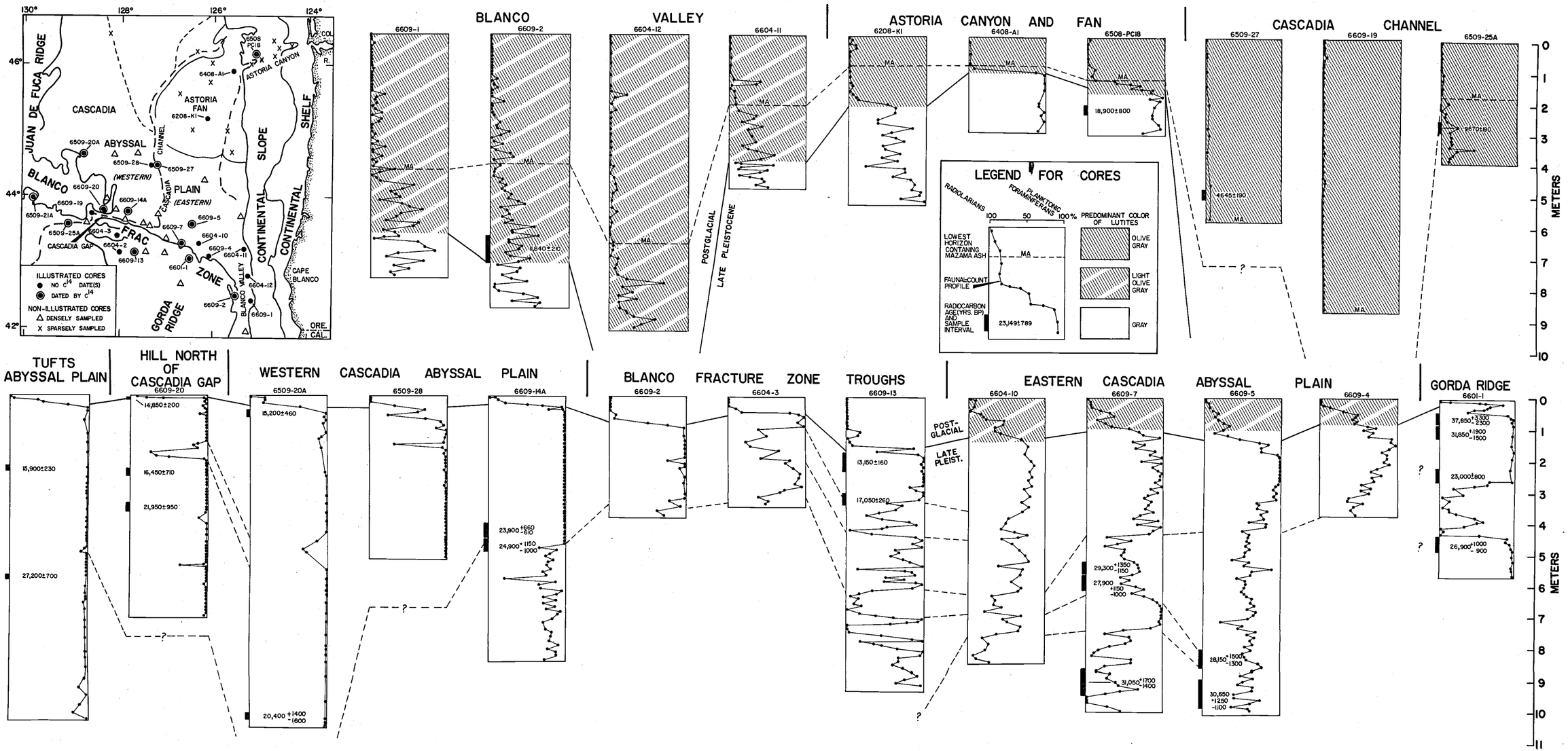

Figure 9. Stratigraphic correlations of relative abundances of radiolarians compared to planktonic foraminiferans, significant lutite color zones and Mazama ash distribution in selected cores from deep-sea environments off Oregon. Inset map shows locations of illustrated and non-illustrated cores analyzed for correlations.

were obtained by using only the organic carbon; the samples taken immediately above or below these intervals were previously dated by using only the carbonate carbon. In all three cases, the dates were close, and discrepancies could be accounted for either by the relative stratigraphic positions of the compared sample intervals or by the margin of error inherent in the method of analysis. (See Appendix 3 for the type of carbon used in all samples, and compare 6609-5-1C14 with -2C14, 6609-7-1C14 with -2C14, and 6609-14A-1C14 with -2C14.)

From the ages indicated by the radiocarbon analyses of the cores (Figure 9), it is evident that relatively high rates of sedimentation are prevalent in all the deep-sea environments studied off Oregon. Even with up to 1055 cm of penetration, the age of the oldest sediment cored is approximately 35,000 or 40,000 years BP (Before the Present). As a result, only the sedimentation regime from the late Pleistocene to the present can be examined. However, this enables the writer to undertake a detailed study of the changes occurring in the more recent stratigraphic record. The generally high sedimentation rates have yielded an expanded stratigraphic section which can be readily examined for temporal variations in the sedimentary record on the order of a few thousand years duration.

The chronology of the radiocarbon ages in core 6601-1 is puzzling. In sequential order, starting from the upper section, the

following dates were obtained down the length of the core: 37, 850; 31, 850; 23, 000; and 26, 900 years BP. The general reversed order of these dates and the fact that the core was obtained from a submarine mountain-slope suggest slumping. Nevertheless, no matter what caused this stratigraphic reversal in dates, it seems justifiable to show the results of the analyses performed for stratigraphic correlations, but not to consider them as evidence in the establishment of general time lines and stratigraphic boundaries.

Planktonic Foraminiferan-Radiolarian Stratigraphy

Changes in climate often greatly influence sedimentational regimes in both marine and continental environments. Recognition of these changes is therefore necessary in order to establish the interrelationships between sedimentary processes, climatic conditions, and the resulting sediment characteristics.

Marine planktonic organisms such as radiolarians and planktonic foraminiferans are generally numerous and sensitive to variations in oceanographic conditions resulting from climatic changes that are essentially synchronous for an area of reasonable size. As a result, stratigraphic time lines having significant paleoclimatic implications can be established on the basis of vertical variations of the species or abundances of these organisms noted in a core. Important and comprehensive studies of the relationship between

planktonic foraminiferal trends and paleoclimatic fluctuations have been made in the Atlantic (Ericson et al., 1961), in the Caribbean (Emiliani, 1966) and in the Pacific off southern California (Bandy, 1960). However, such detailed studies are lacking in the northeastern Pacific Ocean.

The only previous attempt to construct a stratigraphic column in the northeastern Pacific was made by Nayudu (1964a). He obtained five radiocarbon dates from two short gravity cores taken several hundred miles from the continent (Juan de Fuca Ridge and Tufts Abyssal Plain) and tentatively correlated Globigerina-rich sediments with the Vashon (late Wisconsin) glaciation of the adjacent continental area. He also noted that radiolarians were more abundant in the first few centimeters at the tops of the cores. These upper few centimeters of sediment were believed by Nayudu to represent postglacial climatic conditions which he suggested began in the marine environment approximately 12,000 years BP. Nayudu attributed the abundance of globigerinids in the older marine sediments to a high rate of primary production of these planktonic organisms during the Vashon glaciation. This high production rate presumably was caused by intensified atmospheric and oceanic circulation which may have mixed more of the nutrient-rich subsurface water with the surface water.

After considering Nayudu's findings, the author reasoned that

by comparing the abundances of planktonic foraminiferans and radiolarians with respect to each other and irrespective of their total concentration per unit of sediment, the results would be independent of variations in the influx of terrigenous sediment. Hence, the lutites in 40 of the 53 cores presented in this study were sampled at approximately 10-cm intervals to determine the relative abundances of radiolarians compared to planktonic foraminiferans. The other 13 cores were sparsely sampled to establish time lines in them. In all, approximately 1500 faunal counts were made. The faunal distributions for 23 of the densely sampled cores are illustrated in Figure 9. These 23 profiles were selected to demonstrate the variations in the faunal stratigraphy.

One generally well-defined faunal interval, varying in thickness from 2 cm (core 6609-20) to more than 900 cm (core 6609-19) and capping the top of each core, is characterized by 50 percent to nearly 100 percent radiolarians (with 100 percent being equal to the sum of radiolarians and planktonic foraminiferans). Below this interval in 32 of the cores is another interval containing almost 100 percent planktonic foraminiferans. In Figure 9, a time line (solid) is drawn from core to core indicating the selected boundary between the two intervals. The stratigraphic section of variable thickness above this boundary is considered to represent sediment accumulation during postglacial time, while the underlying section of undetermined

thickness is classified as late Pleistocene.

Generalized graphs showing the late Pleistocene and the post-glacial intervals are given for all 53 cores in Plate 1. The faunal boundary between the two time intervals is abrupt, except in the cores where higher rates of sedimentation yield an expanded vertical scale; in these cores a period of transition is clearly evident. In the transition, the relative numbers of radiolarians increase up-section, though numerous oscillations interrupt the trend (e.g., eastern Cascadia Abyssal Plain and Blanco Valley in Figure 9).

Eight radiocarbon dates, selected in order to determine the age of the faunal boundary and to verify its temporal consistency over the entire deep-sea area studied, suggest that the time of faunal change to greater relative abundances of radiolarians is, in fact, fairly consistent. Extrapolations of sedimentation rates were made from the various dated segments down to, or up to, this boundary. Taking into consideration the location of the various sample intervals in the cores, possible fluctuations in rates of sedimentation above and below the boundary, and the margins of error in the radiocarbon dating technique, the author suggests an age of between 12,000 and 13,000 years BP for the time of significant faunal change. An average age of 12,500 years BP is therefore assumed for the boundary. This age is fairly consistent with the findings of Nayudu (1964a) and substantiates his opinion that the faunal transition

probably represents a somewhat rapid shift from glacial to post-glacial climatic conditions in the marine environment of the north-eastern Pacific Ocean.

Additional support for the association of the relative increase in radiolarians with the climatic shift towards present-day conditions is given by Bandy's (1967) study of deep-basin cores off southern California. Although reported only in terms of number per gram of sediment, Bandy found a significant increase in radiolarians at and above the boundary between Pleistocene and Recent (or postglacial) sediments. Frerichs (1968) also noted the same trend for sediments from the Indian Ocean.

Only a few cores penetrated much of the late Pleistocene section (all of these cores are shown in Figure 9). Faunal counts of these cores indicate that some less well-defined radiolarian-rich zones are evident in the late Pleistocene stratigraphic section. Applying a climatic interpretation, it is suggested that slightly warmer intervals during the late Pleistocene are registered by these radiolarian-rich zones. As verified by radiocarbon dating, a few of the radiolarian-rich zones correlate from core to core. However, these zones are not as continuous regionally as is the postglacial section. The faunal variations in the late Pleistocene stratigraphic sections demonstrate better localized correlations than broad regional correlations. Perhaps this localization reflects

the smaller magnitude of the climatic oscillations during the late Pleistocene as compared to the major climatic shift towards non-glacial conditions initiated at the start of postglacial time.

An attempt has been made to generalize the radiolarian-planktonic foraminiferan chronologic profile (Figure 10). This profile is the result of integrating, correlating, and overlapping the stratigraphic sections of 53 cores ranging in length from 30 to 1055 cm. The faunal data are limited for the section below the postglacial-late Pleistocene boundary since only a few cores penetrated this part of the stratigraphic section.

Within the planktonic foraminiferan-dominated late Pleistocene section, there are three possible zones representing time intervals during which fairly abundant numbers of radiolarians were also deposited (Figure 10). The earliest of these intervals, whose time of conception is unknown (>34,000 years BP), terminated approximately 31,000-30,000 years BP. Also, slight increases in radiolarians are generally evident in the period from 28,000 to 25,000 years BP. The final late Pleistocene interval, during which significant numbers of radiolarians were produced, lasted from 18,000 to 16,000 years BP.

In cores taken off southern California, Bandy (1967) found that large numbers of radiolarians (per gram of sediment) were deposited from 28,000 to 26,000 years BP and from 19,000 to 16,000 years BP.

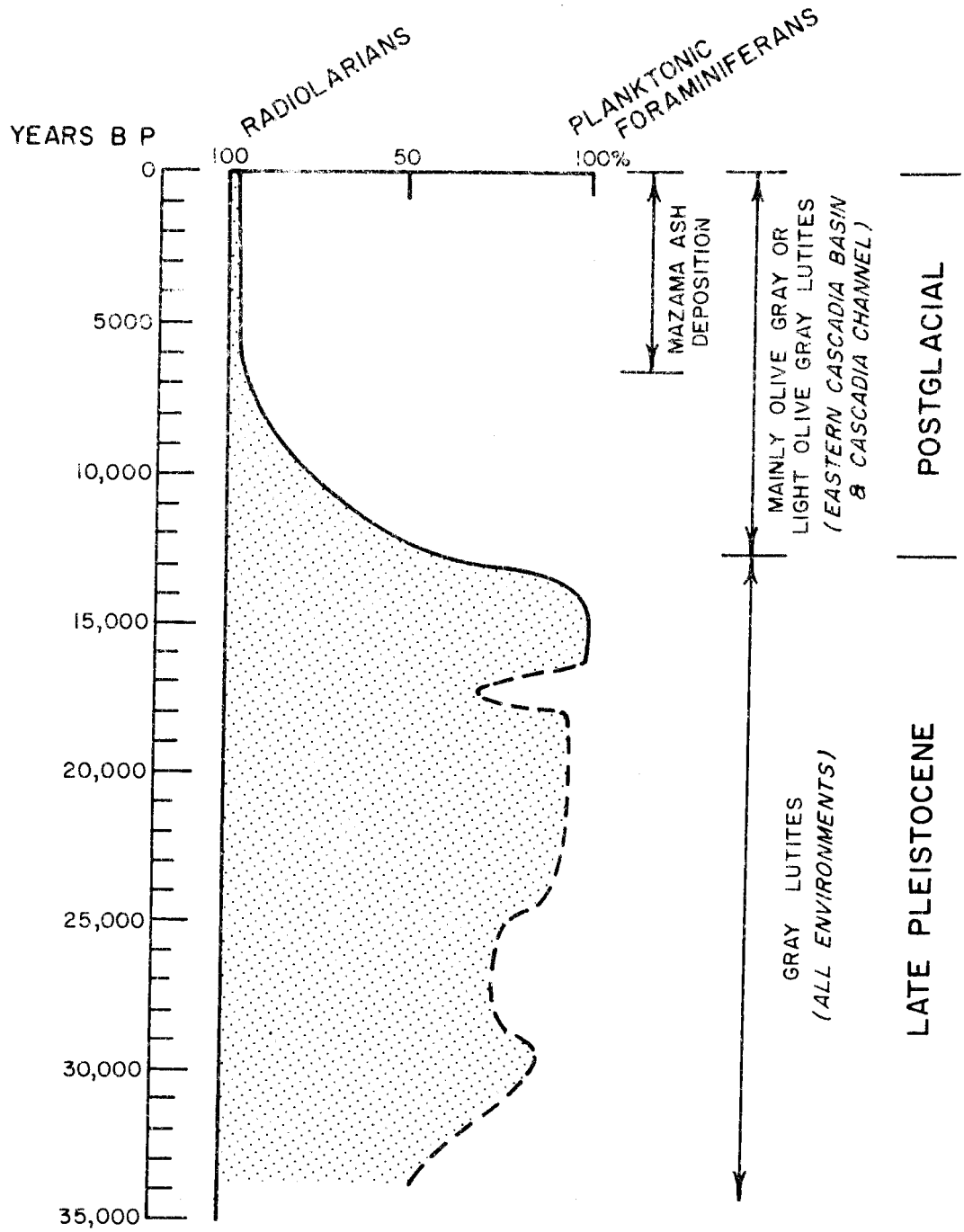

Figure 10. Generalized stratigraphic relationships of faunal trends, lutite color zones, and Mazama ash distribution off Oregon.

These two radiolarian-rich intervals correspond remarkably well with the two radiolarian-rich intervals noted off Oregon. Bandy's data do not extend farther back than approximately 30,000 years BP, so no comparison can be made for the earliest radiolarian-rich interval noted in this study.

In the deep-sea sediments which were deposited off Oregon between 16,000 and 12,500 years BP, the planktonic fauna is consistently composed of nearly 100 percent planktonic foraminiferans (Figure 10). This faunal consistency suggests that the greatest glacial maximum (during the interval studied) occurred just before climatic conditions began to shift towards those of modern times.

Some generalizations can be made about the planktonic foraminiferan-radiolarian profile (Figure 10) and its relationship to the climate during postglacial time. Although a rather abrupt change in the faunal composition occurred approximately 12,500 years BP, the interval from about 12,500 to 7000 years BP shows a somewhat transitional composition between the uppermost radiolarian-dominant section (nearly 100 percent radiolarians) and the planktonic foraminiferan-rich section below. This transitional interval is especially evident in areas of rapid sedimentation, such as Blanco Valley, where the section is expanded and thus affords closer scrutiny. The transition zone seems to reflect a more gradual shift to present-day climatic conditions in the marine environment after the rather abrupt

climatic change which signaled the start of postglacial time approximately 12,500 years BP.

Preliminary studies of cores from the abyssal region off Oregon by Fowler and Duncan (1967) indicate that trends in the species composition of planktonic foraminiferans reflect paleoclimates in a much more subtle way than does the planktonic foraminiferan-radiolarian trend. Most species present are typical of the sub-arctic fauna of Bradshaw (1959). Globigerina pachyderma and G. bulloides combined make up 70 to 80 percent of the assemblage. Globigerina eggeri, G. quinqueloba, Globigerinita glutinata and G. uvula usually comprise the remainder of the fauna. Some species that are more typical of warmer watermasses occur sporadically in low numbers; they are Globoquadrina hexagona, Globigerina digitata and Globigerinoides ruber. There is some indication that G. pachyderma is more abundant in the intervals influenced by relatively cold climates. This species makes up nearly 100 percent of the planktonic fauna in polar areas (Be, 1960).

The coiling directions of G. pachyderma have been used effectively to identify relatively cold and relatively warm watermasses and stratigraphic sections formed under their influence (Ericson, 1959; Bandy, 1960). Left coiling forms indicate cold water and right coiling forms are indicative of warm water. Off Oregon, the coiling direction reversals that have been studied so far (Fowler

and Duncan, 1967) are not nearly as marked as they are elsewhere. Globigerina pachyderma, on the average, coils right about 40 percent of the time in the postglacial, radiolarian-rich interval of core 6609-7 (Figure 11). Below this interval, in the late Pleistocene section, only about five percent (average) of the specimens coil to the right; however, the highest percentages of the right coiling forms (up to 20 percent) occur in the radiolarian-rich intervals.

Stratigraphic Changes in Lutite Color

The abrupt lutite color change (gray lutite overlain by olive gray or light olive gray lutite) in the stratigraphic section of eastern Cascadia Basin marks a significant time boundary. In a detailed study of Astoria Canyon, Carlson (1968) suggested that the olive gray lutite in the Canyon area represents sediment accumulation during postglacial time, whereas the gray lutite is indicative of sedimentation during the closing stages of the Pleistocene. Nelson (1968) also noted the same color change in the Astoria Fan sediments. This color change occurs approximately at the late Pleistocene-postglacial boundary as previously defined by faunal stratigraphy (Plate 1; Figure 9).

The association of color change and faunal transition is also present in the sediments of Blanco Valley and eastern Cascadia Abyssal Plain. However, in these areas the change is from gray to

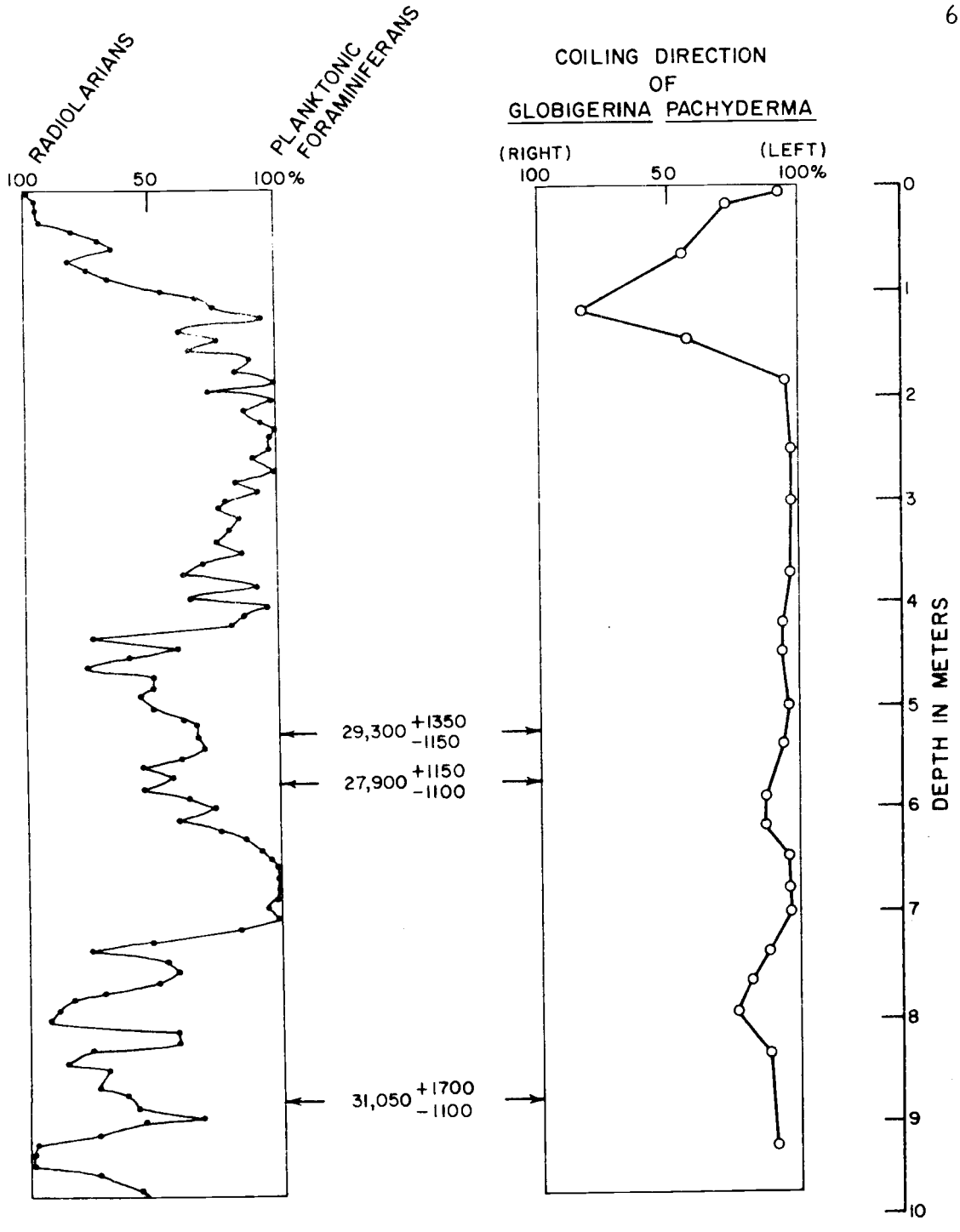

Figure 11. Comparison of the coiling direction of Globigerina pachyderma with the relative abundance of radiolarians and planktonic foraminiferans in core 6609-7 from eastern Cascadia Abyssal Plain. Numbers in the center column are radiocarbon dates.

light olive gray. The radiocarbon date in core 6609-2 (Blanco Valley), which was obtained from the lower part of the light olive gray section just above the color change, is 11,840 years BP (Figure 9). A sedimentation rate extrapolation from this date gives an age of 12,400 years BP for the abrupt change in sediment color. This age is similar to that designated for the late Pleistocene-postglacial faunal boundary (12,500 years BP). Thus, where present, the color break can be used along with the faunal data to identify the time boundary.

The color of the olive gray or light olive gray lutite unit in the postglacial stratigraphic section appears to fade into a gray lutite laterally towards the west away from the continent (Plate 1), with the exception of Cascadia Channel (discussed in Chapter IV). As a result, the color break becomes difficult to recognize in cores from eastern Cascadia Abyssal Plain. In the environments west of Cascadia Channel, no color change can be detected at the late Pleistocene-postglacial faunal boundary, and gray lutite occurs above as well as below it. Also, in Cascadia Channel, where only postglacial sections have been penetrated thus far (Plate 1), thin gray lutite units are even intercalated with the thick olive gray lutite layers described previously (Chapter IV). Thus, it is evident that all gray lutites are not restricted to the late Pleistocene section. However, all of the olive gray and the light olive gray

lutites apparently are restricted to postglacial intervals, and when these colors are present, they identify the sediment as being part of the postglacial section.

On the Alaskan and Tufts Abyssal Plains, Hurley (1960) and Nayudu and Enbysk (1964) found the surface layer of brownish sediment to be strikingly different in biologic content as compared to the underlying sediments. They suggested that the brown material is an important sedimentary unit reflecting recent sedimentation and climatic conditions. However, these authors noted no consistent biologic change associated with the surface brown sediments in Cascadia Basin. Their collective observation is also verified in this study, and the brown lutite capping of variable thickness in the southern Cascadia Basin area (Figure 8) apparently has no consistent association with any time horizon.

Mazama Ash

In addition to counting the relative abundances of planktonic foraminiferans and radiolarians present in the coarse fractions, the general composition of the entire coarse fraction in each sample was noted in a semi-quantitative manner. Unaltered, colorless volcanic ash is also present in sparse to liberal proportions in the upper sections of the postglacial olive gray and light olive gray lutites, and intercalated terrigenous sand-silt layers of Astoria Canyon, Fan

and Channel, Willapa Channel, Cascadia Channel, and Blanco Valley.

When the ash is present in a core, it is only present in the stratigraphic section above a certain horizon. In each core that contains ash, this lowermost horizon is marked in Figure 9 and Plate 1 (designated by "MA"). As a rule, the ash is most abundant near its lowermost stratigraphic limit. Also, the ash content is usually higher in the terrigenous sand-silt layers than in the associated lutite intervals. However, for both sediment types, the abundance of ash decreases proportionately up-section.

Nelson et al. (1968) have studied the ash in the aforementioned cores as well as in additional cores from Astoria Canyon and Astoria Fan. They showed that the deep-sea ash deposits were derived from the continental deposits of the Mt. Mazama eruption (Crater Lake, Oregon) which occurred about 6600 years BP (Rubin and Alexander, 1960; Powers and Wilcox, 1964; Fryxell, 1965). The marine ash has the same indices of refraction (average R.I.=1.505) as the Mt. Mazama ash. Radiocarbon dates in several piston cores indicate that the ash was first introduced into the marine environment sometime between 9600 and 5600 years BP; extrapolations of sedimentation rates suggest that ash deposition began about 6600 years BP or shortly after the eruption of Mt. Mazama. This date is also verified by the stratigraphic position of the lowermost ash horizon in relation to the lutite color break and the faunal transition in the deep-sea

cores; the lowermost Mazama ash layer is located approximately midway between the late Pleistocene-postglacial boundary and the surface.

Royce (1967) has also identified an ash layer in one core from the Willapa Canyon area as being correlative with the Mt. Mazama ash on the continent. He infers that this layer was deposited by air fall. However, Nelson et al. (1968) have shown that the ash, even in the lowermost horizon, was carried to the sea floor by turbidity currents originating from the slumping of debris which accumulated on the continental shelf and slope. A turbidity current origin is evident from the inclusion of displaced shallow water benthic foraminiferans and plant fragments incorporated in the ash-rich sediments. Also, the ash is not found as a blanket deposit over the entire deep-sea area but appears to be prevalent in the environments through which turbidity currents are more apt to flow and eventually deposit sediment. For example, Mazama ash is present in the sediments throughout the entire course of Cascadia Channel, and yet this ash is absent in most of the immediately adjacent environments.

The Mt. Mazama eruption blanketed a very wide area of the northwestern United States with volcanic debris (Fryxell, 1965). No doubt, the land drainage basins were covered or filled with ash, and the rivers began transporting it to the sea almost immediately. The Columbia River is believed to be the largest contributor,

although rivers along the southern coast of Oregon probably contributed some of the volcanic glass to the sediments in Blanco Valley.

The lowermost ash horizon is extremely useful as an approximate time line, especially in those cores that do not penetrate completely through the postglacial section. Provided the ash is not found all the way down to the base of the core, it is assumed that the lowermost ash layer in a core represents deposition very shortly after 6600 years BP. The generalized chronologic sequence of the Mazama ash distribution, the lutite color break, and the planktonic foraminiferan-radiolarian profile are shown in Figure 10.

VI. RATES OF SEDIMENT ACCUMULATION

Knowledge of the variations in sediment accumulation rates both in time and in space is of considerable value in understanding the factors which account for a particular stratigraphic sequence. The depositional rates (cm/1000 years) of the deep-sea sediments off Oregon were extrapolated by using the radiocarbon dates and the established stratigraphic time horizons (Chapter V) and by assuming constant rates of sedimentation for the time intervals concerned.

Extrapolated sedimentation rates, based on the radiocarbon dates, are given in Appendix 4. In each case, an average rate is presented for the core section included between the radiocarbon date and the surface of the core. In those cores having more than one radiocarbon date, rates are calculated for the sections between dated intervals. Where possible, late Pleistocene sedimentation rates are given, which were determined by extrapolating from the older radiocarbon dates up to the younger late Pleistocene-postglacial boundary (12,500 years BP).

Results of the sedimentation rate extrapolations from the lowermost Mazama ash horizon (6600 years BP) and the late Pleistocene-postglacial boundary to the sediment surface are presented in Appendix 5 for all cores. For those cores in which neither of these horizons were penetrated, a minimum rate (>) is given; it is assumed that the

base of the core section represents the lowermost ash horizon (when ash is present in the core) or the late Pleistocene-postglacial boundary, depending upon which is most appropriate for the core in question.

Postglacial Sedimentation

Using the above mentioned sedimentation rate extrapolations, it is possible to present postglacial rates of deposition for most of the deep-sea cores collected (Figure 12). The postglacial sediment accumulation rates range from less than 0.2 cm/1000 years to more than 130 cm/1000 years. This great range in rates of sedimentation is influenced primarily by physiography and, to a lesser degree, by the proximity of the depositional environment to the continent.

The highest rates of deposition are found in Astoria Canyon, Astoria Channel, Willapa Channel, Cascadia Channel, and Blanco Valley, where all rates are in excess of 20 cm/1000 years. Throughout most of the length of Cascadia Channel the sedimentation rates are greater than 50 cm/1000 years. The highest rate found is in the axial depression of Cascadia Channel just beyond Cascadia Gap (Plate 1, core 6609-19), where postglacial sediments have accumulated at a rate of more than 130 cm/1000 years. In contrast, west of this depression the postglacial rate in the Channel is much less, and the highest calculated value is 26 cm/1000 years (core 6509-25A). Rates

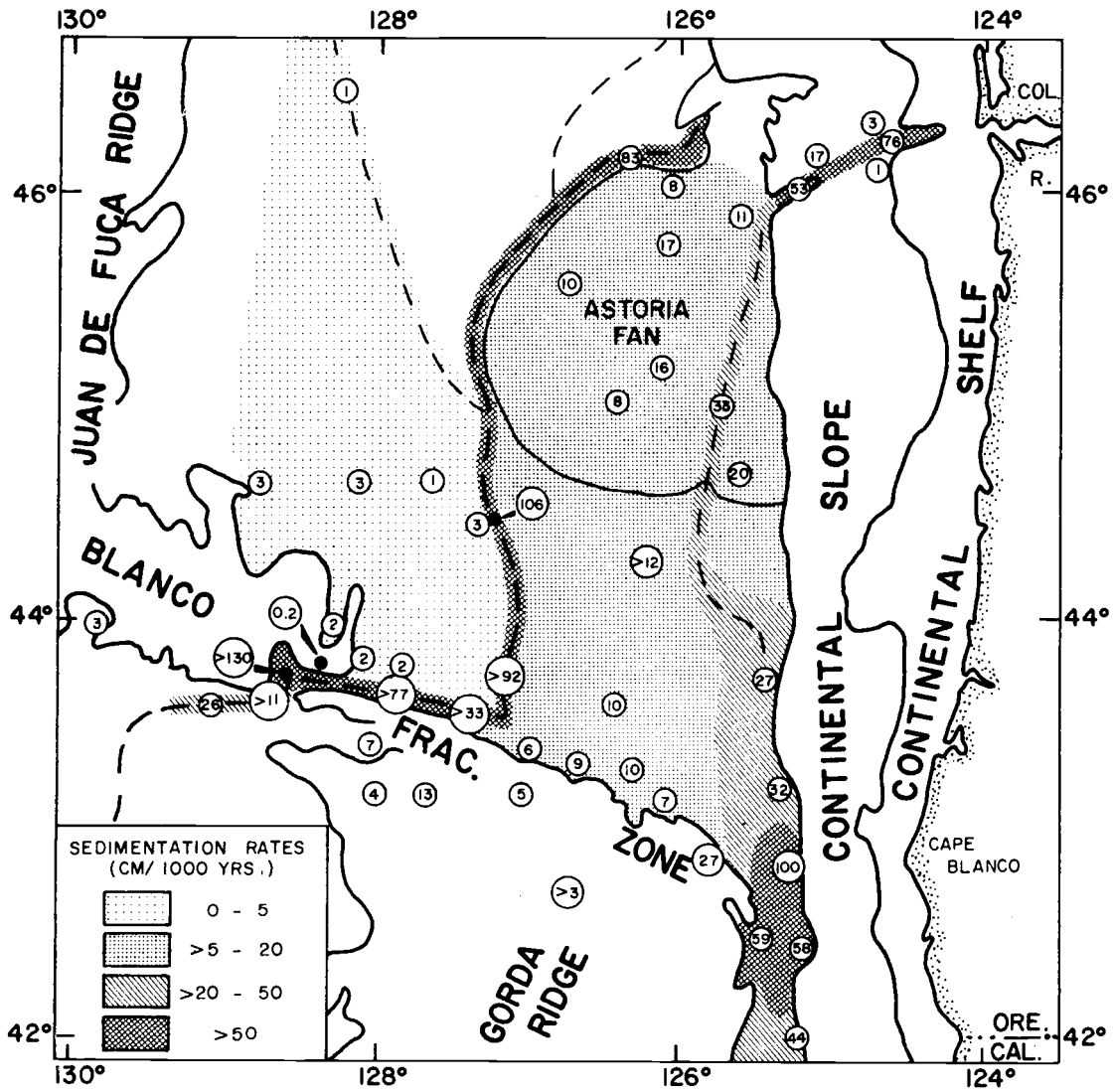

Figure 12. Postglacial rates of sediment accumulation (cm/1000 years) in southern Cascadia Basin and vicinity. Minimum values (>) are indicated for cores which did not penetrate deep enough to reach a known time horizon used for sedimentation rate extrapolations. Data for Astoria Canyon and Astoria Fan from Carlson (1968) and Nelson (1968), respectively.

of over 50 cm/1000 years are also evident on the floors of Astoria Canyon (Carlson, 1968) and Blanco Valley. The highest rate of sedimentation for the walls and the tributary valleys of Astoria Canyon is 17 cm/1000 years (Carlson, 1968).

The rate of postglacial sedimentation for Astoria Fan (Nelson, 1968) and adjoining eastern Cascadia Abyssal Plain varies from 6 to 20 cm/1000 years. This rate is significantly higher than the 1 to 3 cm/1000 years accumulation rate for Vancouver Valley and western Cascadia Abyssal Plain, and it demonstrates that there is an offshore decrease in the rate of deposition.

Sediment accumulation rates in the troughs of the Blanco Fracture Zone are generally low (4 to 13 cm/1000 years), but not as low as those in Vancouver Valley and on western Cascadia Abyssal Plain, even though all of these environments are approximately equivalent distances from the continent. The higher sedimentation rates in the troughs may be due to the added influx of sediments which initially settled out of suspension over adjacent high areas and have since moved slowly down-slope and eventually come to rest on the bottom of the troughs. One high area just north of Cascadia Gap (core 6609-20) yields a correspondingly low postglacial rate of accumulation (0.2 cm/1000 years).

Late Pleistocene versus Postglacial Sedimentation

Low rates of sediment accumulation are frequently related to the non-tectonic phases in an orogenic cycle; a continued supply of sediment to a depositional basin ultimately requires continued uplift of the adjacent land. However, changes in certain factors controlled by a shift from glacial to non-glacial climatic conditions can produce the same results. Broecker, Turekian and Heezen (1958) have demonstrated that there is a correlation between sedimentation rate and extent of continental glaciation in the mid-equatorial Atlantic. They found that the accumulation of sediment decreased abruptly from a much higher glacial rate prior to 11,000 years BP.

To determine if there is a correlation between climatic change and the rate of deep-sea sediment accumulation off Oregon, the writer has compared rates above and below the late Pleistocene-postglacial boundary with one another (Table 2). For the eight cores where estimates for both time intervals are possible, the average rate of late Pleistocene sedimentation is 44 cm/1000 years, while the post-glacial average rate is only 7 cm/1000 years. Because these cores are not representative of all the different depositional environments studied, the average rates are not necessarily indicative of the over-all absolute sedimentation rates for the two time intervals. However, the ratio of these two averages does give some idea of the order

Table 2. Comparison of late Pleistocene and postglacial rates of sedimentation for selected cores. Indicated rates are averages which were determined by extrapolation from radiocarbon age dated intervals as well as from the position of the late Pleistocene-postglacial boundary set at 12,500 years BP.

CORE NUMBER	PHYSIOGRAPHIC ENVIRONMENT	RATE OF SEDIMENTATION (CM/1000 YEARS) POSTGLACIAL	RATE OF SEDIMENTATION (CM/1000 YEARS) LATE PLEISTOCENE
6508-PC18	Tributary valley of Astoria Canyon	13	10
6609-5	Eastern Cascadia Abyssal Plain	11	43
6609-7	Eastern Cascadia Abyssal Plain	9	32
6609-14A	Western Cascadia Abyssal Plain	2	35
6509-20A	Western Cascadia Abyssal Plain	3	121
6609-20	Hill north of Cascadia Gap	0.2	49
6609-13	Blanco Fracture Zone trough	13	29
6509-21A	Tufts Abyssal Plain	3	31

of magnitude of the decrease in sedimentation associated with the shift toward present-day climatic conditions. During the late Pleistocene, sediments appear to have accumulated more than six times as fast as during the postglacial interval. This factor is considerably higher than the factor of 2.4 reported by Broecker, Turekian and Heezen (1958) for the mid-equatorial Atlantic.

Deposition of Terrigenous Sand-Silt Layers

The terrigenous sand-silt layers present in most of the marine sediments cored off Oregon (Plate 1) were deposited mainly by turbidity currents (Chapter IV). The accessibility of turbidity currents to a particular area is reflected in the relative frequency and thickness of these layers.

In the postglacial core sections, from 0 to 89 percent of the sediments (total thickness) are terrigenous sand-silt layers of varying thickness, and these layers make up from 0 to 93 percent of the late Pleistocene sections (Appendix 6). However, a definite temporal relationship is evident when only those cores are considered in which both postglacial and late Pleistocene intervals are represented. The late Pleistocene sections in such cores generally have a higher percentage of terrigenous sand-silt layers than do their postglacial counterparts (Figure 13). On the average, only nine percent of the postglacial stratigraphic section consists of terrigenous sand-silt

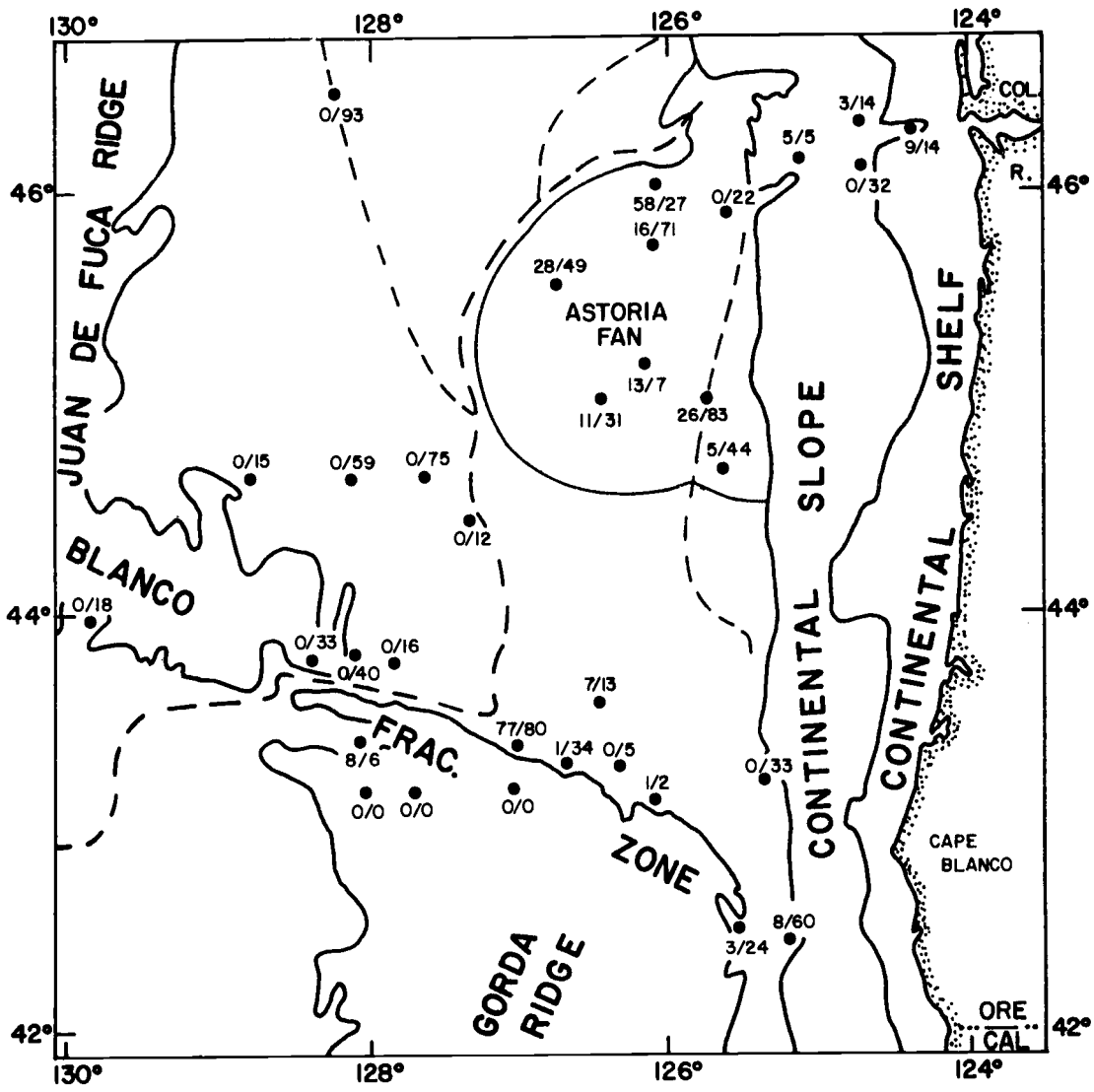

Figure 13. Areal distribution of terrigenous sand-silt layers in late Pleistocene (lower numbers) and postglacial (upper numbers) stratigraphic sections of selected cores in southern Cascadia Basin and vicinity. The numbers are the percents of the total thicknesses of the late Pleistocene and the postglacial core sections which are terrigenous sand-silt layers.

layers, while 32 percent of the late Pleistocene section consists of these layers.

A very striking temporal change in sediment texture is evident in the Vancouver Valley-western Cascadia Abyssal Plain area (Figure 13). Terrigenous sand-silt layers are absent in the postglacial section of this area, while the late Pleistocene section is composed of 12 to 93 percent terrigenous sand-silt layers.

It is evident that, not only was the overall late Pleistocene sedimentation rate higher in the southern Cascadia Basin area but also, there were more and thicker terrigenous sand-silt layers deposited during the earlier interval compared to postglacial time. Since turbidity currents most likely transported the coarser material to the deep-sea environments, it appears that these currents were more active during the late Pleistocene than they are today.

The absence of turbidity current flows in many parts of the world during postglacial time, on the one hand, and the numerous flows during glacial stages, on the other, was previously pointed out by Heezen and Hollister (1964). They suggested that these relationships are due partially to the supply of sediment and partially to the relative stand of sea level. Greater erosion due to intensified glaciation and higher stream gradients (lower sea level) probably supplied more sediment to the marine environment. Even more important, larger volumes of sediment reached the edge of the

continental shelf, because the lower stand of sea level brought the shoreline closer to the shelf edge. In contrast, with the present high stand of sea level, many rivers throughout the world, which formerly must have contributed sediment for the generation of turbidity currents, are now isolated from the deep water by estuaries and broad continental shelf areas. Thus, more sediments (especially the coarser components) presumably are being retained in the shallow water areas.

Primary Productivity of Calcium Carbonate

Calcium carbonate, in the form of tests of marine organisms, often makes up a considerable portion of marine sediments. The lutites in the abyssal environments off Oregon contain from less than 1 to as much as 42 percent calcium carbonate (Appendix 7); most of the calcium carbonate was produced by planktonic foraminiferans.

In order to account for the variation in calcium carbonate content, we must consider the following factors: 1) the higher rate of dissolution of calcium carbonate in deeper depositional environments as compared to shallower ones (Berger, 1967); 2) temporal and areal variations in rates of deposition of non-carbonate sediments; and 3) temporal and areal changes in the primary production of organisms producing calcium carbonate tests. The relative

significance of each of these factors was examined for the lutites from core sections in which both the calcium carbonate content and the rate of sedimentation (postglacial or late Pleistocene) were known. In Table 3 and in Figure 14, the sedimentation rate and the calcium carbonate content of the sediments are compared with the water depths in which they were deposited.[1]

In order to determine the relative importance of the factors influencing the concentration of calcium carbonate in the deep-sea sediments, let us first assume that 1) the contribution of calcium carbonate (by primary organic production) to the various sedimentary environments has been constant with time, and 2) the differences in calcium carbonate content are inversely proportional to both the rate of non-carbonate sedimentation and the solution rate of calcium carbonate. If these assumptions are correct, the variations in the calcium carbonate content of the sediments taken from the same water depths should be compensated for when the calcium carbonate

---

[1] Since only the lutites are considered here, the sedimentation rates, given in Table 3 and used in Figure 14, are estimates for the average depositional rates of the lutites only. These rates were calculated by assuming that the intercalated terrigenous sand-silt layers were deposited instantaneously as well as discontinuously, while the finer grained sediments were deposited continuously. (Gorsline and Emery, 1959). The lutites account for most of the time that elapsed between dated horizons in the core intervals for which sedimentation rates were extrapolated.

Table 3. Comparison of sedimentation rate, calcium carbonate content, and water depth for deep-sea sediments of late Pleistocene and postglacial intervals.

CORE NUMBER	AGE OF SAMPLE INTERVAL	WATER DEPTH (FATHOMS)	RATE OF SEDIMENTATION * (CM/1000 YRS.)	% $CaCO_3$ **	% $CaCO_3$ X SED. RATE
6508-PC18	Postglacial	845	20	0.6	12
6509-20A	Late Pleistocene	1528	164	7.3	1200
6509-25A	Postglacial	1823	25	0.7	17
6509-27	Postglacial	1696	82	0.5	41
6604-3	Postglacial	1741	6	0.0	0
6604-11	Postglacial	1646	32	0.1	3
6609-1	Postglacial	1656	46	0.6	28
6609-2	Postglacial	1646	56	0.5	28
6609-4	Postglacial	1590	7	0.0	0
6609-5	Postglacial	1602	10	0.4	4
6609-5	Late Pleistocene	1602	33	3.0	99
6609-7	Postglacial	1566	9	0.4	4
6609-8	Postglacial	2343	5	0.4	2
6609-13	Postglacial	2196	13	2.1	26
6609-13	Late Pleistocene	2196	29	14.1	409
6609-14A	Postglacial	1610	2	1.3	3
6609-14A	Late Pleistocene	1610	40	5.2	208
6609-16	Postglacial	1515	2	3.5	7
6609-20	Postglacial	1420	0.2	31.7	6
6609-20	Late Pleistocene	1420	49	28.4	1392
6609-20	Late Pleistocene	1420	20	41.8	826

*Refers to accumulation rate of lutites only.

**Average calcium carbonate values for lutite samples from the stratigraphic sections for which sedimentation rate extrapolations were determined.

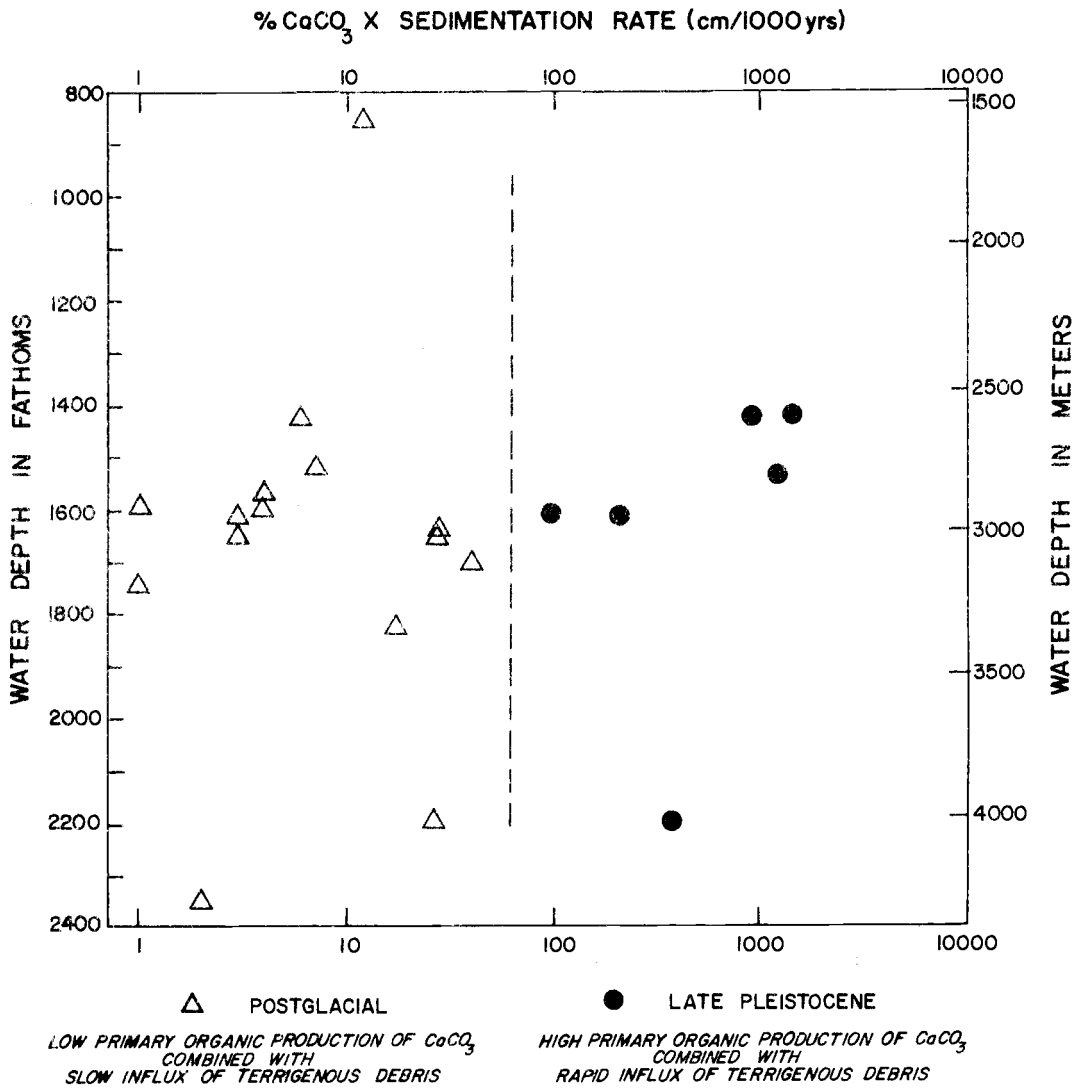

Figure 14. Plot of water depth versus percent calcium carbonate times sedimentation rate of late Pleistocene and postglacial lutites in selected deep-sea cores off Oregon. Refer to Table 3 for additional details.

concentration is multiplied by the sedimentation rate (cm/1000 years). For example, the resulting product for a sediment having a high calcium carbonate content because of a slow, non-carbonate sedimentation rate, should be equivalent to a sediment having a low calcium carbonate content because of a rapid, non-carbonate influx. For sediments from different water depths, the product values should not be equivalent to each other but should decrease with increase in water depth (dissolution of calcium carbonate increases with depth).

In Figure 14 and in Table 3, it is clear that the concentration of calcium carbonate is not noticeably inversely proportional to either the rate of non-carbonate sedimentation or the water depth. The highest product values occur in the late Pleistocene sediments, thus indicating that both carbonate and non-carbonate sediments were deposited at a higher rate during the late Pleistocene than during the postglacial time. One of the prime factors accounting for the variations in calcium carbonate content in the lutites off Oregon must therefore be a change in the rate of primary production of calcium carbonate-producing organisms accompanying the shift from glacial to non-glacial climatic conditions.

The higher calcium carbonate concentrations in the late Pleistocene sediments and the relatively lower concentrations of the same in the postglacial sediments have previously been noted in both the mid-equatorial Atlantic Ocean (Broecker, Turekian and

Heezen, 1958) and the Indian Ocean (Olausson, 1960). Arrhenius (1952, 1963) did not study the postglacial sediments in the eastern equatorial Pacific Ocean, but he did find that the calcium carbonate content (planktonic foraminiferans and coccoliths) was higher in sediments of the Pleistocene glacial stages (Wisconsin, Illinoian, etc.) and lower in those of the interglacial stages (Sangamon, Yarmouth, etc.) in this area. Divergence of the trade-wind drift currents produces upwelling of the nutrient-rich intermediate water along the equator. Hence, Arrhenius attributed the higher calcium carbonate content to more active water circulation brought about by increased trade-wind intensity during the glacial stages; the increased oceanic circulation brought more nutrients to the surface which supported the production of more planktonic organisms which, in turn, resulted in more calcium carbonate in the sediments.

Conflicting results have been obtained from calcium carbonate analyses run on North Atlantic Ocean cores (Olausson, 1965). A few of the cores show trends similar to those noted above (i.e., the calcium carbonate content is higher in the late Pleistocene sediments than in the postglacial sediments). However, the majority of the cores from the North Atlantic have lower calcium carbonate concentrations in their late Pleistocene sections than in their postglacial sections. Since the influx of non-carbonate sediments and the production of calcium carbonate by marine organisms are

independently controlled, their relative contributions can vary independently of each other both in time and in space. It is quite possible that a higher late Pleistocene influx of the non-carbonate debris in many parts of the North Atlantic actually masks the increase in calcium carbonate.

In the abyssal sediments off Oregon, the tests of planktonic foraminiferans account for most of the calcium carbonate content. Hence, as suggested by Nayudu (1964a), it is evident that the production of planktonic foraminiferans was much greater during the late Pleistocene than at present. Although little is known about the production rate of the radiolarians, the previously discussed variations in abundance of radiolarians compared to planktonic foraminiferans (Chapter V) may thus be due primarily to changes in the production rate of the latter while the former remained nearly constant.

VII. MINERALOGY OF SAND-SIZE SEDIMENTS

Where possible, layers containing an abundance of sand-size grains were selected from both late Pleistocene and postglacial stratigraphic sections of the various deep-sea environments under study to determine the mineralogical variations in both light and heavy components. The selected samples also were analyzed for grain size composition and are classified as terrigenous sand-silt layers, basaltic glass lutites, and basaltic sand layers (Chapter V). Prime emphasis in this mineralogical study is placed on identifying sediment source areas and tracing the systems of dispersal for the coarser grained, bottom-transported sediments in the deep-sea area off Oregon.

Light Mineral Fraction

The overall textural properties and the light fraction composition of sand-size components form the bases for various classifications of sandy sediments and concepts associated with tectonic and source area control of sedimentation. Van Andel (1960, 1964) and Folk (1956) have argued that textural characteristics are almost entirely controlled by the depositional environment and are virtually independent of sediment source and basin tectonics, whereas, light mineral associations reflect source area composition and tectonic

stability or instability. With this concept in mind, we will ignore the overall textural composition and only consider the sand-size light fractions of sediments that display a considerable range in sorting and, in many cases, are composed predominantly of constituents finer than 62 microns.

Components present in the light mineral fraction of the deep-sea sediments off Oregon include quartz, potash feldspar, plagioclase feldspar, rock fragments, mica, colorless volcanic glass, and dark brown volcanic glass (Appendix 8). In order to determine the relative abundances of stable and unstable grains, which reflect source area composition and tectonic stability or instability, the author used a classification scheme that was adapted from Williams, Turner and Gilbert (1958, pp. 289-297). This system is based on three end-member groups, quartz + chert + quartzite (stable), feldspars (unstable), and rock fragments + volcanic glass (unstable).

According to the above classification, the light mineral fractions of the deep-sea sediments off Oregon are characterized as lithic, arkosic, or volcanic sands (Figure 15). The abundance of unstable grains demonstrates the tectonic instability of the various source areas.

The sand-size sediments from the Blanco Fracture Zone-Gorda Ridge transition area (Plate 1, cores 6601-1, 6609-6, -8) are almost entirely composed of unstable grains which are generally

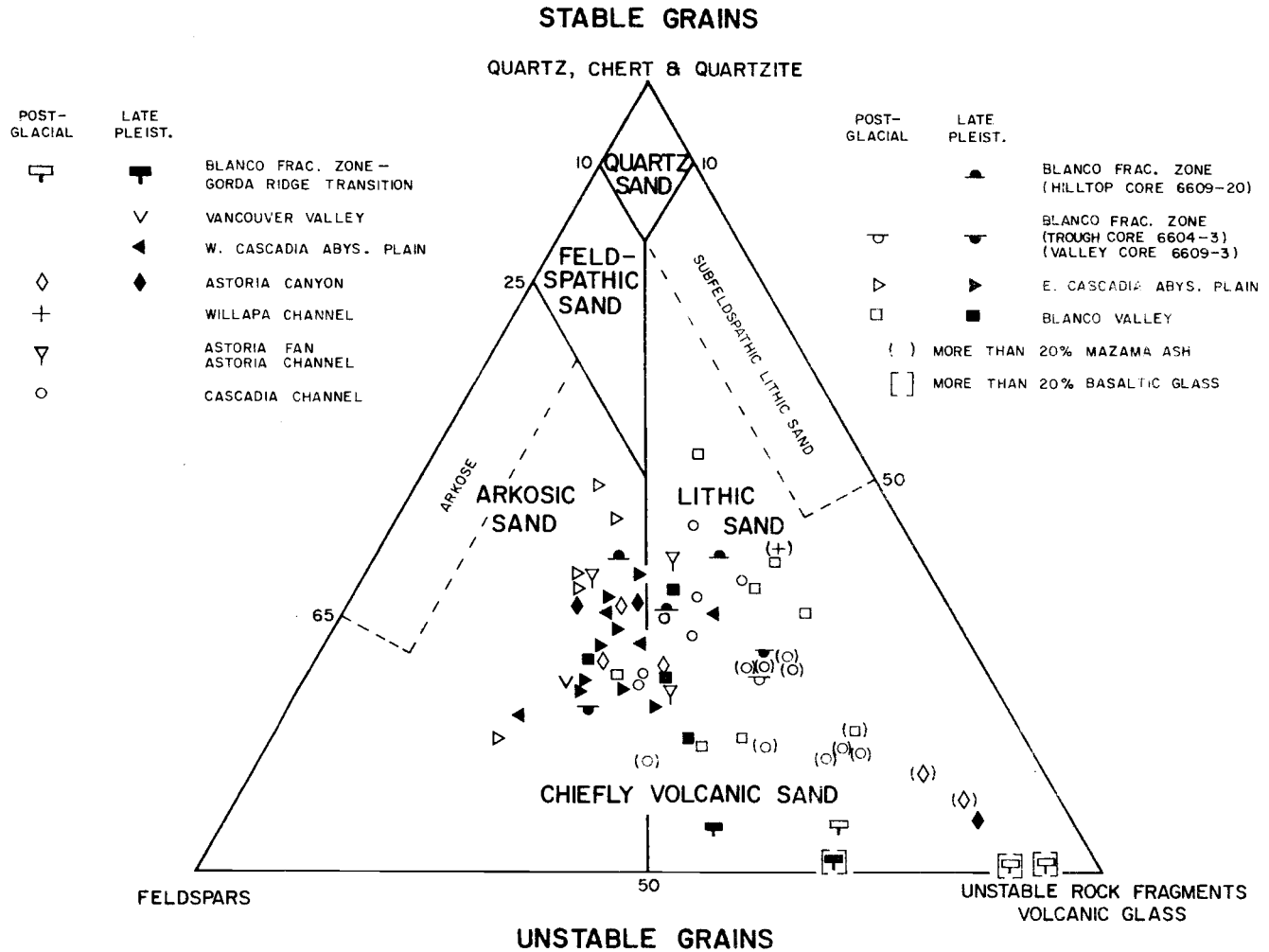

Figure 15. Triangular diagram of the light mineral compositions of the total sand fraction of sediments in various deep-sea environments off Oregon and petrographic classification of sand types (after Williams, Turner, and Gilbert, 1958). Values for Astoria Canyon from Carlson (1968).

angular. An abundance of basaltic glass (dark brown) is present in the transition area; this glass is absent in the adjacent areas. The characteristics and the restricted distribution of the sand-size sediments in the transition area, combined with the presence of topographic barriers which make the area inaccessible to turbidity current flows, suggest that the sand-size grains are the by-products of local submarine volcanic activity.

Very high percentages of unstable grains are also noted in other depositional environments (Figure 15; Cascadia Channel, Blanco Valley, and Astoria Canyon); in these environments colorless volcanic glass generally is a considerable portion of the unstable grains. The index of refraction of the glass (average R.I.=1.505) indicates that it is from the Mt. Mazama eruption (6600 years BP). The stratigraphic positions of the glass-rich sediments indicate that the sediments were deposited after the eruption of Mt. Mazama (see Chapter V).

Potash/plagioclase feldspar ratios indicate that debris from extrusive and intrusive basic igneous rocks is being deposited in the deep-sea environments in large volumes compared to debris from other rock types (Table 4). Plagioclase feldspar is far more abundant than potash feldspar in the deep-sea sediments; on the average the ratio of potash feldspar to plagioclase feldspar is 0.3. In the sediments from the Blanco Fracture Zone-Gorda Ridge transition

Table 4. Ratio of potash feldspar to plagioclase feldspar in sediments from the deep-sea environments. Data for Astoria Canyon from Carlson (1968).

Physiographic environment	Potash feldspar / Plagioclase feldspar Mean	(Range)	Number of samples
Astoria Canyon	0.5	(0.3-0.7)	8
Astoria Fan and Channel	0.6	(0.5-0.6)	3
Willapa Channel	0.4	-------	1
Vancouver Valley	0.5	-------	1
Cascadia Channel	0.3	(0.1-0.6)	16
Eastern Cascadia Abyssal Plain	0.4	(0.2-0.7)	14
Western Cascadia Abyssal Plain	0.4	(0.3-0.5)	4
Blanco Valley	0.3	(0.1-1.1)	12
Blanco Fracture Zone (trough core 6604-3, valley core 6609-3)	0.3	(0.1-0.5)	3
Blanco Fracture Zone (hilltop core 6609-20)	0.3	(0.1-0.5)	3
Blanco Fracture Zone--Gorda Ridge transition area	0.0	(0.0-0.1)	7

area, potash feldspar is almost nonexistent.

Heavy Mineral Fraction

Heavy minerals comprise 0 to 18 percent and average five percent by weight of the entire sand fraction in the deep-sea sediments (Appendix 9). In most of these sediments practically all of the heavy minerals are in the 62- to 125-micron size fraction. However, a few of the sediments contain coarser heavy grains. Because variations in the grain size and sorting of the sediments may obscure similarities between heavy mineral suites originally derived from the same source (van Andel, 1964, p. 228; Wilde, 1965), only those heavy mineral grains within the 62- to 125-micron size fraction are included in the counts (Appendix 9).

In the 62- to 125-micron fraction of the deep-sea sediments, 42 heavy mineral species and varieties are present, but less than one-half of these occur frequently; the remainder exist only in minor quantities or as trace minerals. The mica content, ranging from 0 to 87 percent (by count), shows a great variation in relation to the total heavy mineral assemblage but is generally far more abundant where the total sand content is low. Biotite is more plentiful than muscovite, although the ratio of biotite to muscovite varies irregularly. Chlorite constitutes a very small percentage of the micaceous minerals. Alteration of some of the more unstable ferromagnesian

mineral grains is common and presents a problem in identification; weathered grains may account for 1 to 63 percent of the assemblage. Opaque grains, mainly magnetite and ilmenite, make up 0 to 12 percent of the heavy mineral fraction.

Non-opaque, non-micaceous heavy minerals, excluding unidentifiable altered ferromagnesian minerals, constitute 13 to 89 percent of the heavy fraction. Quantitatively important mineral groups, species, and varieties are actinolite-tremolite; clinopyroxene, predominantly augite but also including traces of titanaugite and tentatively identified diopside; epidote group, including clinozoisite-zoisite and epidote; garnet, colorless to pink types; hornblende, including common, blue-green, and brown varieties; hypersthene, commonly with magnetic inclusions and glassy rims; and olivine. Other minerals that occur in trace amounts are aegirineaugite, andalusite, apatite, basaltic hornblende, chloritoid, corundum, dumortierite, enstatite, glaucophane, kyanite, monazite, rutile, serpentine, sillimanite, sphene, spodumene, tourmaline (brown), and zircon.

Some of the sediments examined are so fine-grained that the heavy minerals in their sand fractions do not exist over the full range of the 62- to 125-micron size class selected for this study. High concentrations of mica in the heavy mineral assemblages of these fine-grained samples demonstrate the effect of selective sorting.

To minimize this effect, samples with less than 1 or 2 percent sand and containing 25 percent or more mica in their heavy fractions are excluded from subsequent discussions pertaining to regional heavy mineral trends.

In order to determine more completely the sources of the sediments and trace the routes of sediment dispersal in the deep-sea environments, the author included available heavy mineral data from the Oregon continental shelf (Bushnell, 1964; Runge, 1966; Chambers, 1967) and coastal rivers of Oregon and northern California (Kulm, 1968) in the present study. In addition, the heavy mineral fractions (62-125 microns) of four Columbia River sediment samples (Appendix 10; CR-1, -2, -3, -4) were analyzed by the writer. These four samples were collected at points 5, 9, 15, and 25 miles (9, 17, 27, and 46 km) upstream from the river mouth in the main channel.

Kulm (1968) originally counted three heavy mineral size intervals (62-125, 125-250, and 250-500 microns) for all fluvial samples taken near the mouths (but upstream of tidal influence) of 25 major coastal rivers and streams south of the Columbia River to, and including, the Klamath River in northern California. To facilitate comparisons with the deep-sea data, the author has considered herein only the results from the 62- to 125-micron fractions of the river sediments.

In the Oregon continental shelf studies by Runge (1966), Bushnell (1964), and Chambers (1967), all heavy minerals greater than 62 microns were identified without further size-interval differentiation. To compensate for this lack of size distinction, the writer considered only the results from sediment samples with mean diameters less than 125 microns; because heavy mineral grains are hydraulically equivalent to larger size light mineral grains (Rittenhouse, 1943), it is assumed that at least most of the heavy minerals in these selected samples will be less than 125 microns and thus fall within the specified 62- to 125-micron interval.

In general, all the heavy mineral species and varieties present in the deep-sea environments off Oregon are also present in the continental shelf and coastal river sediments. Various ratios of different heavy minerals were examined for possible systematic areal or temporal patterns. The ratio of clinopyroxene to hornblende (hereafter referred to as "CP/H ratio") was the most successful in revealing systematic trends for both marine and fluvial sediments. The relative abundance of clinopyroxene and hornblende is a very consistent indicator of the source area contributing sediment to the deep-sea environments. The minerals included in the CP/H ratio constitute the majority of the non-opaque and non-micaceous constituents and therefore adequately represent the entire heavy mineral suite. Although glaucophane occurs in trace quantities, the

presence or absence of this metamorphic mineral is also helpful in identifying source areas.

Continental Source Areas

On the bases of the natural boundaries of the continental watershed basins (outlined by Hagenstein et al., 1966) and the CP/H ratio and the glaucophane content of the river sediments, four continental source areas producing dissimilar sediments are evident (Figure 16; Table 5). These source areas are 1) the Klamath and South Coast Basins, 2) the Umpqua and Mid-Coast Basins, 3) the North Coast Basin, and 4) all basins ultimately drained by the Columbia River.

Assuming a direct correlation between runoff and sediment load, the annual rates of freshwater discharge shown for the four source areas (Figure 16) serve as rough approximations of the relative amounts of sediment transported to the sea from the various drainage basins. The mean CP/H ratio and the glaucophane content indicated for each continental source area (Table 5) are weighted averages of the mineral values for all the rivers sampled within a particular basin. These weighted averages are obtained by dividing the sum of the various river mineral values multiplied by their respective weights (river runoff) by the sum of the weights (total runoff of all rivers in a particular basin). Data for the river

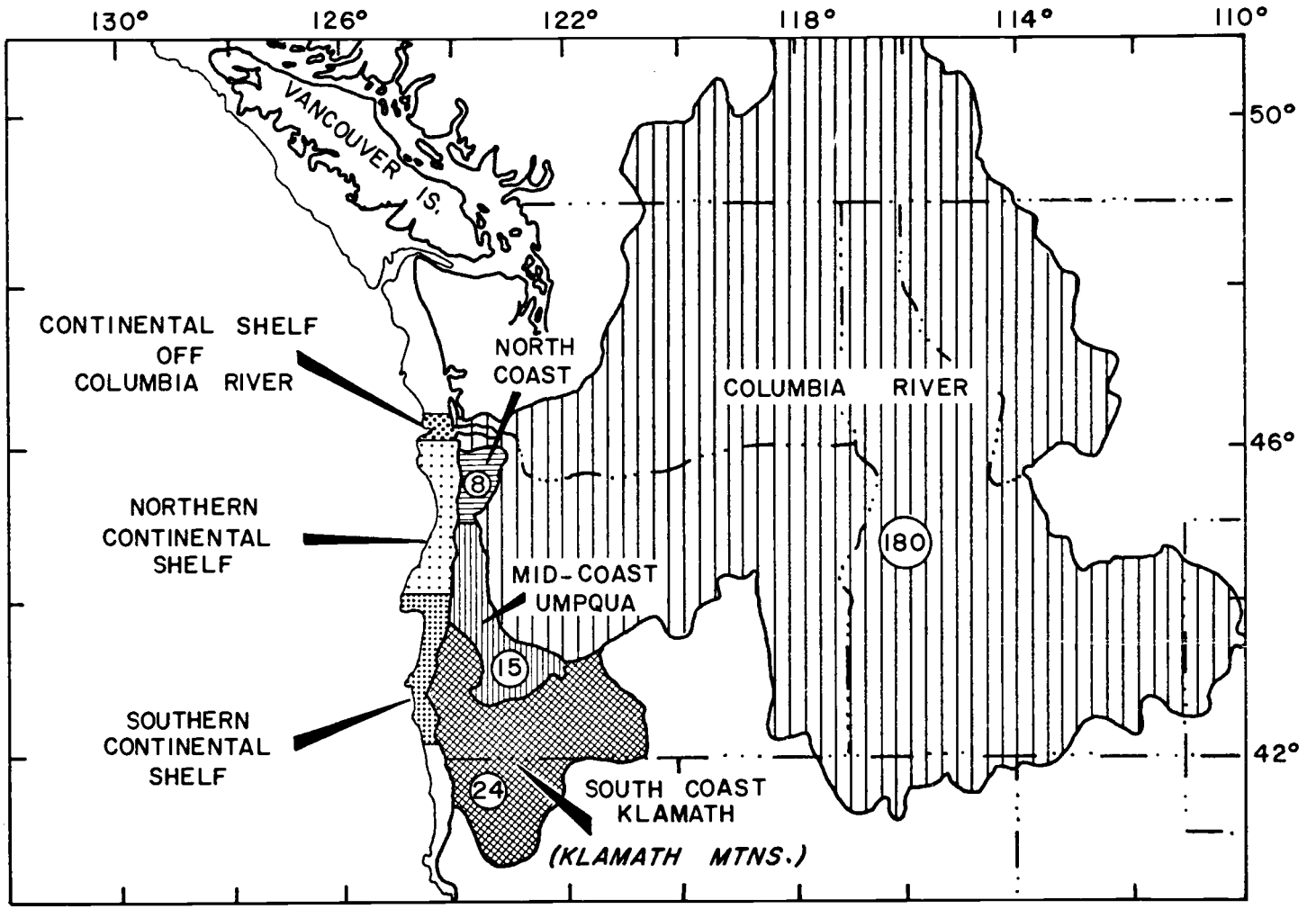

Figure 16. Northwestern United States continental drainage basins and continental shelf areas off Oregon characterized by certain heavy mineral compositions (given in Table 5). Average annual runoff (circled numbers) in millions of acre feet is given for each land drainage system.

Table 5. Significant heavy mineral characteristics for sediments of the continental shelf off Oregon and the adjacent continental drainage basins. Refer to Figure 16 for geographic locations. Data for river samples, except for Columbia River, from Kulm (1968). Continental shelf heavy mineral data from Bushnell (1964), Runge (1966) and Chambers (1967). Certain mineral values (*) for the continental basins are weighted averages of the mineral values for all the rivers included within a particular basin.

ENVIRONMENT	CLINOPYROXENE/HORNBLENDE RATIO		NUMBER OF SAMPLES	% SAMPLES CONTAINING GLAUCOPHANE
	MEAN	RANGE		
CONTINENTAL DRAINAGE BASINS				
COLUMBIA RIVER	1.25	(1.16-1.38)	4	0
NORTH COAST	56.80*	(10.60-112.00)	7	0
MID-COAST, UMPQUA	6.39*	(0.93-31.20)	5	0
SOUTH COAST, KLAMATH	0.53*	(0.14-4.85)	10	78*
CONTINENTAL SHELF AREAS				
OFF COLUMBIA RIVER	1.03	(0.75-1.40)	3	0
NORTHERN	1.10	(0.38-3.40)	12	42
SOUTHERN	0.36	(0.19-0.65)	29	86

and basin runoff rates were obtained from Lockett (1965), Hagenstein et al. (1966), and the U. S. Geological Survey surface water records for California (1964) and for Oregon (1966).

South Coast and Klamath Basins. The principal watershed basins draining most of the Klamath Mountains of southwestern Oregon and northwestern California are the South Coast and the Klamath Basins. Rising more than 9000 feet (2750 m), the Klamath Mountains expose Paleozoic and Mesozoic metasedimentary, metavolcanic, and sedimentary rocks that have been intruded by granitoid and ultrabasic rocks (Baldwin, 1964). The main streams draining most of this mountainous area are the Rogue and the Klamath Rivers, both of which have their head waters in the Pliocene to Recent lava flows of the High Cascades to the east. Along the coast, the Smith, Chetco, Pistol, Elk, Sixes, Coquille, Coos, and Millicoma Rivers drain the western slopes of the Klamath Mountains and the Miocene-Pliocene and Quaternary marine formations of the southern tip of the low (1500 feet, 460 m) Oregon Coast Range. The combined sediment from all the above named rivers strongly reflects the influence of the metamorphic terrane of the Klamath Mountains which is characterized by a heavy mineral assemblage commonly containing glaucophane and possessing a low CP/H ratio (mean 0.5).

Umpqua and Mid-Coast Basins. The river sediments indicate that these two basins are devoid of glaucophane and have a combined

mean CP/H ratio of 6.4. The watershed basin of the Umpqua River extends into the northern tip of the Klamath Mountains and part of the Cascade Mountains to the east but is mainly confined to the southern Oregon Coast Range. Most of the southern Coast Range is composed of volcanic (basalt) and sedimentary rocks of the Eocene Umpqua Formation (Baldwin, 1964). This formation is generally equivalent to the Siletz River Volcanics farther north but contains a larger percentage of sedimentary rock. The Siuslaw, Alsea, Yaquina, and Siletz Rivers of the Mid-Coast Basin drain the central Oregon Coast Range. Along the crestline of the Coast Range, these rivers cut through the massive arkosic and micaceous sandstones and sandy siltstones of the Tyee Formation (Middle Eocene) that are intruded by numerous dikes and sills (mainly granophyric gabbro) (Baldwin, 1964). On the seaward side of the crestline, the rivers are mainly eroding Oligocene-Miocene marine sandstones and mudstones.

North Coast Basin. The rivers sampled in the North Coast Basin are the Nestucca, Tillamook, Trask, Wilson, Miami, Nehalem, and Necanicum. They drain the northern Coast Range which has a central core consisting of thick submarine volcanic flows, breccias, and tuffaceous sedimentary rocks of the Early Eocene Siletz River Volcanics (Baldwin, 1964). These volcanics and the widespread exposures of Late Eocene and Oligocene tuffaceous sedimentary rocks (Allen and Van Atta, 1964) produce the glaucophane-free,

extremely high CP/H ratio (mean 56.8) sediment present in the North Coast Basin rivers.

Columbia River Basins. Sharply contrasting to the North Coast Basin, the sediments of the Columbia River Basins contain roughly equivalent amounts of clinopyroxene and hornblende (mean CP/H ratio 1.25). As also noted by Glenn (1967), glaucophane is absent in Columbia River sediments. When compared to the discharge of the other drainage areas discussed, it is obvious that the load of this river and its tributaries should dominate the terrigenous sediments of the adjoining marine environments. The Columbia watershed spans several physiographic and geologic provinces (Fenneman, 1931). Most of the Tertiary hypersthene-augite andesites and Pliocene to Recent basalts of the Cascade Mountains and the vast Miocene tholeiitic basalt flows of the Columbia Plateau region are included in the drainage system (Waters, 1955). In Washington, Columbia River tributaries drain the metamorphosed sedimentary rocks and granitic batholiths of the northern Cascades. The western slope of the Rocky Mountains (Idaho, Montana, Washington, southern British Columbia, and part of Wyoming) drains into the Pacific Ocean via the Columbia River and its largest tributary, the Snake River. These mountains consist of a group of distinct high ranges of differing rock types. Sedimentary rocks from Precambrian to Cenozoic in age, in places metamorphosed, crop out over large areas. Large

Mesozoic batholiths, of which the Idaho Batholith is a well-known example, intrude the sediments in the western part of the range.

Continental Shelf Heavy Mineral Distribution

The continental shelf off Oregon can be divided into three sediment zones based on CP/H ratios and glaucophane content (Figure 16; Table 5). These zones are 1) the southern shelf area, from Heceta Head (44°08'N) south to at least Cape Sebastian (42°19'N; 2) the northern shelf area, from Heceta Head north to Tillamook Head (45°58'N); and 3) the shelf area adjacent to the Columbia River mouth.

The low CP/H-ratio values (mean 0.4), plus the usual presence of glaucophane, indicate that the Klamath Mountains (Klamath and South Coast Basins) are the source of sediments for the southern continental shelf. The presence of sediments from the Klamath Mountains is still evident on the northern continental shelf where glaucophane is found in most of the sediments. The CP/H ratio for the northern shelf (mean 1.1) is certainly lower than that of the adjoining Oregon Coast Range (Umpqua and Mid-Coast Basins mean = 6.4; North Coast Basin mean = 56.8) which suggests that comparatively little sediment is added to the shelf from this region. As expected, continental shelf sediments off the Columbia River mouth do not contain glaucophane and have a CP/H ratio (mean 1.0) closely

resembling that of the Columbia River sediments (mean 1.25). The freshwater discharge and the sediment load of the Columbia River is nearly four times that of the combined Oregon coastal drainages to the south (Figure 16), and its load should dominate the sedimentation on the adjacent shelf area and mask all other sources. However, since many of the continental shelf samples south of the Columbia River contain glaucophane, presumably derived from the Klamath Mountains, it appears that the net longshore transport on the shelf is to the north. This net northward transport is verified by textural studies of northern Oregon and Washington continental shelf sediments (Gross, McManus, and Hsin-yi Ling, 1967) and by investigations of the radionuclides included in sediments from the Columbia River (Gross, 1966; Gross and Nelson, 1966).

Heavy Mineral Dispersal Patterns for Deep-Sea Environments

Heavy mineral assemblages from the various deep-sea environments can be divided into four groups on the bases of CP/H ratio and glaucophane content (Figure 17). Considering both areal and temporal systematic variations in these assemblages, four heavy mineral provinces are evident. These provinces are 1) Province A, generally confined to the Blanco Fracture Zone-Gorda Ridge transition area; 2) Province B, restricted to late Pleistocene sediments in

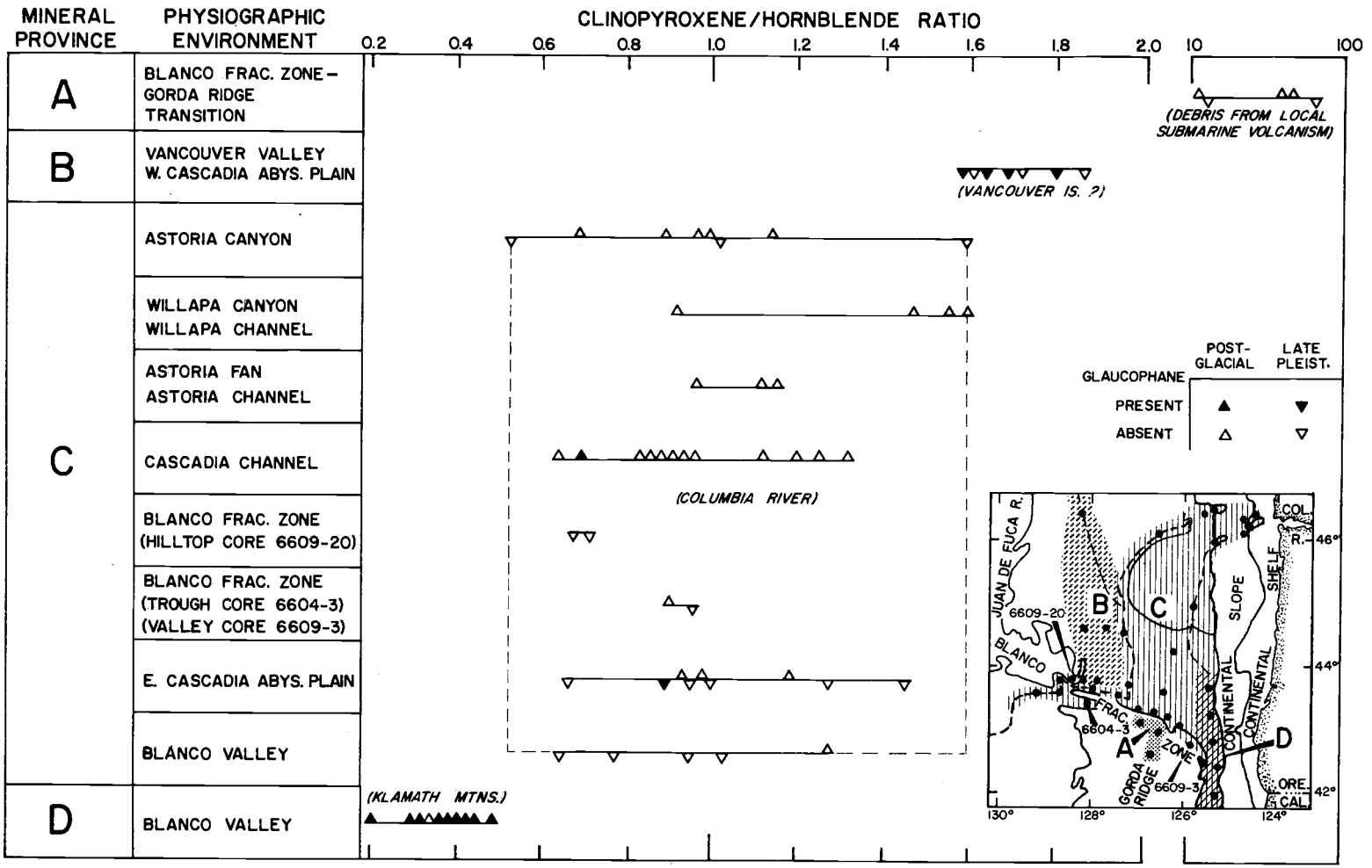

Figure 17. Clinopyroxene/hornblende ratio and glaucophane content of the heavy mineral sand fraction (62-125 microns) of sediments in various deep-sea environments, and geographic distribution of the deep-sea heavy mineral provinces in southern Cascadia Basin and vicinity. Note that Province D overlies Province C in Blanco Valley. Main source areas of sediments indicated in parentheses ( ).

the Vancouver Valley-western Cascadia Abyssal Plain area; 3) Province C, encompassing both late Pleistocene and postglacial sediments in the several depositional environments of southeastern Cascadia Basin in addition to the entire length of Cascadia Channel--even out beyond Cascadia Gap onto Tufts Abyssal Plain; and 4) Province D, restricted to the postglacial sediments of Blanco Valley. The mineralogical compositions of the non-opaque, non-micaceous heavy mineral suites are shown in Figure 18 and listed in Table 6 for these four heavy mineral provinces.

Province A. In Province A, angular grains of augite dominate the heavy mineral assemblage and produce an extremely high CP/H ratio (mean 52.0). Olivine is more abundant when compared to the other provinces, and glaucophane is absent (Figure 18; Table 6). These factors, combined with the accompanying distinct light mineral assemblage (Figure 15; Table 4), support a local submarine volcanic origin for the sand-size debris in the Blanco Fracture Zone-Gorda Ridge transition area.

Province B. The heavy mineral assemblage of the terrigenous sand-silt layers comprising Province B (Vancouver Valley-western Cascadia Abyssal Plain) is characterized by the occasional presence of glaucophane and particularly by a relatively high CP/H ratio (mean 1.70) (Figures 17, 18; Table 6). The geographic location of Province B, combined with its heavy mineral assemblage, eliminates any of

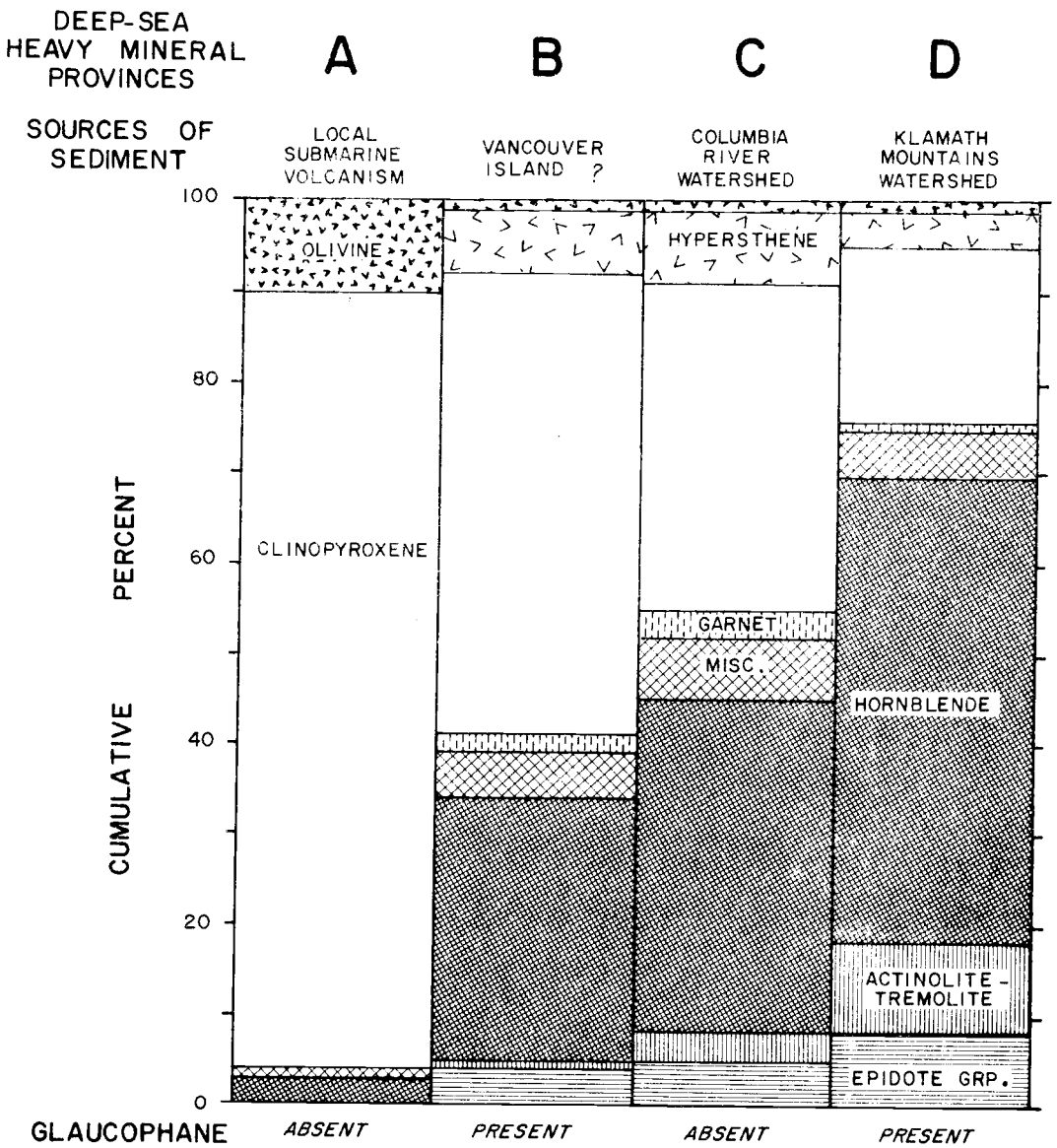

Figure 18. Mean cumulative percent compositions of the non-opaque, non-micaceous heavy minerals (62-125 microns) for the deep-sea heavy mineral provinces in southern Cascadia Basin and vicinity. See Figure 16 for geographic locations of the mineral provinces.

Table 6. Non-opaque, non-micaceous heavy mineral compositions for deep-sea heavy mineral provinces off Oregon. Mean and range values are given in percent. See Figure 17 for province locations.

	HEAVY MINERAL PROVINCES			
	A	B	C	D
PERCENT OF NON-OPAQUE, NON-MICACEOUS HEAVY MINERALS				
ACTINOLITE-TREMOLITE	Absent	1(0-2)	3(0-10)	10(8-17)
CLINOPYROXENE**	86(71-98)*	51(45-54)	36(22-42)	19(11-25)
EPIDOTE GROUP***	0(0-1)	4(3-4)	5(3-8)	8(5-11)
GARNET	Absent	2(1-3)	3(0-8)	1(0-1)
HORNBLENDE +	3(1-5)	29(26-33)	37(23-47)	52(45-56)
HYPERSTHENE	Absent	7(5-9)	8(0-16)	4(2-7)
OLIVINE	10(0-28)	1(0-3)	1(0-2)	1(0-3)
MISCELLANEOUS ++	1(0-1)	5(1-7)	7(3-10)	5(3-7)
Aegirineaugite		0.0	0.8	0.1
Andalusite		0.1	0.2	0.5
Apatite		0.7	0.5	0.1
Basaltic hornblende		1.6	1.3	0.4
Enstatite	0.6	0.5	1.2	1.6
Glaucophane		0.2	0.0	0.9
Kyanite		0.2	0.1	0.3
Rutile	0.1	0.1	0.8	0.1
Sillimanite		0.0	0.3	0.0
Sphene		1.0	1.2	0.3
Tourmaline		0.0	0.1	0.1
Zircon		0.3	0.2	0.2
Number of samples	5	7	39	10
Clinopyroxene/Hornblende ratio	52.0 (17.8-87.5)	1.70 (1.58-1.86)	0.98 (0.51-1.60)	0.37 (0.20-0.50)
Percent of samples containing Glaucophane	0	57	7	90

*Range of values shown in parentheses ( ).

**Predominantly consists of augite but may include minor amounts of titan-augite and tentatively identified diopside; does not include aegirineaugite.

***Epidote, clinozoisite and zoisite.

+Includes common, blue-green and brown hornblende.

++Other non-opaque, non-micaceous heavy minerals not listed and rarely present include chloritoid, corundum, dumortierite, monazite, serpentine and spodumene.

the previously discussed land drainage basins as the principal source contributing coarse clastics to the Vancouver Valley-western Cascadia Abyssal Plain area.

Since Vancouver Valley has its head at the base of the continental slope off Vancouver Island, sediments derived from the Island could be dispersed to the designated abyssal area by bottom transport along Vancouver Valley. Vancouver Island is covered with exposures of Late Triassic to Jurassic sedimentary rocks composed chiefly of volcanic debris (Vancouver Group; White, 1959); extensive influx of the erosion products of these rocks may have supplied relatively large quantities of clinopyroxene (augite) which would in turn account for the high CP/H ratio found in Province B. The granite-injected (Cretaceous) metamorphic rocks that crop out on southern Vancouver Island (White, 1959; Goddard et al., 1965) may be the source of the glaucophane occurring in the terrigenous sand-silt layers of Province B.

In the Vancouver Valley-western Cascadia Abyssal Plain area, terrigenous sand-silt layers are present in the late Pleistocene deposits but are absent in the overlying postglacial section (Figure 13). This restriction of the terrigenous sand-silt layers to the late Pleistocene section suggests that the heavy mineral assemblage (and terrigenous sand-silt layers) in Province B are derived from glacial moraines and outwashes associated with extensive late Pleistocene

glaciation by a lobe of the Cordilleran glacier which extended over Vancouver Island as well as over northwest Washington and British Columbia (Flint, 1957, p. 309). The maximum late Pleistocene glacial advance occurred 15,000 years BP during the Vashon Stade (Armstrong et al., 1965), but the ice had retreated considerably by 12,500 years BP (late Pleistocene-postglacial boundary in the deep-sea section off Oregon). Gross, McManus and Hsin-yi Ling (1967) have observed that no major local sources appear to be presently contributing sediment to the Vancouver Island shelf. River-borne sediments from the Island are now being discharged into long, narrow glacially-scoured inlets which generally have sills at their entrances. As a result, these inlets act as settling basins and prevent both suspended and bottom-transported sediments from moving seaward. Thus, as noted in the deposits of Province B, the flow of sediments to the deeper marine environments was greatly curtailed with the last retreat of the glaciers.

Province C. Heavy mineral characteristics (mean CP/H ratio 1.0, glaucophane absent) as well as geographic location indicate that Province C has received most of its sand-size sediment from the load of the Columbia River (mean CP/H ratio 1.25, glaucophane absent) during both late Pleistocene and postglacial time. As previously shown, little sediment from the Columbia River is presently moving on the bottom across the continental shelf south of the river mouth (net

longshore movement on the shelf of bottom-transported sediments is to the north). This lack of transport to the south suggests that most of the terrigenous sand found in the abyssal environments of Province C passed over the continental shelf and slope by way of Astoria and Willapa Canyons.[2] Terrigenous sand-silt layers in the axes of these canyons have heavy mineral assemblages characteristic of Columbia River sediment (Figure 17).

Cascadia Channel forms the western boundary for the dispersal of Columbia River sands in Cascadia Basin. However, the heavy mineral assemblage of the Channel's terrigenous sand-silt layers indicates that Columbia River sediments are passing westward through the southwest margin of Cascadia Basin onto Tufts Abyssal Plain by way of Cascadia Channel. The presence of a Columbia River heavy mineral assemblage in a terrigenous sand-silt layer from core 6604-3 (Figure 17; Plate 1) suggests that occasional Channel overflows (turbidity currents) may have supplied the few terrigenous sand-silt layers found in the shallow Blanco Fracture Zone trough south of Cascadia Gap. The most probable place for the overflows to occur is where Cascadia Channel is sharply deflected

---

[2] Heavy mineral data for Astoria and Willapa Canyons were obtained from Carlson (1968) and Royce (1964), respectively. These workers did not analyze discrete size fractions within the sand-size interval; thus, as with the continental shelf heavy mineral data, only values from samples with mean diameters less than 125 microns were used.

to the right in the vicinity west of Cascadia Gap (43°35'N, 128°45'W).

Columbia River sand reaches Cascadia Channel from Willapa Canyon by way of Willapa Channel. Sands from the Columbia River may also enter Cascadia Channel through numerous small valleys radiating out from Astoria Canyon on Astoria Fan (Nelson, 1968). These valleys presumably enter the Channel at points along its south-trending section section in Cascadia Basin.

Since Vancouver Valley leads into Cascadia Channel, it is most likely that a portion of the late Pleistocene sediment load, which was transported along the bottom of the Valley from the Vancouver Island area, spilled into Cascadia Channel. However, direct proof of this is lacking; none of the piston cores penetrated through the thick postglacial sediment layer in Cascadia Channel into late Pleistocene sediments.

The terrigenous sand-silt layer present in core 6609-3 (Figure 17; Plate 1) from the eastern part of the Blanco Fracture Zone contains a typical Columbia River heavy mineral assemblage. The presence of this layer suggests that occasional bottom-transported terrigenous sediment may pass through a gap in the prominent west-northwest trending ridge (bordering southern Cascadia Basin) and come to rest in low areas behind the ridge.

Province D. In Blanco Valley, a stratigraphic change is evident in the heavy mineral assemblage of the terrigenous sand-silt

layers; the heavy mineral assemblage constituting Province D (Figure 18; Table 6) is found in terrigenous sand-silt layers which overlie sediments that contain a heavy mineral assemblage belonging to Province C (Figures 17, 19). All late Pleistocene layers analyzed have heavy mineral assemblages of Columbia River provenance. These layers form a late Pleistocene tongue of Province C sediment which extends southward into Blanco Valley from Cascadia Basin. One terrigenous sand-silt layer studied in the lower portion of the postglacial section of core 6609-1 (extrapolated age = 8500 years BP) also contains a Columbia River heavy mineral suite (Figure 19). All other postglacial terrigenous sand-silt layers analyzed in Blanco Valley belong to Province D; this province has a heavy mineral assemblage (mean CP/H ratio 0.4, glaucophane present) indicative of Klamath Mountain provenance (mean CP/H ratio 0.5, glaucophane present).

Relatively few, thin terrigenous sand-silt layers are present in the postglacial section of Blanco Valley (Figures 13, 19); this decrease in terrigenous sand-silt layers attests to a generally diminished supply of coarse, bottom-transported sediment reaching the Valley in postglacial time. The most reasonable explanation for the postglacial change in heavy mineral provenance and the accompanying decrease in terrigenous sand-silt is a decrease in supply of coarse clastics originating from the Columbia River; the large

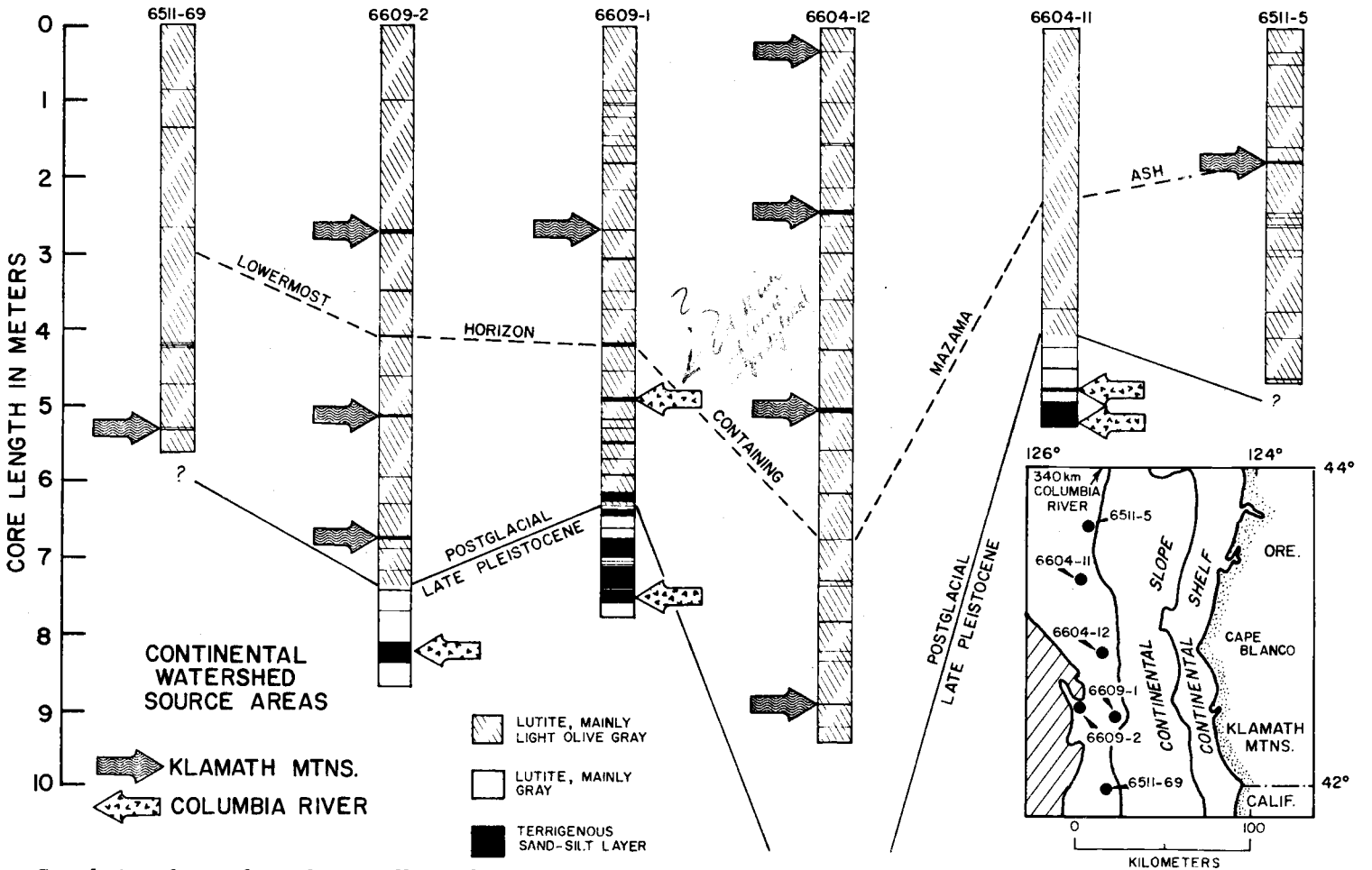

Figure 19. Correlation of cores from Blanco Valley and heavy mineral evidence for postglacial change of principal continental source area contributing sediment to Blanco Valley. Inset map gives core locations in Blanco Valley.

volumes of Columbia River sand-silt which reached Blanco Valley in the late Pleistocene seem to have completely masked the smaller, local contribution of Klamath Mountains sediment at that time.

During the late Pleistocene and occasionally during the early part of postglacial time, Columbia River sediments were transported by turbidity currents at least as far south in Blanco Valley as 42° 26' N (core 6609-1). These turbidity currents were probably generated near the head of Astoria Canyon and then flowed down the Canyon to Blanco Valley by way of Astoria Channel. As previously demonstrated (Chapter VI, Figure 13), turbidity currents were not as extensive in postglacial time. Postglacial flows originating near Astoria Canyon apparently did not have sufficient volumes of debris to reach as far south as Blanco Valley. With the smaller influx of Columbia River sediment in the postglacial interval, the contribution of debris from the Klamath Mountains is more dominant.

VIII. X-RAY CLAY MINERALOGY OF LUTITES

In a detailed X-ray diffraction study of clay minerals in sediment cores from Astoria Canyon and Astoria Fan, Russell (1967) reported the presence of montmorillonite, illite, and chlorite and the absence of vermiculite, kaolinite, and mixed-layer clays. Although all of the sediments contained similar clay mineral assemblages, he noted that a change took place in the character of the clay X-ray traces below a certain stratigraphic horizon in the cores. The X-ray peaks for montmorillonite, illite, and chlorite are higher and sharper in the clays from the lower portions of some core sections. Russell also observed that, rather than altering gradually with depth in the core, the peak characteristics changed abruptly along the certain stratigraphic horizon; the abruptness of the change implied that a slow, continual process of marine diagenesis could not account for the resulting stratigraphic sequence. Russell suggested that the abrupt stratigraphic change was due to a shift from glacial to non-glacial conditions, and that the position of the stratigraphic change in clay mineralogy coincided with the boundary between Pleistocene and postglacial sedimentation for Astoria Canyon and Astoria Fan as defined by Carlson (1968) and by Nelson (1968), respectively.

The broader, regional significance of the stratigraphic trend

in clay mineralogy, found by Russell, and its association with stratigraphic boundaries defined in the present study (Chapter V) was investigated by the writer using additional samples from adjoining abyssal areas. Late Pleistocene and postglacial samples representing the typical lutites of the various deep-sea environments were analyzed for possible lateral as well as vertical clay mineral trends. To facilitate direct comparison with Russell's work, the writer employed the same laboratory techniques. The semi-quantitative methods suggested by Biscaye (1965) were then applied on the X-ray traces to determine the relative abundances of chlorite, illite, and montmorillonite present in the less than 2-micron fraction of the lutites. These semi-quantitative methods were also applied on traces previously run by Russell (1967) and by Allen (1966) for sediments from cores presented in this study. The results of the semi-quantitative calculations for the clay mineral compositions of all the samples are given in Appendix 10.

Postglacial Clay Mineral Facies

The large postglacial contribution of fine sediment from the Columbia River to the deep-sea environments within southern Cascadia Basin and Blanco Fracture Zone is evident in the clay mineralogy. Variations in the clay mineral percentage compositions of the postglacial lutites, plotted on a ternary diagram (Figure 20),

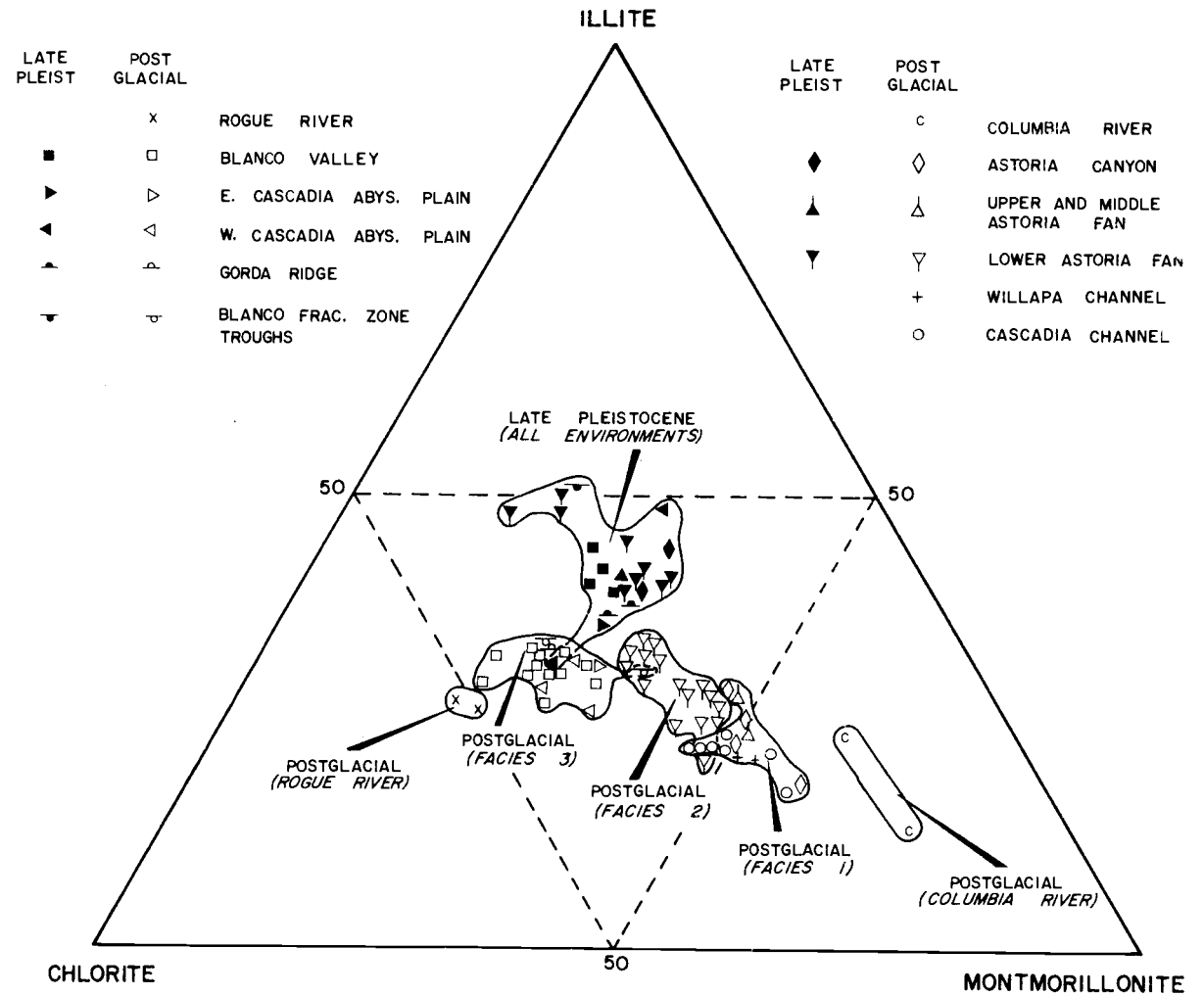

Figure 20. Ternary diagram of weighted peak-area percentages of chlorite, illite, and montmorillonite in late Pleistocene and postglacial lutites from various environments. The percentages are computed from tracings of magnesium-glycerol solvated slides of the clay fraction (<2 microns).

can be interpreted primarily as a function of distance from the mouth of the Columbia River; from this point source, a gradational clay mineral facies pattern radiates outward into the deep-sea environments (Figure 21). The percent of montmorillonite generally decreases while the percents of chlorite, to a greater extent, and illite, to a lesser extent, increase with distance from the point source.

Sediments in the Columbia River itself (samples were taken at points 30 and 250 km upstream from the mouth of the river and were processed by Russell, 1967) have the highest percentages of montmorillonite (mean values: chlorite 16%, illite 19%, and montmorillonite 65%). This high montmorillonite content confirms the sediment source and conforms to the systematic lateral changes in clay mineral composition in the southern Cascadia Basin-Blanco Fracture Zone area. Studies of South Pacific Ocean (Griffin and Goldberg, 1963) and southwestern Indian Ocean (Biscaye, 1965) clays have shown that a high montmorillonite content is usually associated with sediments derived from volcanic rock provinces. Thus, the high content of montmorillonite in the Columbia River clays is probably due to the influx of weathering products from the vast exposures of volcanic rock on the Columbia River Plateau, in the Cascade Mountains, and on the eastern flank of the Oregon Coast Range (Waters, 1955); all of these areas are included in the Columbia

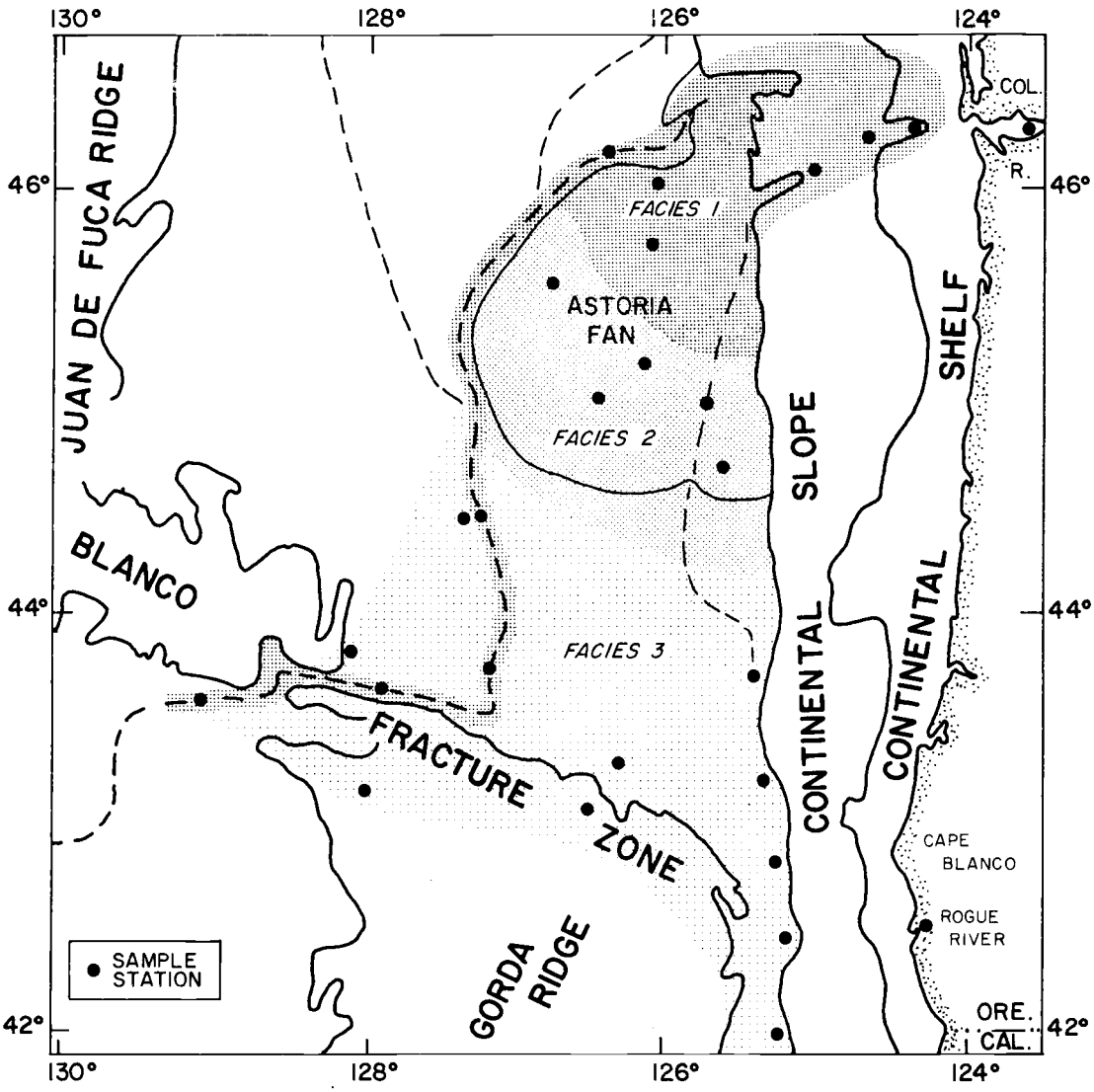

Figure 21. Distribution of postglacial clay mineral facies reflecting the relative contribution of the Columbia River clay load to different marine environments in southern Cascadia Basin and vicinity.

River drainage area (Figure 1).

The radiating pattern of clay mineral variations with distance from the Columbia River mouth in the deep-sea environments can be divided into three facies (Figures 20, 21). Clays from Astoria Canyon, upper and middle Astoria Fan, and Willapa Channel form Facies 1 which has the highest deep-sea montmorillonite content (mean values: chlorite 27%, illite 22%, and montmorillonite 51%). Although unsampled, the clays from lutites in Willapa Canyon most likely belong to this high montmorillonite facies. Lutites from lower Astoria Fan belong to Facies 2 which has an intermediate amount of montmorillonite (mean values: chlorite 30%, illite 29%, and montmorillonite 41%), while the lutites farther away in the areas of eastern and western Cascadia Abyssal Plain, Blanco Valley, Blanco Fracture Zone, and Gorda Ridge form Facies 3. The latter facies has the lowest content of montmorillonite and the highest content of chlorite (mean values: chlorite 40%, illite 28%, and montmorillonite 32%).

The layers of postglacial, olive gray lutite in Cascadia Channel (Plate 1) are an exception to the radiating facies trend (Figure 21). Collectively, these lutite layers form a thick but narrow ribbon of sediment in the Channel and have the clay mineral composition of Facies 1. These deposits transect both Facies 2 and 3 along the course of Cascadia Channel out to Tufts Abyssal Plain. It is clear

that Cascadia Channel has received these finer grained sediments essentially in an undiluted state directly from submarine environments close to the mouth of the Columbia River which are characterized by Facies 1. These channel sediments most likely were periodically transported along the bottom and entered Cascadia Channel through Willapa Channel or the small fan valleys originating on the upper and middle portions of Astoria Fan. Once entering Cascadia Channel, the montmorillonite-rich sediments remained within the confines of the Channel and followed its course, eventually settling somewhere along the channel bottom. Further discussion of the mechanism of bottom transport of the olive gray lutites is given in Chapter IX.

From the clay mineral distribution pattern noted in the southern Cascadia Basin-Blanco Fracture Zone area, it appears that the clays produced in the Columbia River drainage area have a lower chlorite and higher montmorillonite content than do other drainage areas emptying into the northeastern Pacific. With increased distance from the Columbia River, the clay composition apparently changes as a result of dilution with clays from other land sources that contribute different amounts of chlorite, illite, and montmorillonite. Clays from the Rogue River (Figure 20; Plate 1, sample RR-1), which drains part of the Klamath Mountains in southwestern Oregon, have a relatively high chlorite content (mean values: chlorite 51%,

illite, 26%, and montmorillonite 23%). These Klamath Mountain clays represent a local southern source that could dilute the Columbia River Clay mineral composition. However, it is very unlikely that the relatively small drainage area of the Klamath Mountains contributes enough chlorite to account completely for the distribution pattern (Figure 21). Griffin and Goldberg (1963) found that the chlorite content of clays in the northeastern Pacific Ocean is generally higher than that of other Pacific Ocean areas. They attribute this higher chlorite content to continental sources in the coastal regions of Canada, Alaska, and the Aleutian Islands. Perhaps a combination of influxes of both the far northern and the local southern sources of chlorite-rich clays best explains the clay mineral distribution pattern noted in the marine environments of southern Cascadia Basin and adjoining Blanco Fracture Zone.

Late Pleistocene versus Postglacial Clay Minerals

In contrast to the systematic lateral variations in clay mineral composition of the postglacial section, no facies changes are evident in the late Pleistocene clay mineral assemblage (Figure 20). Variations in peak-area characteristics for chlorite, illite, and montmorillonite in a typical late Pleistocene lutite compared to postglacial lutites are shown in Figure 22. More illite and less chlorite and montmorillonite (mean values: chlorite 29%, illite 42%, and

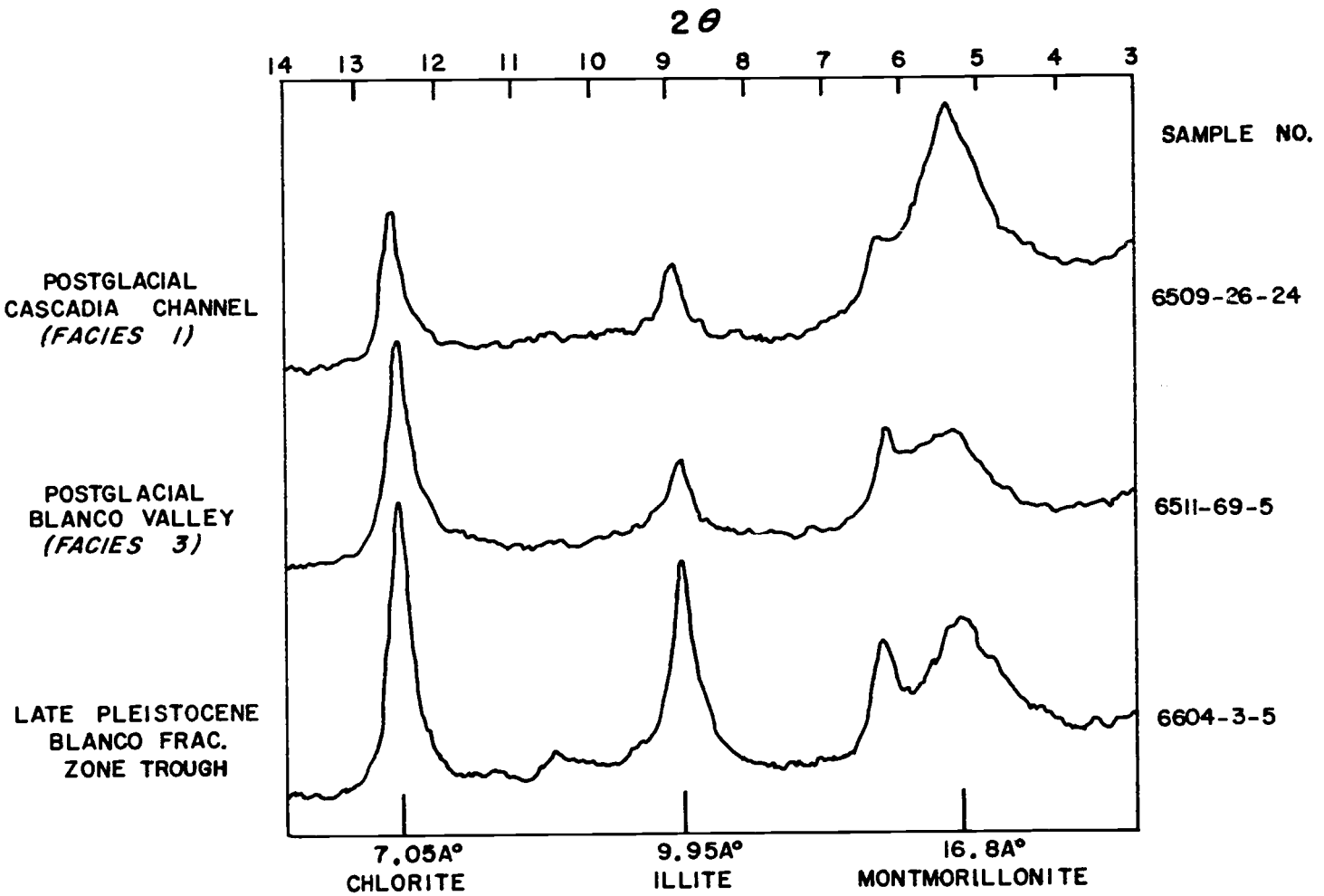

Figure 22. Typical X-ray diffraction traces indicating environmental and temporal variations of peak-area characteristics of illite, chlorite, and montmorillonite in deep-sea lutites.

montmorillonite 29%) are present in the late Pleistocene lutites compared to those of the postglacial interval. As previously mentioned, Russell (1967) has demonstrated that the change in peak characteristics of the X-ray traces associated with different age deposits is not due to marine diagenesis. Supporting evidence for a lack of marine diagenesis can best be seen in the ratios of chlorite to illite and of montmorillonite to illite plotted against stratigraphic depth in cores from lower Astoria Fan and Blanco Valley (Figure 23). The abrupt changes in the ratios are associated with the late Pleistocene-postglacial boundary previously defined on the basis of faunal and lutite color stratigraphy. The lack of an abrupt change in the montmorillonite-illite ratio in Blanco Valley (core 6609-1) probably reflects a dilution of the montmorillonite-rich Columbia River clay by the local influx of montmorillonite-poor clays from the Klamath Mountains.

Presumably the Columbia River watershed area has been the main source of both late Pleistocene and postglacial clay-size debris in the southern Cascadia Basin area. Since marine diagenesis does not appear to be the cause of the stratigraphic change in clay mineral composition, Russell (1967) suggests that a change in weathering processes in the continental source area probably accounts for the differences between late Pleistocene and postglacial clay mineral compositions in the deep-sea environments. Compared to the

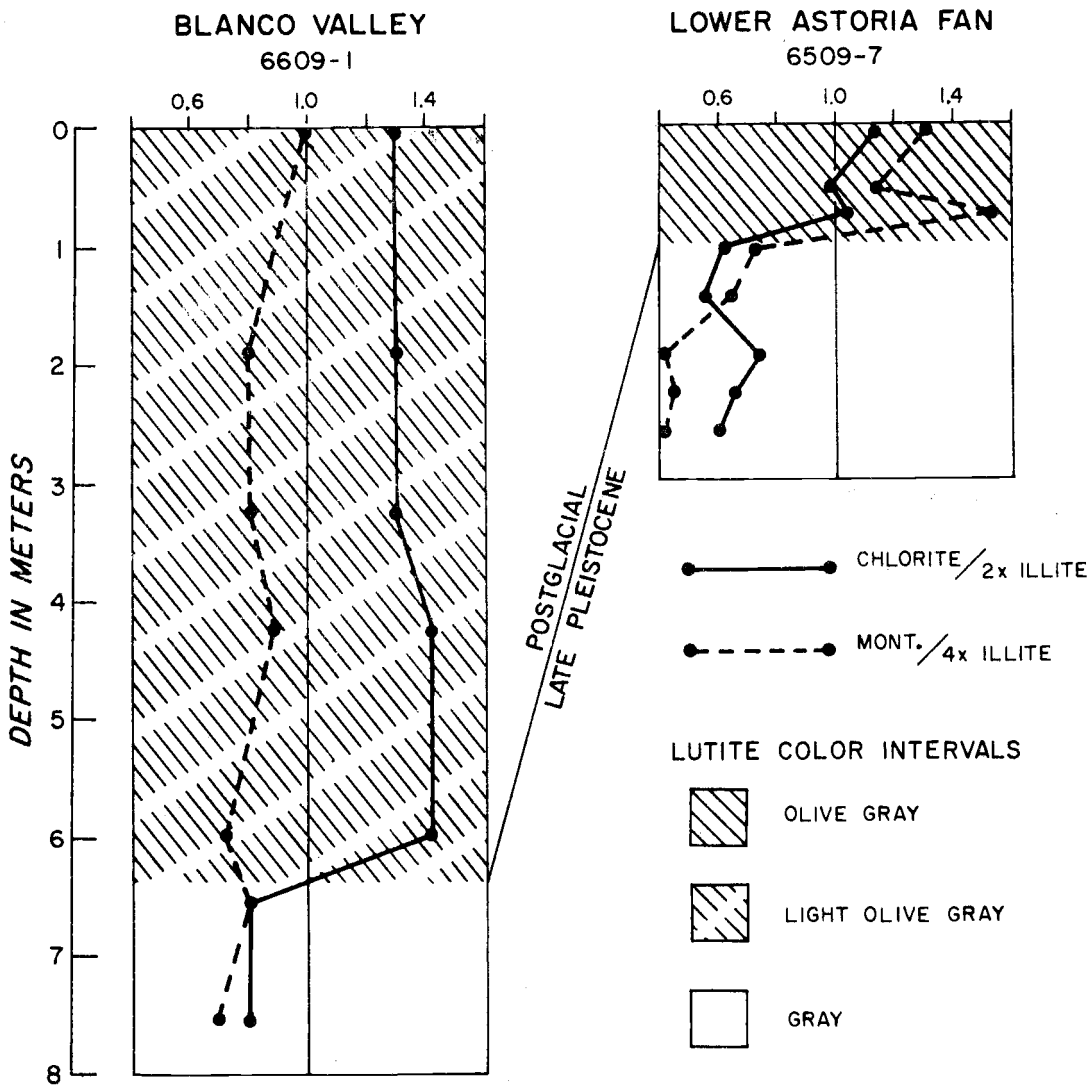

Figure 23. Chlorite-illite and montmorillonite-illite ratios as functions of depth in selected cores.

postglacial interval, detritus produced on the continent during glacial times most likely was subjected to more mechanical and less chemical weathering; the greater influence of mechanical weathering during the Pleistocene may have resulted in the production of larger quantities of illite (Russell, 1967).

The late Pleistocene-postglacial stratigraphic change in the clay mineral composition could also be due to a change in the relative contributions of sediments from different source rocks within the watershed area of the Columbia River. Much of the Rocky Mountains area ultimately drained by the Columbia River was subjected to severe glaciation during the late Pleistocene (Flint, 1957, p. 309). Partially metamorphosed sedimentary rocks of Precambrian to Cenozoic age crop out over large areas of the Rocky Mountains. Grim (1953, p. 356) has noted that montmorillonite tends to disappear in sedimentary rocks older than the Mesozoic Period, and either chlorite or illite is more abundant. Due to the intense erosion by late Pleistocene glaciers, the Rocky Mountains probably produced more sediment in a very finely ground state (glacial flour) than is presently being produced from the same area. It is therefore possible that the increased glacial erosion during the late Pleistocene of the older sedimentary rocks in the Rocky Mountains may have released more illite to the Columbia River drainage basin and thus produced the higher content of illite noted in the late

Pleistocene marine lutites.

The lack of systematic lateral changes in the late Pleistocene clay mineral composition for the deep-sea environments is puzzling (Figure 20). Perhaps the enormous periodic floods of the Columbia River during the Pleistocene (Bretz, Smith and Neff, 1956; Richmond et al., 1965; Malde, 1965; Lowry and Baldwin, 1952) carried such large volumes of sediment to the sea, that the resulting plumes of muddy water completely covered the study area with one clay mineral facies.

IX. GRAIN SIZE AND COARSE FRACTION COMPOSITIONS OF LUTITE

Terrigenous particles make up the bulk of the lutites in the deep-sea environments off Oregon, and variations in the lutite grain size compositions (percent sand, silt and clay) are significant since they reflect conditions in the depositional environment, mode of sediment transport, and distance from the source. Other materials, such as marine organisms and authigenic minerals, are present in rather small quantities because of the relatively rapid introduction of the terrigenous particles.

Results of grain size and coarse fraction (>62 microns) analyses on selected lutite samples are shown in Appendix 11. The coarse fraction constituents group into four major categories: 1) terrigenous debris--including plant fibers, mica, colorless volcanic glass, and other minerals and rock fragments of continental origin; 2) planktonic fauna--embracing diatoms, radiolarians, and foraminiferans; 3) submarine volcanic debris--chiefly basaltic glass (dark brown) but including other rock fragments and minerals believed to be by-products of submarine volcanism; and 4) miscellaneous components--including those of in situ origin as well as other non-differentiated constituents generally occurring in trace amounts.

Some confusion may arise if the reader assumes that the same

percentages of constituents which occur in the coarse fractions of the lutites are also present in the smaller size fractions. The coarse fraction generally is less than a few percent of each sample, and some of the components are mainly present only in this size fraction. Thus, the coarse fraction may not be representative of the entire sediment composition. However, the coarse fraction composition adds valuable information to the study because it gives some insight into the relative importance of certain factors that influence the overall character of the sediment.

Postglacial Lutites

Environmental trends are evident in the mean sand-silt-clay composition and the coarse fraction composition of sediments representing the typical postglacial lutites in the various depositional environments (Figure 24; Table 7). Much of the sediment in the Blanco Fracture Zone-Gorda Ridge transition area (cores 6601-1, 6609-6, -8 in Plate 1) is basaltic glass lutite. This sediment has a higher percentage of sand-size constituents in comparison to the lutites of adjacent environments and represents an accumulation of debris from two discrete sources. Most of the clay- and silt-size components are presumably of continental origin and were transported to the area by suspension in the water mass. In contrast, the sand-size sediment consists mainly of basaltic glass, basaltic rock

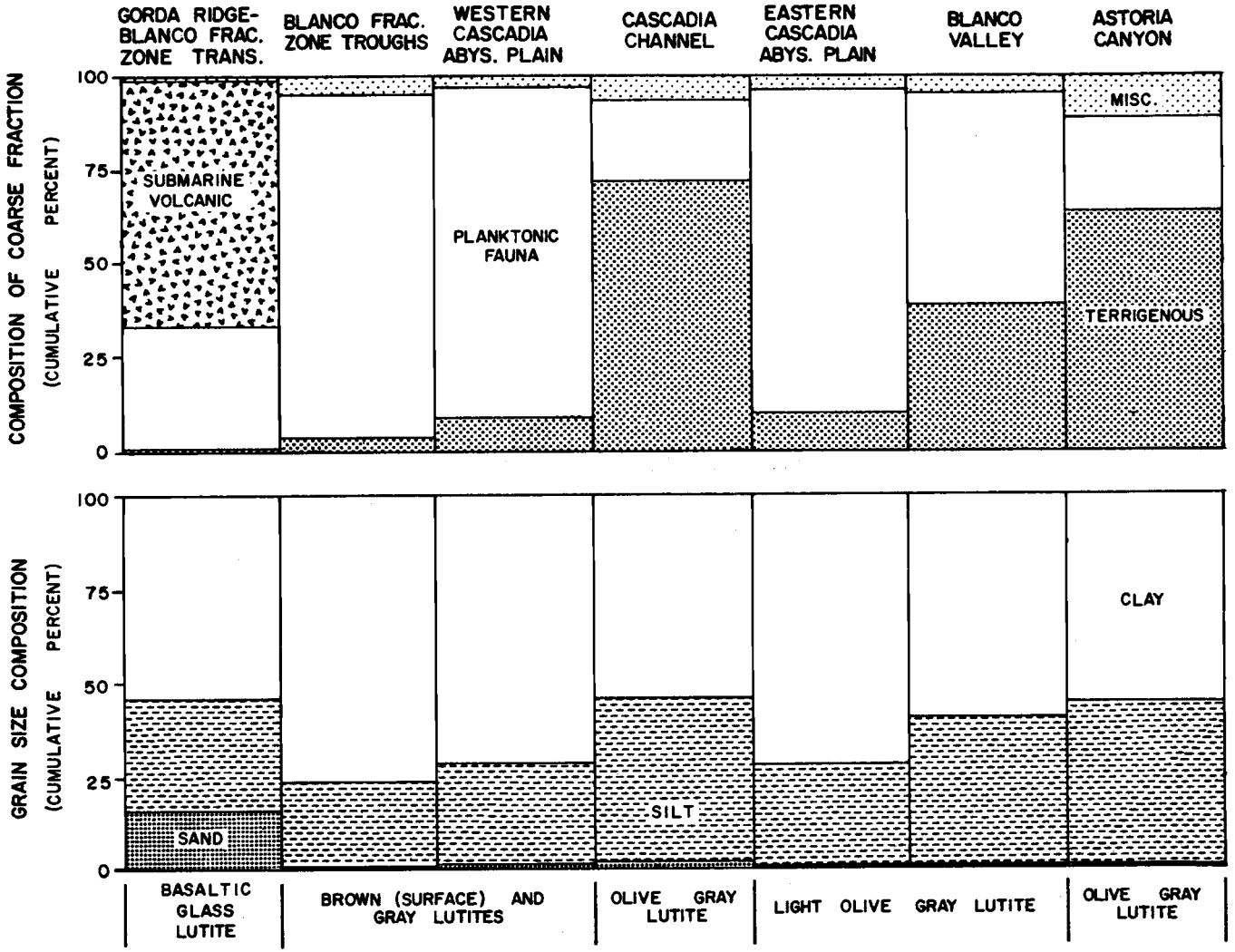

Figure 24. Postglacial mean coarse fraction and grain size compositions of lutites which are typical of the various deep-sea environments. Refer to Table 7 for additional details. Data for Astoria Canyon from Carlson (1968).

Table 7. Grain size and coarse fraction compositions of typical postglacial lutites in various deep-sea environments. Mean and range values are given in percents. Data for Astoria Canyon from Carlson (1968).

	PHYSIOGRAPHIC ENVIRONMENT	GORDA RIDGE-BLANCO FRAC. ZONE TRANS.	BLANCO FRAC. ZONE TROUGHS	WESTERN CASCADIA ABYSSAL PLAIN	EASTERN CASCADIA ABYSSAL PLAIN	BLANCO VALLEY	CASCADIA CHANNEL	CASCADIA CHANNEL	ASTORIA CANYON
PERCENT OF COARSE FRACTION	TERRIGENOUS DEBRIS (total)	1(0-2)	4(0-9)	8(0-19)	8(3-19)	38(11-86)	29(8-67)	76(28-92)	63(45-90)
	Plant fibers	Absent	1(0-2)	0(0-1)	2(1-3)	9(0-23)	6(1-13)	39(8-72)	26(9-49)
	Mica	1(0-1)	1(0-5)	1(0-3)	1(0-1)	5(2-20)	5(2-18)	10(3-24)	8(5-13)
	Colorless vol. glass	0(0-1)	Absent	1(0-1)	Absent	6(0-67)	2(0-7)	9(0-39)	3(0-9)
	Other min. & rk. frag.	Absent	2(0-7)	6(0-17)	5(2-16)	18(4-53)	16(3-45)	18(3-49)	26(10-65)
	PLANKTONIC FAUNA (total)	32(17-47)	90(81-98)	90(80-98)	88(79-93)	57(12-81)	63(32-85)	17(3-43)	25(4-42)
	Diatoms	0(0-1)	5(2-7)	1(0-7)	5(1-17)	17(0-36)	3(0-9)	8(1-22)	17(3-36)
	Radiolarians	31(17-46)	85(74-93)	89(74-94)	80(70-89)	37(9-70)	57(22-84)	9(2-36)	8(1-22)
	Foraminiferans	1(0-2)	Absent	0(0-2)	3(0-11)	3(0-12)	3(0-10)	0(0-1)	Absent
	SUBMARINE VOLCANIC DEBRIS	66(48-82)	Absent	Absent	Absent	Absent	Absent	Absent	Absent
	MISCELLANEOUS (total)	1(0-4)	6(0-16)	2(1-5)	4(1-9)	5(1-21)	8(1-16)	7(0-29)	12(1-19)
	Benthic foraminiferans	1(0-2)	2(0-2)	1(1-3)	2(1-2)	2(0-4)	4(1-8)	1(0-2)	2(0-4)
	Pyrite	0(0-2)	3(0-15)	0(0-2)	0(0-1)	2(0-19)	3(0-10)	2(0-22)	Absent
	Other*	0(0-1)	1(0-8)	1(0-3)	2(0-7)	1(0-3)	1(0-4)	4(0-27)	10(1-18)
SIZE	PERCENT SAND	16(3-45)	1(1-2)	2(1-3)	1(1-2)	1(0-1)	1(0-3)	2(0-12)	1(1-4)
	PERCENT SILT	29(16-35)	22(19-27)	26(20-38)	26(24-30)	39(31-50)	35(26-50)	43(28-47)	42(38-48)
	PERCENT CLAY	55(39-62)	77(72-80)	72(60-79)	73(69-74)	60(49-68)	64(65-73)	55(42-71)	57(52-61)
NUMBER OF SAMPLES		5	6	8	5	13	10	16	13
SEDIMENT TYPE(S)		BASALTIC GLASS LUTITE	BROWN & GRAY LUTITE		LIGHT OLIVE GRAY LUTITE		GRAY LUTITE	OLIVE GRAY LUTITE	

*Other--fecal pellets, glauconite, pollen, sponge spicules and unidentified grains.

fragments, and plagioclase feldspar grains that are from local submarine volcanic sources.

The Blanco Fracture Zone troughs on the western side of Gorda Ridge (cores 6604-2, -3, 6609-13) and the western Cascadia Abyssal Plain are environments of slow postglacial hemipelagic sedimentation (Figure 12). Most of the postglacial sediments in these areas reflect this in their fine-grained nature and the abundance of planktonic organisms (predominantly radiolarians) in their coarse fractions (Figure 24). The stratigraphic sections consist chiefly of gray lutite with a surface covering of brown lutite which may be up to 20 cm thick (Figure 8). Because the sedimentation rates in these environments are low, the brown lutite makes up a considerable portion of the postglacial sections. However, no differences in grain size, biological, or lithological compositions are associated with the vertical color change from gray to brown in these particular localities, so the data from the different colored lutites of the postglacial interval are averaged together for the general environmental descriptions (Figure 24).

The lutites in the Fracture Zone troughs are the finest grained of all the sediments in the study area. In comparison, western Cascadia Abyssal Plain lutites, although also very fine grained, are slightly coarser and have more terrigenous components in their coarse fractions.

The postglacial stratigraphic section of eastern Cascadia Abyssal Plain consists chiefly of light olive gray lutite with coarse fraction and grain size compositions very similar to those of the brown (surface) and the gray lutites of western Cascadia Abyssal Plain (Figure 24). In contrast, the light olive gray lutites in Blanco Valley are coarser and have a higher percentage of terrigenous components, though the planktonic organisms are still the most plentiful coarse fraction constituents. A notably coarser grain size composition characterizes the olive gray lutites which dominate the postglacial sections of Cascadia Channel and Astoria Canyon. Terrigenous components make up the majority of the coarse fraction in these sediments.

In most of the above physiographic environments, the lutites appear to be hemipelagic deposits consisting of blanket-like layers of fine terrigenous sediments. These sediments most likely were transported to the deep-sea environments by a slow continuous seaward diffusion process in which the fine sediments drift laterally while they settle through the water column and eventually are deposited particle-by-particle on the sea floor. As a rule, both the particle size and the terrigenous components of the coarse fraction decrease with increasing distance from the continental source areas. This decrease reflects the effect of settling velocity; the finer debris settles more slowly than the coarser material and thus travels

farther from the source before coming to rest on the bottom.

The thick layers of olive gray lutite in Cascadia Channel represent a marked deviation from the above trend. All along the course of the Channel the olive gray lutite layers are coarser and have more terrigenous components in their coarse fractions than do the lutites in adjacent environments (Figure 24). The incongruent nature of these Channel lutite layers suggests that they are not the product of the slow continuous hemipelagic sedimentation which affects the abyssal environments in a more uniform manner.

The postglacial section in Cascadia Channel is composed of cyclic units consisting of a relatively thin basal terrigenous sand-silt layer grading upward into a thick olive gray lutite bed which is capped with a thin, gray lutite layer (previously discussed in Chapter IV). Detailed grain size and coarse fraction studies of the stratigraphic section in Cascadia Channel by other workers (Kulm and Griggs, 1966; Griggs, Kulm and Carey, 1968) have shown that the terrigenous sand-silt layers are the basal units of turbidity current deposits. The olive gray lutite intervals represent the finer grained sediments which take longer to settle out of the turbid suspensions. Both the terrigenous sand-silt and the olive gray lutite layers contain benthic foraminiferans indigenous to continental shelf and slope environments (Duncan, 1966; Griggs, 1966); the presence of these displaced benthic foraminiferans suggests a turbidity current

origin. Heavy mineral and clay mineral data (Figures 17, 22) indicate that these turbidity current deposits were introduced into the Channel through a connecting tributary system originating in the vicinity of Astoria and Willapa Canyons.

The olive gray lutites of Cascadia Channel have similar coarse fraction and grain size compositions as those of the Astoria Canyon area (Figure 24). However, the lutites in these two areas were deposited in different manners. In the vicinity of Astoria Canyon, the lutites were chiefly deposited in a particle-by-particle manner (Carlson, 1968); these lutites owe their relatively coarse grain size composition and high percentage of coarse fraction terrigenous constituents to the close proximity of the Columbia River which releases copious amounts of suspended debris to the marine environments. In contrast, the olive gray lutites of Cascadia Channel represent sediments that were originally deposited in the Astoria Canyon-Willapa Canyon area by a particle-by-particle process and then later re-transported and deposited by turbidity currents.

Kulm and Griggs (1966) and Griggs, Kulm and Carey (1968) demonstrated that the thin gray lutite layers capping the cyclic units in Cascadia Channel consist chiefly of very fine terrigenous particles and the remains of pelagic organisms, both of which slowly but continually rain down on the sea floor. These thin gray layers accumulated particle-by-particle and represent long intervals of

time between turbidity currents in the Channel.

In general, the gray lutites in Cascadia Channel are much finer grained and have fewer terrigenous components in their coarse fractions than do the olive gray lutites (Figure 25; Table 7). However, when compared to the postglacial hemipelagic lutites found on both eastern and western Cascadia Abyssal Plain, the gray lutite layers in the Channel are coarser and have more terrigenous components. If the gray lutites in the Channel have the same origin as the lutites on eastern and western Cascadia Abyssal Plain, there should be a closer similarity in their compositional characteristics than actually exists. A possible solution to this dilemma may be found in the work of Griggs, Kulm and Carey (1968). Their work demonstrates that burrowing organisms re-colonize in the Channel sediments after each turbidity current and re-work the sediments in the upper portion of the flow. This re-colonization is indicated by the mottling of gray lutite within the upper portions of the underlying olive gray lutite. The re-working of the sediments by the organisms may introduce some of the coarser olive gray lutite debris into the gray lutite layers and thus explain whey they are intermediate in grain size and coarse fraction characteristics.

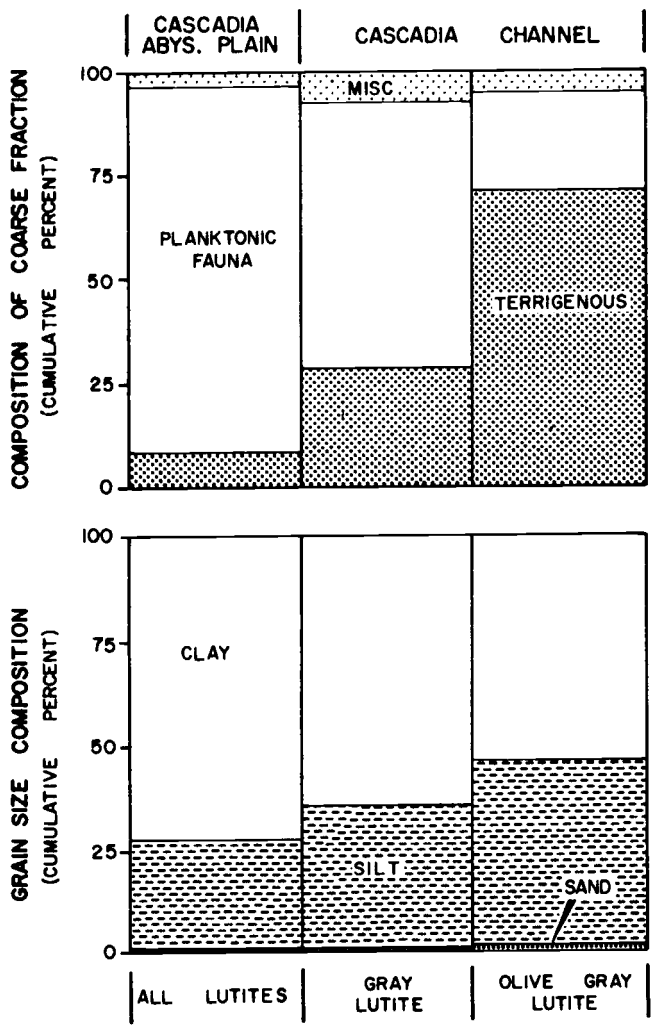

Figure 25. Mean coarse fraction and grain size compositions of the different postglacial lutites in Cascadia Channel compared to Cascadia Abyssal Plain lutites. Refer to Table 7 for additional data.

Similarities and Contrasts between Late Pleistocene and Postglacial Lutites

Where sufficient core penetration and sub-sampling permitted, grain size and coarse fraction compositions of typical late Pleistocene lutites in some of the deep-sea areas were analyzed; compilations of these analyses are shown in Figure 26 and listed in Table 8.

Although the late Pleistocene coverage is not as extensive as that for the postglacial section, it is evident that proximity to source areas is a significant factor governing the grain size and coarse fraction compositions of the hemipelagic sediments from both age intervals. The late Pleistocene lutites in Astoria Canyon, eastern and western Cascadia Abyssal Plain, and the Blanco Fracture Zone troughs also show a decrease in grain size and coarse fraction terrigenous components with increase of distance from the continental source areas. The presence of submarine volcanic debris in the lutites of the late Pleistocene as well as the postglacial section of the Blanco Fracture Zone-Gorda Ridge transition area indicates that this area has been producing significant quantities of volcanic sediments throughout the time interval studied.

As previously pointed out (Figures 9, 10), the most significant difference in coarse fraction composition of the late Pleistocene sections compared to the postglacial ones is the planktonic fauna.

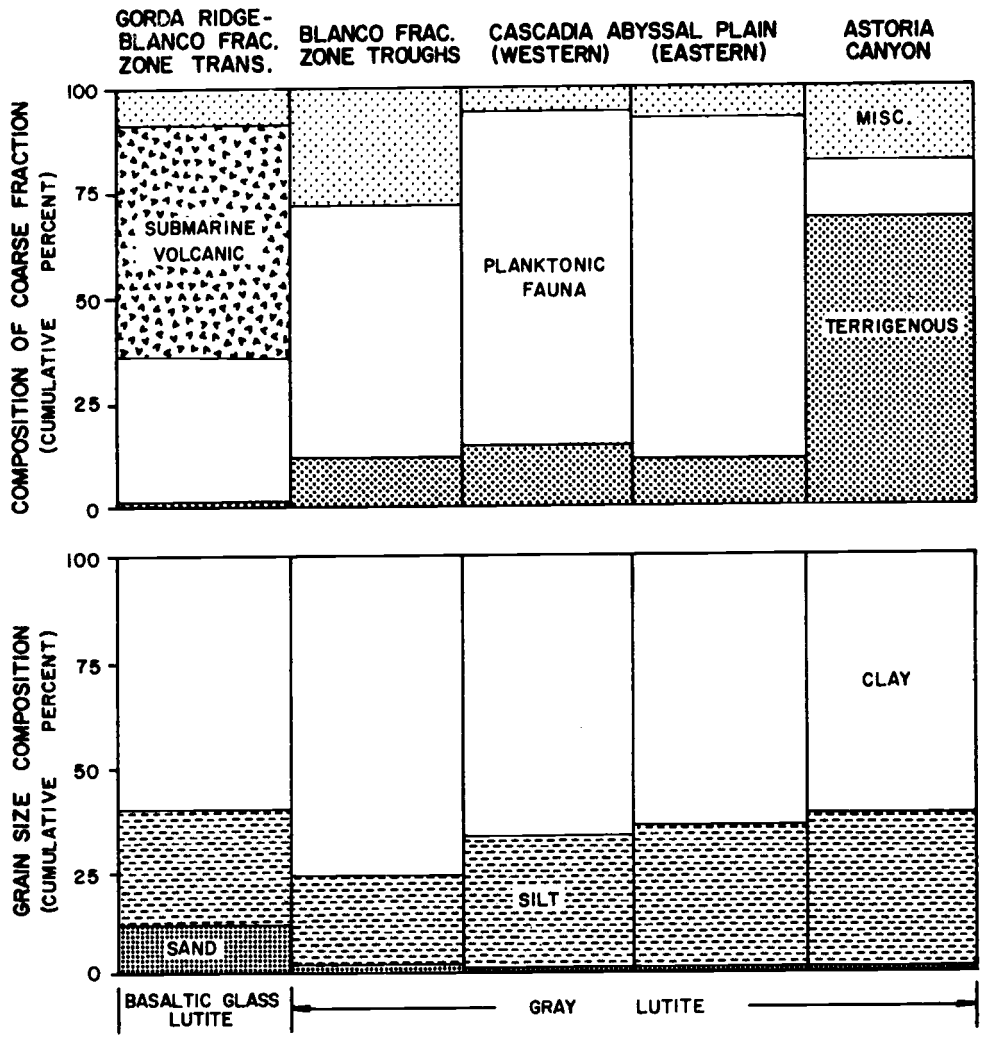

Figure 26. Mean coarse fraction and grain size compositions of late Pleistocene lutites from various deep-sea environments. Refer to Table 8 for additional details. Data for Astoria Canyon from Carlson (1968).

Table 8. Grain size and coarse fraction compositions of typical late Pleistocene lutites in various deep-sea environments. Mean and range values are given in percents. Data for Astoria Canyon from Carlson (1968).

	PHYSIOGRAPHIC ENVIRONMENT	GORDA RIDGE-BLANCO FRAC. ZONE TRANS.	BLANCO FRAC. ZONE TROUGHS	WESTERN CASCADIA ABYSSAL PLAIN	EASTERN CASCADIA ABYSSAL PLAIN	ASTORIA CANYON
PERCENT OF COARSE FRACTION	TERRIGENOUS DEBRIS (total)	1(0-1)	12(6-27)	15(0-50)	11(1-30)	69(17-96)
	Plant fibers	0(0-1)	1(0-2)	0(0-1)	1(0-2)	6(1-24)
	Mica	1(0-1)	4(1-15)	2(0-4)	2(0-9)	20(5-37)
	Colorless vol. glass	Absent	1(1-2)	Absent	0(0-2)	1(0-7)
	Other min. & rk. frag.	Absent	6(3-10)	13(0-48)	8(0-29)	42(7-74)
	PLANKTONIC FAUNA (total)	34(15-63)	60(34-83)	80(49-96)	82(62-92)	13(1-34)
	Diatoms	Absent	Absent	Absent	0(0-2)	1(0-2)
	Radiolarians	1(1-1)	26(1-76)	3(0-15)	22(0-46)	2(0-8)
	Foraminiferans	33(14-62)	34(7-71)	77(49-94)	60(22-85)	10(1-33)
	SUBMARINE VOLCANIC DEBRIS	57(17-81)	Absent	Absent	Absent	Absent
	MISCELLANEOUS (total)	8(0-19)	28(11-48)	5(0-16)	7(2-15)	18(0-66)
	Benthic foraminiferans	6(0-15)	20(10-46)	3(0-5)	5(2-11)	7(0-32)
	Pyrite	Absent	2(0-11)	Absent	1(0-9)	11(0-63)
	Other*	2(0-4)	6(1-11)	2(0-13)	1(0-4)	0(0-3)
SIZE	PERCENT SAND	12(2-23)	2(0-7)	1(0-4)	1(1-3)	1(0-1)
	PERCENT SILT	28(27-28)	22(8-30)	32(19-47)	35(25-44)	37(28-49)
	PERCENT CLAY	60(49-71)	76(66-90)	67(52-80)	64(55-72)	62(51-72)
NUMBER OF SAMPLES		3	7	11	12	13
SEDIMENT TYPE		BASALTIC GLASS LUTITE	GRAY LUTITE			

*Other--fecal pellets, glauconite, pollen, sponge spicules and unidentified grains.

Radiolarians dominate the postglacial sections, while planktonic foraminiferans generally are more abundant in the late Pleistocene sections (compare Tables 7 and 8). In both age intervals, diatoms constitute a minor part of the planktonic fauna.

X. ORGANIC CARBON CONTENT OF LUTITES

The organic carbon content (dry weight of total sediment) in 76 representative lutite samples varies from zero to nearly three percent (Appendix 7). In terms of sediment ages and regional distributions, the variations in reported values are significant.

Postglacial Distribution

In a preliminary study of marine surface sediments off the Oregon-Washington coast, Gross (1967) found that the largest concentrations of organic carbon occur in lutites from the outer portion of the continental shelf, on the continental slope, and in eastern Cascadia Basin. The surface lutites lying seaward of Cascadia Channel (western Cascadia Abyssal Plain) contain substantially less organic carbon.

Data gathered in the present study on organic carbon content of postglacial lutites (Figure 27) show trends that are generally consistent with those reported by Gross. The brown (surface) and the gray lutites in the Blanco Fracture Zone troughs and on western Cascadia Abyssal Plain have the lowest organic carbon values. Somewhat higher values are found in the light olive gray lutites abounding on eastern Cascadia Abyssal Plain and in Blanco Valley, while the highest organic carbon values occur consistently in the

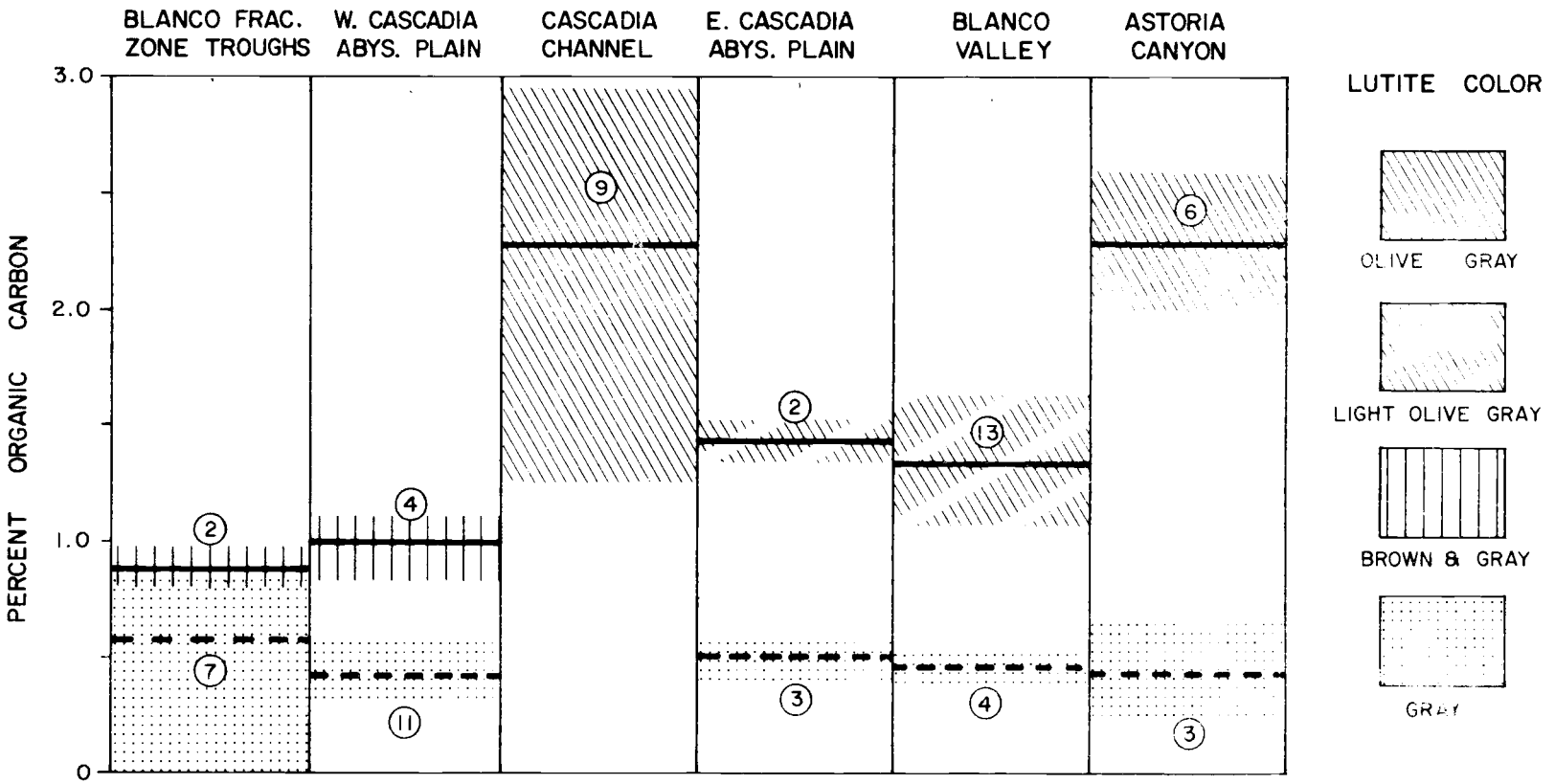

Figure 27. Percent organic carbon in lutites which are typical of the various deep-sea environments for late Pleistocene and postglacial intervals. The mean values for the late Pleistocene (heavy dashed line) and the postglacial (heavy solid line) intervals are indicated for each environment. The stippled areas and the lined areas show the typical lutite present in each environment and time interval as well as the range of values for organic carbon content. Circled numbers indicate the number of samples analyzed. Data for Astoria Canyon from Carlson (1968).

olive gray lutites which dominate the postglacial stratigraphic sections of both Astoria Canyon and Cascadia Channel.

The thick olive gray lutite layers in Cascadia Channel, being of turbidity current origin, again interrupt the regional trends displayed by the lutites with their high organic carbon content. In contrast, the thin gray lutite layers, which cap the turbidity current deposits and represent hemipelagic sedimentation, have much lower organic carbon values (Figure 28). These values are more directly comparable with those of the Cascadia Abyssal Plain lutites and conform with the regional organic carbon values (compare Figure 28 with Figure 27).

Several factors influence the regional distribution of organic carbon content in the postglacial deep-sea lutites. Gross (1967) concluded that a variation in rate of destruction of organic matter is the dominant factor accounting for the regional distribution, and that the rate of destruction of organic matter is largely controlled by the dissolved oxygen concentration in the bottom water. Gross based his conclusions on the following: 1) there appears to be a slight association between the high organic carbon values for the lutites on the continental slope and the depth of the oxygen minimum; 2) the primary production in the surface waters off Oregon and

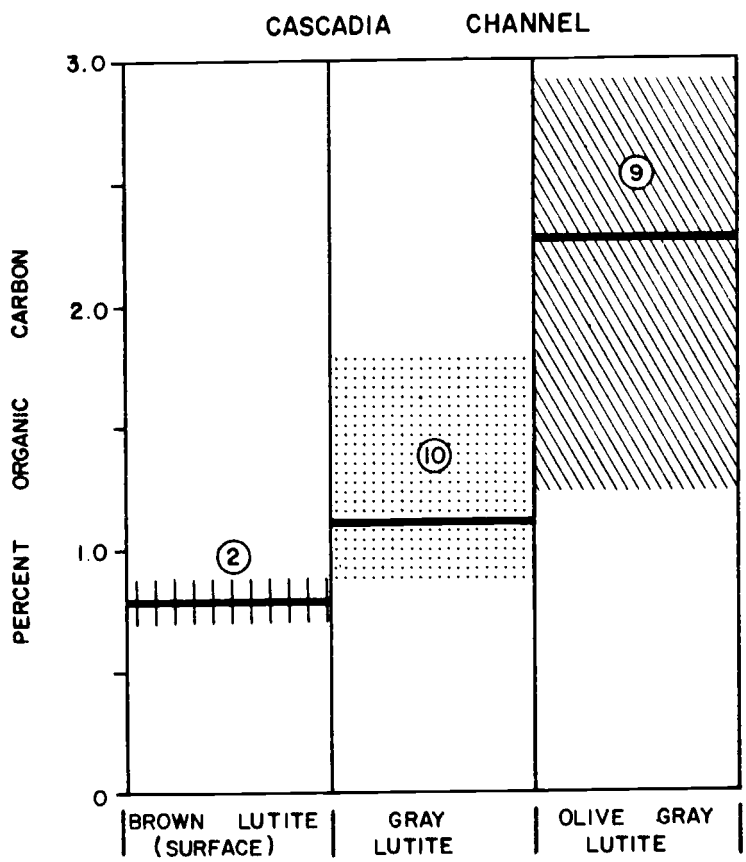

Figure 28. Percent organic carbon in the different postglacial lutites present in Cascadia Channel. The mean value (heavy line), range of values (lined or stippled area) and number of samples analyzed (circled) are given for each lutite. Data for the gray lutite in Cascadia Channel from Griggs, Kulm and Carey (1968).

Washington is essentially uniform (Anderson, 1964); and 3) no appreciable amount of organic matter is being contributed to the ocean by rivers (assumed by Gross).

Data gathered in this study suggest that Gross's assumption of a lack of significant contribution of organic matter from rivers is erroneous; higher concentrations of plant fibers are present in the coarse fractions of lutites which also have higher organic carbon values (compare Figures 27 and 28 with Tables 7 and 8, respectively). Thus, an appreciable amount of the organic matter in the lutites plant material which was brought to the ocean by rivers, and the general offshore decrease in organic carbon content of the postglacial lutites (Figure 27) may primarily be controlled by proximity to the continent; those deep-sea environments closer to the continent may receive proportionately more organic matter settling through the water column than those farthur away from the land area.

The rate of sediment accumulation also plays an important role in determining the organic carbon content of the sediments. Emery (1960, p. 228-230, 265-266) has shown that the highest concentration of organic matter in marine sediments occurs under optimum conditions of neither too rapid nor too slow a rate of deposition of detrital sediments. A very slow rate of detrital deposition results in extensive destruction of the organic matter by biological activity, or non-biological oxidation, or both, before it is buried sufficiently

to be protected from such destruction. In contrast, a very rapid rate of deposition results in the dilution or masking of organic matter. In the postglacial section off Oregon, the organic carbon content in the lutites generally decreases with a decrease in sedimentation rate (compare Figure 27 with Figure 12); this relationship suggests that extensive destruction of the organic matter by biological activity and non-biological oxidation, a consequence of slow burial (low sedimentation rate), is more important than dilution resulting from the rapid influx of lithogenous components.

In Cascadia Channel, the high organic carbon content of the olive gray lutites, deposited by turbidity currents, is a residual trait. The sediments comprising these layers were originally deposited closer to the continent under conditions which produce lutites with high organic carbon content. Subsequently, when these organic-rich sediments were re-transported and rapidly deposited by turbidity currents at their present depositional sites in the Channel, their inherently high organic carbon values were preserved. The rapid deposition and burial of these sediments apparently prohibited appreciable loss of the organic material by the destructive processses which act on organic matter at the sediment-water interface. In contrast, the thin hemipelagic gray lutite layers, which cap each turbidity current deposit in the Channel and have low organic carbon values, accumulated slowly and therefore did

permit sufficient time for much of the organic matter to be destroyed prior to burial.

Late Pleistocene versus Postglacial Organic Carbon Content

Unlike the postglacial lutites, there is no apparent regional trend in organic carbon content in the late Pleistocene lutites. In all the physiographic environments, these older sediments consistently have low organic carbon values which average around 0.5 percent (Figure 27). These values generally are from two to five times lower than those of the postglacial sections in the same environments. The most striking difference occurs in Astoria Canyon where the organic carbon content of the postglacial lutites is five times higher than that of the late Pleistocene lutites (Figure 27).

Although some destruction of organic matter continues after burial (Emery, 1960, p. 228-230), the low organic carbon values in the late Pleistocene lutites cannot be attributed solely to the progressive destruction of organic matter with time. If the low organic carbon values in the older lutites were solely due to continued destruction after burial, the values should decrease gradually with depth in the core. However, as demonstrated in cores from Blanco Valley (Figure 29), an abrupt decrease in organic carbon content occurs at the late Pleistocene-postglacial boundary which was

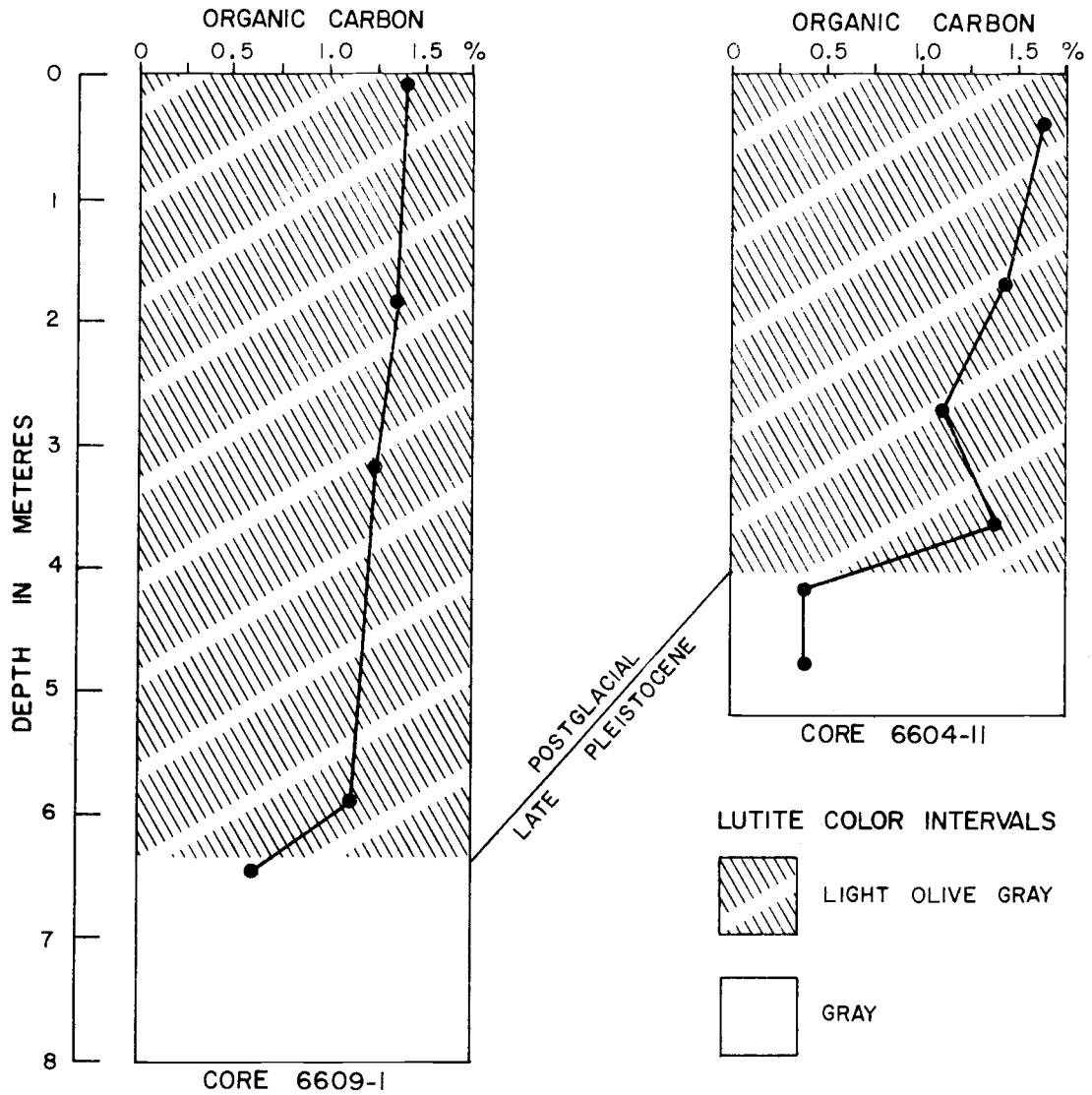

Figure 29. Percent organic carbon in lutites from late Pleistocene and postglacial stratigraphic sections of selected cores from Blanco Valley.

previously established on the bases of faunal stratigraphy and lutite color differences. Since the late Pleistocene rate of sedimentation off Oregon is about six times higher than that of postglacial time (Chapter VI), it is possible that the low organic carbon values in the older lutites are chiefly the result of dilution. Assuming that the organic contribution was similar to the present day input, the larger influx of continental lithogenous material during the late Pleistocene would be sufficient enough to dilute or to mask the organic carbon content in the lutites and thus account for the stratigraphic difference in organic carbon.

Effect of Organic Matter on Lutite Color

An inverse relationship exists between the areal pattern of brown (surface) lutite thickness (Figure 8) and the organic carbon content in the postglacial lutite section; that is, as the organic carbon content increases, the thickness of the brown lutite layer decreases. No consistent time boundary is associated with the lower limit of the brown lutite to suggest that it is a discrete sedimentation unit representing a change of environmental conditions or sediment source. The brown lutite also has no unique clay mineral, grain size, or coarse fraction composition.

Oxidation-reduction potential (Eh) analyses, run on three trip-weight cores (Figure 30) immediately after they were brought aboard

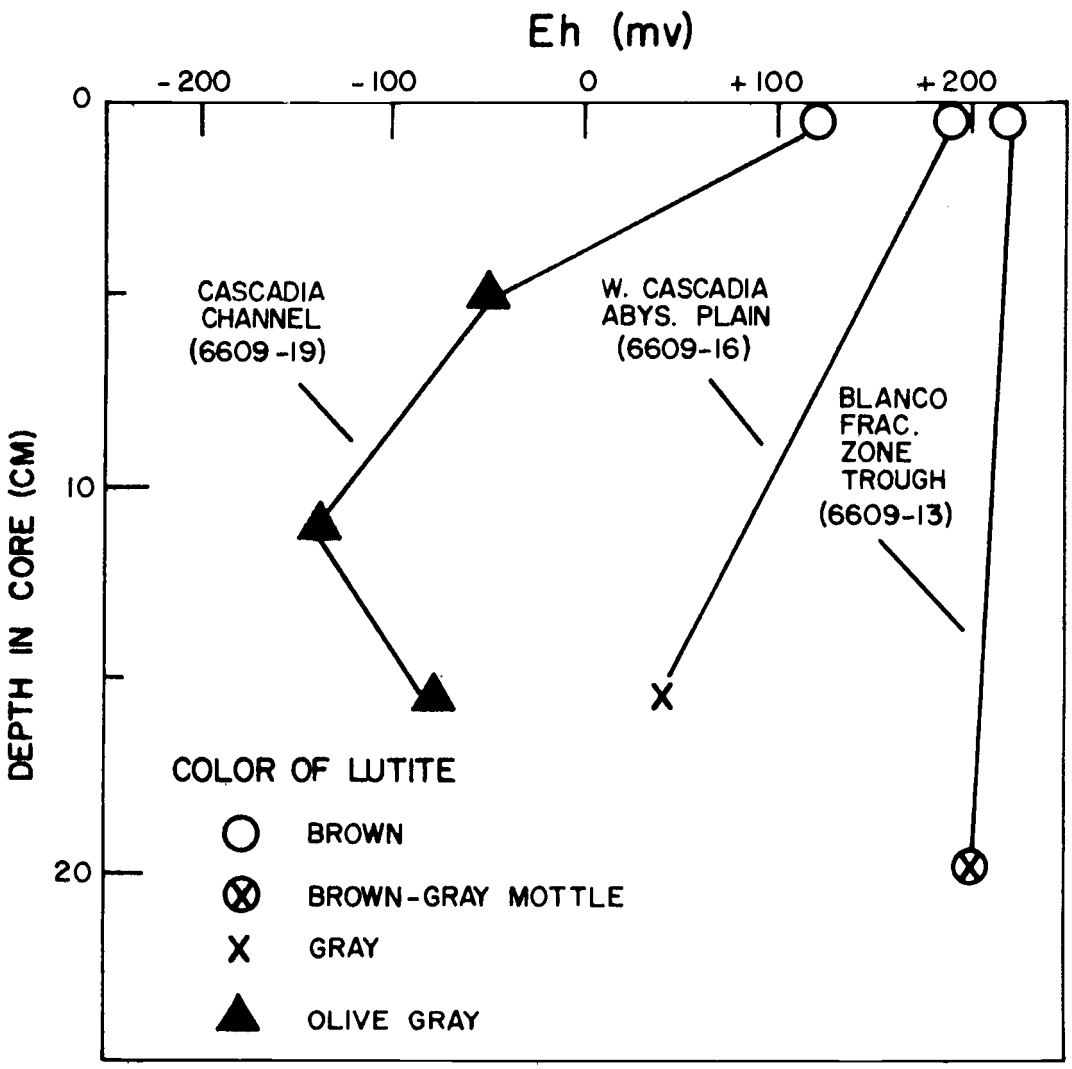

Figure 30. Eh values in selected trip-weight cores as a function of variety of lutite and of depth in core.

ship, show that the brown lutite always has a high positive Eh value (aerobic conditions).[3] The Eh values generally decrease towards negative values with depth in all cores; this decrease is not a linear function of depth but rather it is associated with a change in lutite color. Negative Eh values (anaerobic conditions) are present in the olive gray lutite of Cascadia Channel (core 6609-19) at depths of 5, 12, and 16 cm below the sediment-water interface. In contrast, on western Cascadia Abyssal Plain (core 6609-16) the gray lutite, 15 cm below the interface, still has a slightly positive Eh value. An even higher positive Eh value is recorded at a depth of 20 cm below the interface for the gray and brown mottled lutite in core 6609-13 from a Blanco Fracture Zone trough.

The chief cause of the shift from positive to negative Eh values and the development of reducing conditions at depth in marine sediments is believed to be the oxidation of organic matter which exhausts the supply of oxygen dissolved in the interstitial waters, and,

---

[3] Because Eh depends on the ratios of the concentrations of the oxidized and reduced forms of many chemical systems in the sediment, the state of equilibrium, temperature, pH, and other factors (ZoBell, 1946), little use can be made of absolute measured values; however, Emery (1960, p. 264-267) found that Eh generally decreases from positive to negative values with depth in marine sediments; the depth of zero Eh is closely identified with the first appearance of hydrogen sulfide and can be used as an approximate indicator of the replacement by hydrogen sulfide of dissolved oxygen in the interstitial water, and thus of a change from aerobic to anaerobic conditions.

because of the absence of burrowing animals below a certain depth in the sediment, new supplies of oxygen are not made available (Emery, 1960, p. 265-266). Since brown lutites are only found at or near the surface in the oxidized zone, they most likely reflect oxidizing conditions and the state of oxidation of iron compounds in the surface sediments.

The association of decreasing thickness of the brown lutite layer with increasing organic carbon content in the underlying lutites suggests that the dissolved oxygen in the interstitial waters is more rapidly depleted in lutites with a higher organic carbon content. This rapid depletion of oxygen results in a thinner surface layer in which strong oxidizing conditions can prevail. Furthermore, it appears that, with burial and subsequent shift to anaerobic conditions, the state of oxidation of iron compounds changes; this change results in the disappearance of the brown color. With the elimination of the brown masking color, the lutites become gray, light olive gray, or olive gray. Of the lutite characteristics examined in this study (clay mineralogy, grain size and coarse fraction composition, percent calcium carbonate and organic carbon), the color of the lutite below the brown surface layer seems to depend mainly on the amount of organic matter (organic carbon) present in the sediment. Those lutites with a high organic content become olive gray; those with intermediate quantities turn light olive gray, and those with lower

amounts change to gray (see Figure 27 for comparison of organic carbon content to lutite color).

Along the course of Cascadia Channel the brown lutite layer at the surface is very thin and in places possibly even absent (Figure 8). When the brown lutite layer is present, its organic carbon content is much lower than that of the underlying olive gray lutite layers of turbidity current origin but very similar to that of the hemipelagic gray lutite layers which cap each turbidity current deposit (Figure 28).[4] This similarity of organic carbon content between the brown and the gray lutites implies that the brown surface layer represents the present-day period of hemipelagic sedimentation since the last episode of turbidity current activity in the Channel.

---

[4]As shown in Figure 28, the organic carbon values for the brown lutite (surface) are slightly lower than those for the gray lutite (subsurface). This slight discrepancy is probably due to regional variations in environmental conditions affecting the sections of the Channel that were sampled. The brown lutite samples are from two cores west of Cascadia Gap (6509-25A, 6609-19), while all ten gray lutite samples are from cores in the south-trending section of Cascadia Channel that transects Cascadia Abyssal Plain along 127° W longitude.

XI. SUBMARINE VOLCANISM AND TECTONISM ASSOCIATED WITH SEA-FLOOR SPREADING

The concept of sea-floor spreading has offered a reasonable explanation for the origin of oceanic rises and ridges and the tectonics of the sea floor (Hess, 1962; Vine and Matthews, 1963; Vine and Wilson, 1965; Wilson, 1965; Vine, 1966). The nature of the movements on transverse offsets of the ridges and rises, the tectonically active and young crests, the high crestal heat flow, and the symmetric magnetic anomalies all can generally be accounted for by this concept.

Magnetic anomaly patterns in the northeastern Pacific Ocean (Raff and Mason, 1961) indicate that the north-northeast trending Juan de Fuca and Gorda Ridges are axes perpendicular to which the sea floor is spreading and material is being added to the crust (Vine, 1966). The Blanco Fracture Zone, which connects these two ridges, forms a major west-northwest transecting interruption in the pattern of magnetic anomalies and is the site of considerable seismic activity (Hurley, 1960; McManus, 1965). This activity most likely results from crustal adjustments to stresses caused by the expansions and differential movements of the juxtaposed blocks forming the flanks of the two ridge systems (Wilson, 1965; Vine, 1966).

Volcanism Associated with Sea-Floor Spreading along Gorda Ridge

The grain size, clay mineral, heavy mineral, and light mineral analyses of the deep-sea sedimentary deposits from the Blanco Fracture Zone-Gorda Ridge transition area (cores 6601-1, 6609-6, -8 in Plate 1) indicate that this area is receiving fine terrigenous sediment through hemipelagic sedimentation processes and coarse volcanic debris from local submarine sources. There is no direct evidence as to the age of the volcanic activity which ultimately produced the debris. Unaltered volcanic sediments are present in both the late Pleistocene and the postglacial stratigraphic sections of the area. However, it is reasonable to assume that the activity was fairly recent (no earlier than the Pleistocene Epoch). Most likely, the activity is associated with the growth and expansion of the young crestal zone of the Gorda Ridge.

Greenstones in the Blanco Fracture Zone

Unstratified angular sand- to pebble-size greenstone fragments, set in a matrix of hemipelagic sediment (greenstone lutite; see discussion in Chapter IV), are present in a core (6604-6) from one of the Blanco Fracture Zone troughs (Figure 31; Plate 1). The angular fragments are of local origin and most likely represent accretion of

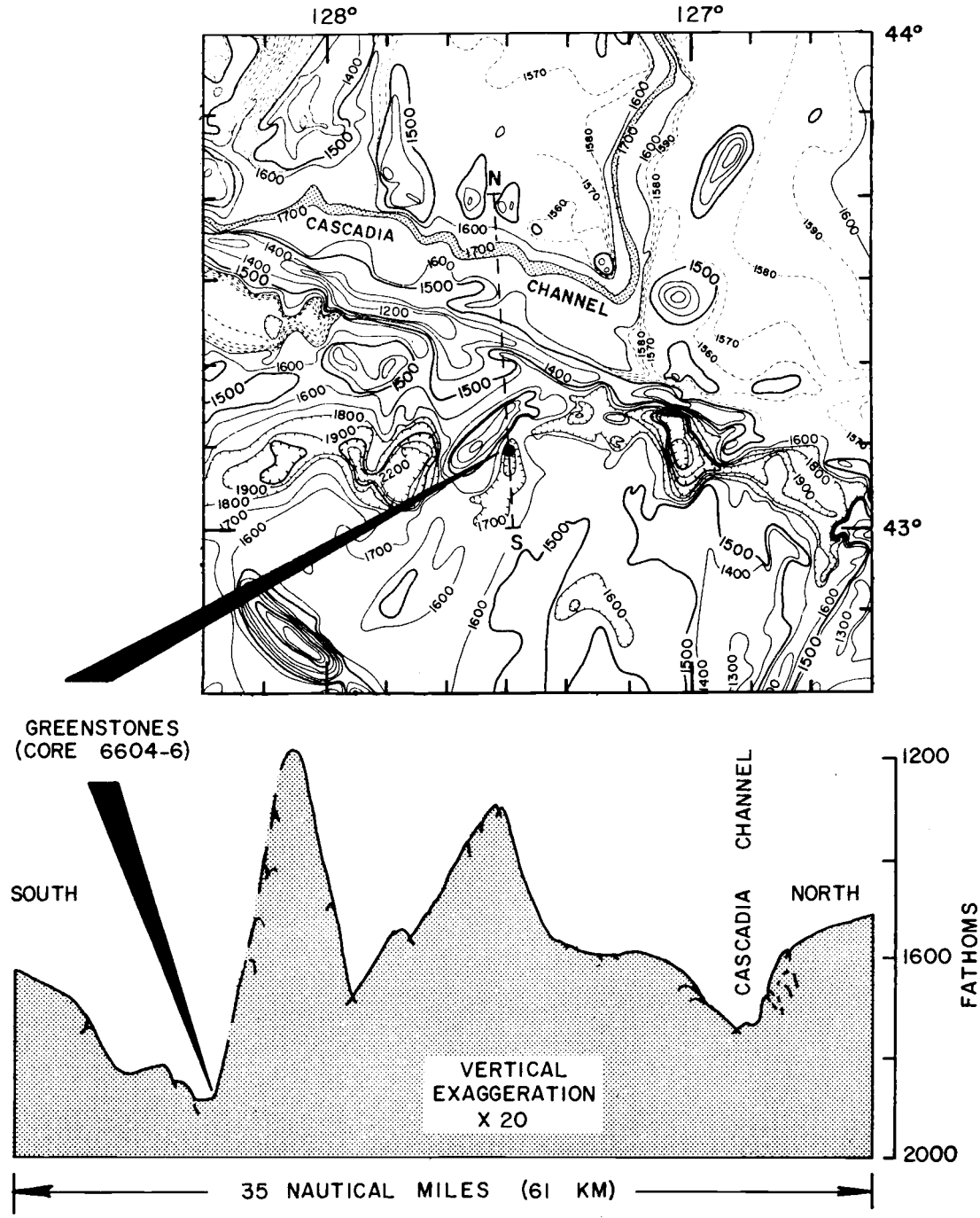

Figure 31. Bathymetric map and PDR profile of the Blanco Fracture Zone showing the location of core 6604-6 containing greenstones.

debris from the northwest wall (average slope 11°) of the trough.

Melson (1967) examined six representative samples of these greenstone fragments and concluded that they are mainly derived from submarine volcanic flows of fine- to medium-grained basalts and porphyritic olivine basalts (see Appendix 2 for complete sample descriptions). Some fragments have typical greenschist facies mineralogy (epidote, chlorite, actinolite, and partially albitized plagioclase microlites and phenocrysts; replacement of olivine by chlorite and of augite by actinolite), although others show little clear cut metamorphic alteration. Melson (1967) also noted that the greenstone assemblage from the Blanco Fracture Zone is very similar to the greenstone assemblage from the 22°N area of the Mid-Atlantic Ridge (Melson and van Andel, 1966).

The occurrence of metamorphosed rocks (greenstones) has been documented from the Carlsberg Ridge in the Indian Ocean (Cann and Vine, 1966) as well as from the Mid-Atlantic Ridge (Melson et al., 1966; Melson and van Andel, 1966). Their presence is attributed to regional metamorphism of the lower part of a gradually thickening crust, followed by uplift and tectonic displacement of the overburden (Melson and van Andel, 1966; van Andel and Bowin, 1968). Van Andel and Bowin (1968) postulate that in the more rapidly spreading sea floor areas (>2.0-2.5 cm/year), plastic flow will occur closer to the sea floor and perhaps even to the sea floor itself; but where the

spreading rate is slower, the upper level of the crust will respond by brittle fracturing, underthrusting, and extensive surfacial structural rearranging which would expose the metamorphosed rock sections.

Since the Gorda Ridge appears to be spreading at a rate of 1.0 cm/year (van Andel and Bowin, 1968), surficial structural rearrangement in the vicinity is to be expected. The location and the original igneous nature of the greenstones in the Blanco Fracture Zone trough suggest that they represent older crestal basalt flows of Gorda Ridge which were later buried, metamorphosed and displaced to the northwest by subsequent flows and spreading along the crest of the ridge. It is inferred that vertical displacement exposed the metamorphosed basalt flow on the wall of the trough, and fragments of the material are now accreting on the bottom of the trough along with finer grained hemipelagic sediments.

Uplift North of Cascadia Gap

Uplift of the abyssal hilly area north of Cascadia Gap is suggested by the stratigraphic sequence observed in core 6609-20 (Figure 32). The lower portion of the 850-cm long core consists of cyclic units of irregularly graded terrigenous sand-silt layers capped with gray lutite layers. These cyclic units imply slow hemipelagic sedimentation frequently interrupted by rapid

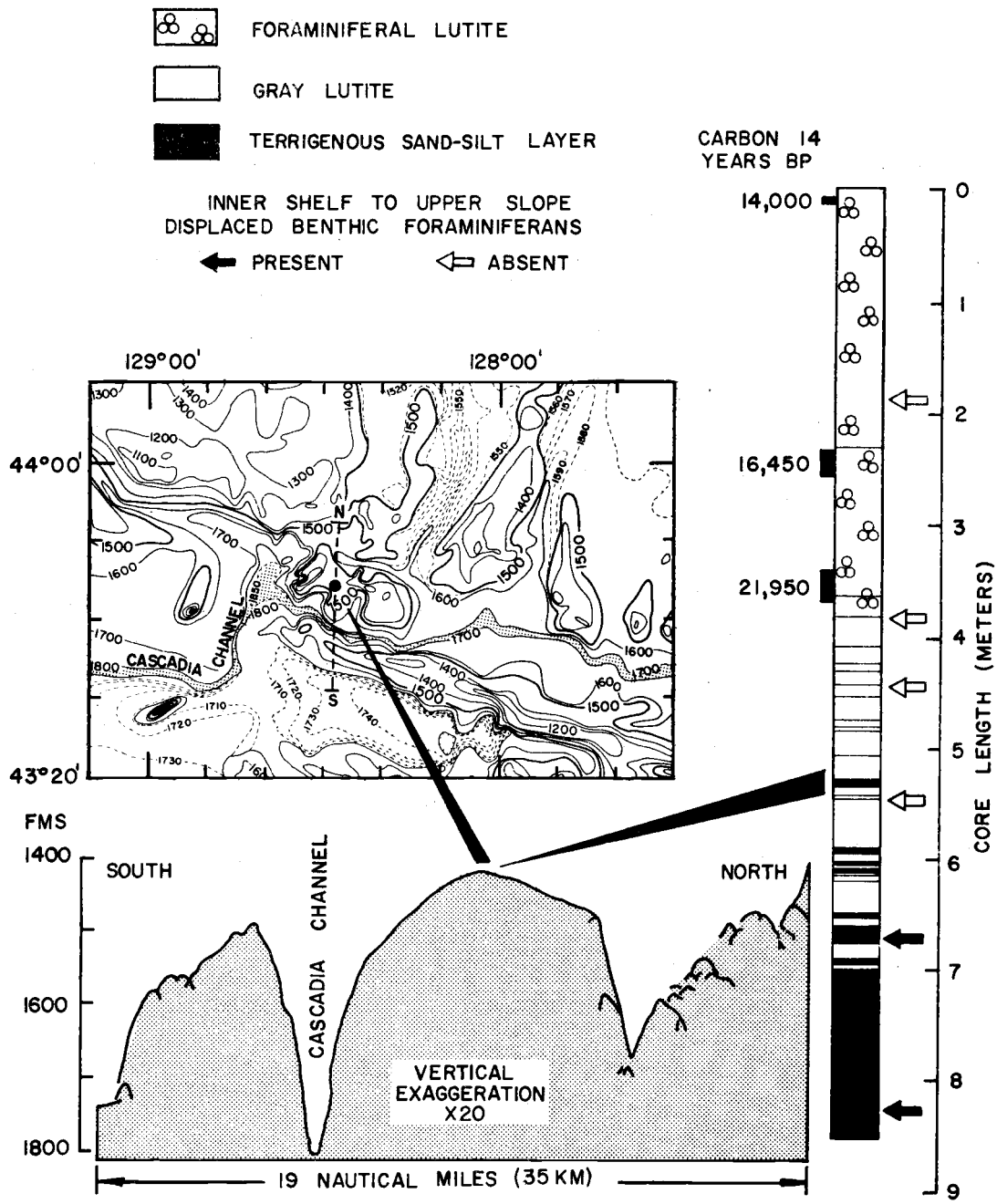

Figure 32. Sediment description of core 6609-20, and bathymetric map and PDR profile of the location of the coring station on the submarine hill north of Cascadia Gap. See Table 9 for species of displaced benthic foraminiferans present in terrigenous sand-silt layers.

discontinuous turbidity current deposition. The terrigenous sand-silt layers have heavy mineral assemblages indicative of Columbia River origin (Figure 17). These layers generally become progressively thinner up the core and are absent in the upper portions. The upper portion of the core generally consists of foraminiferal lutite interbedded with occasional gray lutite layers. Radiocarbon dates indicate that the entire stratigraphic sequence is of late Pleistocene age, except for a very thin postglacial layer (2 cm thick) of brown lutite which caps the core. This thin layer indicates a very slow present-day rate of sediment accumulation.

Two of the lowermost and thickest terrigenous sand-silt units in the core contain displaced benthic foraminiferans that are indigenous to inner shelf to upper slope environments (Figure 32; Table 9). The majority of the displaced species are characteristic of an inner shelf assemblage. Four other thin terrigenous sand-silt layers higher in the core do not contain displaced benthic species.

The entire stratigraphic sequence in core 6609-20 suggests that the hilly area was gradually uplifted and thus became progressively more inaccessible to turbidity currents and their resultant deposits. Assuming that the terrigenous sand-silt layers near the bottom of the core were deposited at the present sea floor depths surrounding the hill, a minimum uplift of 250 fathoms (460 m) is implied for this area. Furthermore, providing that no hiatus in

Table 9. Displaced benthic foraminiferans in terrigenous sand-silt layers of core 6609-20 from a submarine hill north of Cascadia Gap. Water depth at coring station is 1420 fathoms (2600 m). Identification by Fowler (1968).

INNER SHELF SPECIES (0-27 fms) (0-50 m)

Buliminella elegantissima

Cibicides lobatulus

Elphidium incertum clavatum

Elphidium incertum incertum

Elphidium magellanicum

Elphidium microgranulosum

Quinqueloculina stalkeri

MIDDLE SHELF SPECIES (27-55 fms) (50-100 m)

Nonionella japonica

Nonionella labradorica

Nonionella miocenica

OUTER SHELF-UPPER SLOPE SPECIES (80-140 fms) (150-250 m)

Bolivina pacifica

Trifarina angulosa

Uvigerina juncea

UPPER SLOPE SPECIES (110-275 fms) (200-500 m)

Bolivina bicostata

Bolivina spissa

Epistominella pacifica

deposition has occurred, sedimentation rate extrapolations based on radiocarbon dates suggest that this amount of uplift took place during the last 25,000 to 30,000 years BP.

Local Subsidence in Cascadia Channel

Very recent tectonic movements may be inferred where the axis of Cascadia Channel is depressed 70 fathoms (128 m) just west of Cascadia Gap (Figure 5). As previously discussed, the postglacial sediments in Cascadia Channel, both upchannel and downchannel from the depression, are mainly turbidity current deposits. Apparently, upon entering the Channel, the turbidity currents generally remained within its confines. Portions of the current loads, at least in early postglacial time, were transported through Cascadia Basin and out west onto Tufts Abyssal Plain by way of Cascadia Gap. However, the surface brown lutite (hemipelagic sediment) in the segment of the Channel west of the depression is much thicker than that to the east (Figure 8). This thicker unit implies that the last few turbidity current flows may not have passed beyond the presently depressed portion of the Channel. Postglacial rates of sediment accumulation in the Channel also abruptly decrease beyond the depression (Figure 12). Within the depression itself, a very high rate of sediment accumulation is evident; the last three turbidity current flows have piled up a minimum of 860 cm of sediment. In other portions of the

Channel, individual flow units are typically less than 100 cm thick. It is thus evident that this depression is functioning as a sediment trap and has temporarily cut off the flow of sediment through Cascadia Channel out onto Tufts Abyssal Plain to the west.

Mazama ash (Chapter V), which was transported by turbidity currents, is present in substantial percentages both upchannel and downchannel from the depression. Since deposits containing the ash are known to be younger than 6600 years BP (Nelson et al., 1968), it is reasonable to infer that this graben-like structure formed during the past 6600 years.

XII. SUMMARY OF GEOLOGIC HISTORY

Late Pleistocene and postglacial sedimentation in the deep-sea environments off Oregon has been controlled mainly by paleoclimatic conditions, eustatic sea level fluctuations, and submarine physiography. Mechanisms of sediment transport, proximity to sediment sources, and influx of debris from different sources also influenced the nature of the sediments. To a certain extent, the submarine volcanic eruptions in the Blanco Fracture Zone-Gorda Ridge transition area, and the eruption of Mt. Mazama, all within the time interval studied, have affected the character and the distribution of the deep-sea sediments, off Oregon.

The relative abundances of radiolarians and planktonic foraminiferans deposited in the deep-sea sediments off Oregon appear to have responded to climatic variations during late Pleistocene and postglacial time (Figures 9, 10, 33). Greater production of planktonic foraminiferans compared to radiolarians seems to have occurred during glacial advances, while radiolarians are relatively more abundant during times of glacial retreat. The greater abundance of calcium carbonate in the late Pleistocene sediments compared to those of the postglacial interval (Figures 14, 33) suggests that the rate of production of planktonic foraminiferans is greatly influenced by climatic conditions. It appears that the stratigraphic

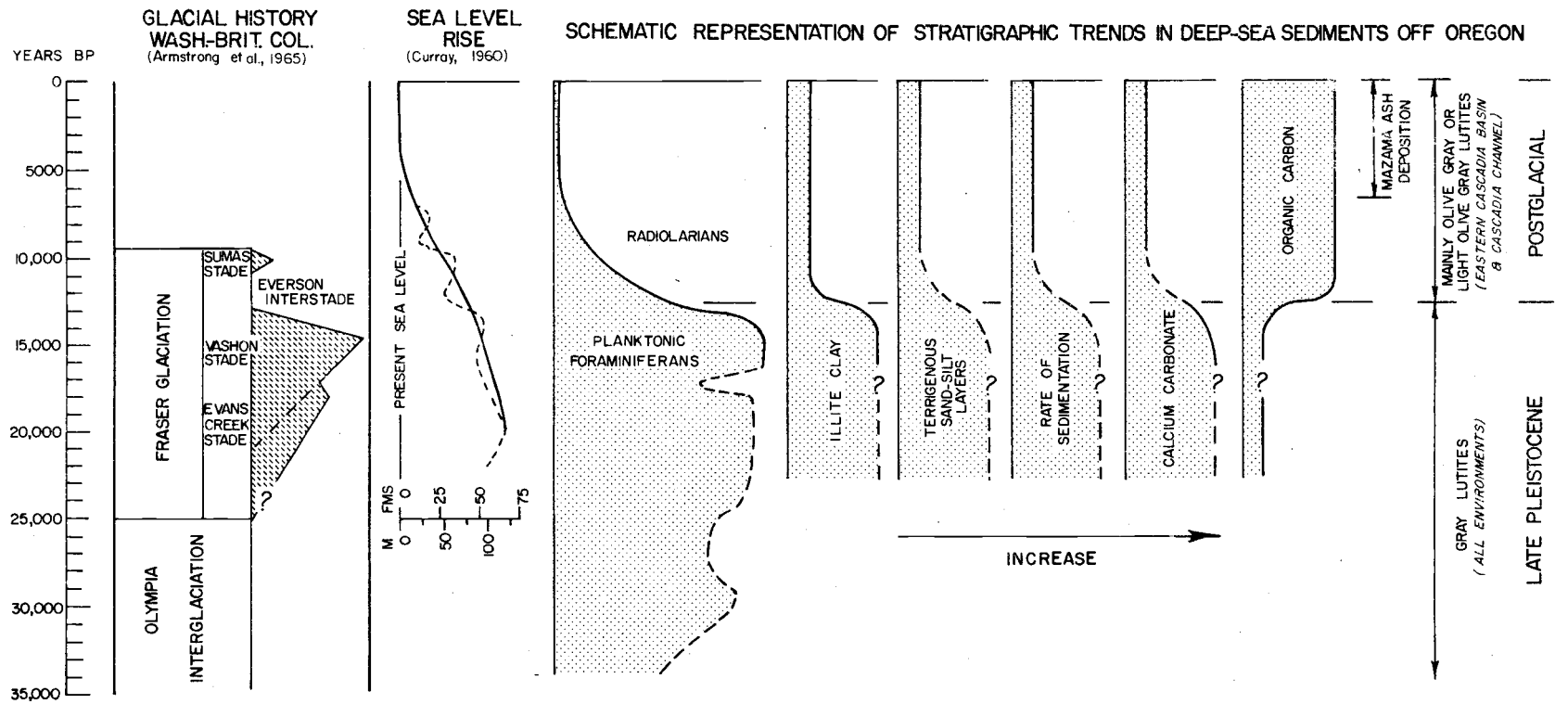

Figure 33. Summary of significant late Pleistocene and postglacial sediment characteristics for the deep-sea environments off Oregon and their relationship to the rise of sea level and the glacial history of southwestern British Columbia and northwestern Washington.

variations in relative abundances of the two groups of planktonic organisms are the result of a somewhat constant production rate of the radiolarians, while the production rate of planktonic foraminiferans oscillated considerably. The concept suggested by Arrhenius (1963) and by Nayudu (1964a) seems to offer a reasonable explanation for the observed stratigraphic variations in the abundance of planktonic foraminiferans: the high productivity of planktonic foraminiferans during glacial times may have been caused by intensified atmospheric and oceanic circulation which presumably mixed more nutrient-rich subsurface water with the surface water.

Some similarities are evident in the climatic events recorded in the deep-sea planktonic foraminiferan-radiolarian stratigraphy and in the late Wisconsin glacial advances and retreats of Cordilleran glacier ice as defined by Armstrong et al. (1965) for the Puget Lowlands of southwestern British Columbia and northwestern Washington (Figure 33). In this region, a non-glacial episode (Olympia Interglaciation) started at least 36,000 years BP and continued until 25,000 years BP when the Cordilleran glacier ice advanced into the northern part of the Lowlands. This advance signified the start of Fraser Glaciation. The deep-sea faunal stratigraphy off Oregon generally indicates a period of moderate glacial conditions during the Olympia Interglaciation, but there is also indicated a possible glacial advance of small magnitude from

approximately 31,000 to 28,000 years BP that is not recorded in the Puget Lowlands. Fraser Glaciation reached its maximum extent in the Lowlands after 15,000 years BP, but a slight recession is evident both in the deep-sea faunal stratigraphy and in the continental glacial stratigraphy from about 18,000 to 16,000 years BP (Figure 33, between Evans Creek and Vashon Stades). In the deep-sea, the accelerated production of planktonic foraminiferans between 16,000 and 12,500 years BP is reasonably coincidental with the time of maximum glacial advancement during the Fraser Glaciation (Vashon Stade). During the marked recession of the glaciers between 13,00 and 11,000 years BP (Everson Interstade), the relative production of planktonic foraminiferans began decreasing rapidly compared to radiolarians. The most abrupt change in the faunal stratigraphy occurred about 12,500 years BP which is herein considered as the start of postglacial time and sedimentation in the deep-sea environments.

The slight glacial advance on land at the end of Fraser Glaciation (Sumas Stade) is not noticeably evident in the marine faunal stratigraphy. Instead, the faunal trends indicate that numerous small fluctuations in climate may have occurred between 12,500 years BP and approximately 7000 years BP as the climatic conditions generally approached those of the present time.

Four heavy mineral provinces (A, B, C, and D) are

distinguished in the deep-sea environments off Oregon chiefly on the basis of the CP/H ratio (clinopyroxene/hornblende) and the presence or absence of glaucophane (Figures 17, 18; Table 6). Province A (mean CP/H ratio = 52.0, glaucophane absent) characterizes the Blanco Fracture Zone-Gorda Ridge transition area. The late Pleistocene and the postglacial sediments in this area consist mainly of basaltic glass lutite with some layers of basaltic rubble or sand; all of these deposits suggest that the area is receiving sediment from both continental and submarine sources. The fine-grained debris is chiefly terrigenous and was deposited particle-by-particle as it settled through the water column; whereas, the coarse-grained sediment, which is the by-product of submarine volcanic activity, was derived from local submarine sources. Province B (mean CP/H ratio = 1.7, glaucophane occasionally present) is restricted to the late Pleistocene section of the Vancouver Valley-western Cascadia Abyssal Plain area. The terrigenous sand-silt layers in this area were probably derived from the vicinity of Vancouver Island. Province C (mean CP/H ratio = 1.0, glaucophane absent) occurs in southeastern Cascadia Basinand in Cascadia Channel; the terrigenous sand-silt layers in this province were derived from the Columbia River drainage basin and are found in both the late Pleistocene and the postglacial deposits. The late Pleistocene and the early postglacial terrigenous sand-silt layers in Blanco Valley also have

heavy mineral assemblages indicative of a Columbia River origin. However, most of the terrigenous sand-silt layers in the postglacial section of this valley have heavy mineral assemblages which are included in Province D (mean CP/H ratio = 0.4, glaucophane present) and were derived from the Klamath Mountains (Figure 19).

During the late Pleistocene, coarse detritus from glacial moraines and outwashes from the glaciated areas of Vancouver Island may have been transported southward by turbidity currents moving through Vancouver Valley to western Cascadia Abyssal Plain and Cascadia Channel (Figure 34). Meanwhile, turbidity currents, originating in the vicinity of Astoria and Willapa Canyons, distributed large quantities of coarse debris (terrigenous sand-silt layers) from the Columbia River to the environments of southeastern Cascadia Basin. Turbidity currents, presumably originating near Astoria Canyon, transported large volumes of debris as far south as Blanco Valley by way of Astoria Channel. This large volume of Columbia River sediment seems to have completely masked the more locally derived sediments from the Klamath Mountains which, no doubt, moved across the southern Oregon continental shelf and slope and accumulated in Blanco Valley at the base of the continental slope during the late Pleistocene. Columbia River sediments presumably were transported in large volumes to Tufts Abyssal Plain through Cascadia Gap by way of Cascadia Channel (no direct evidence of

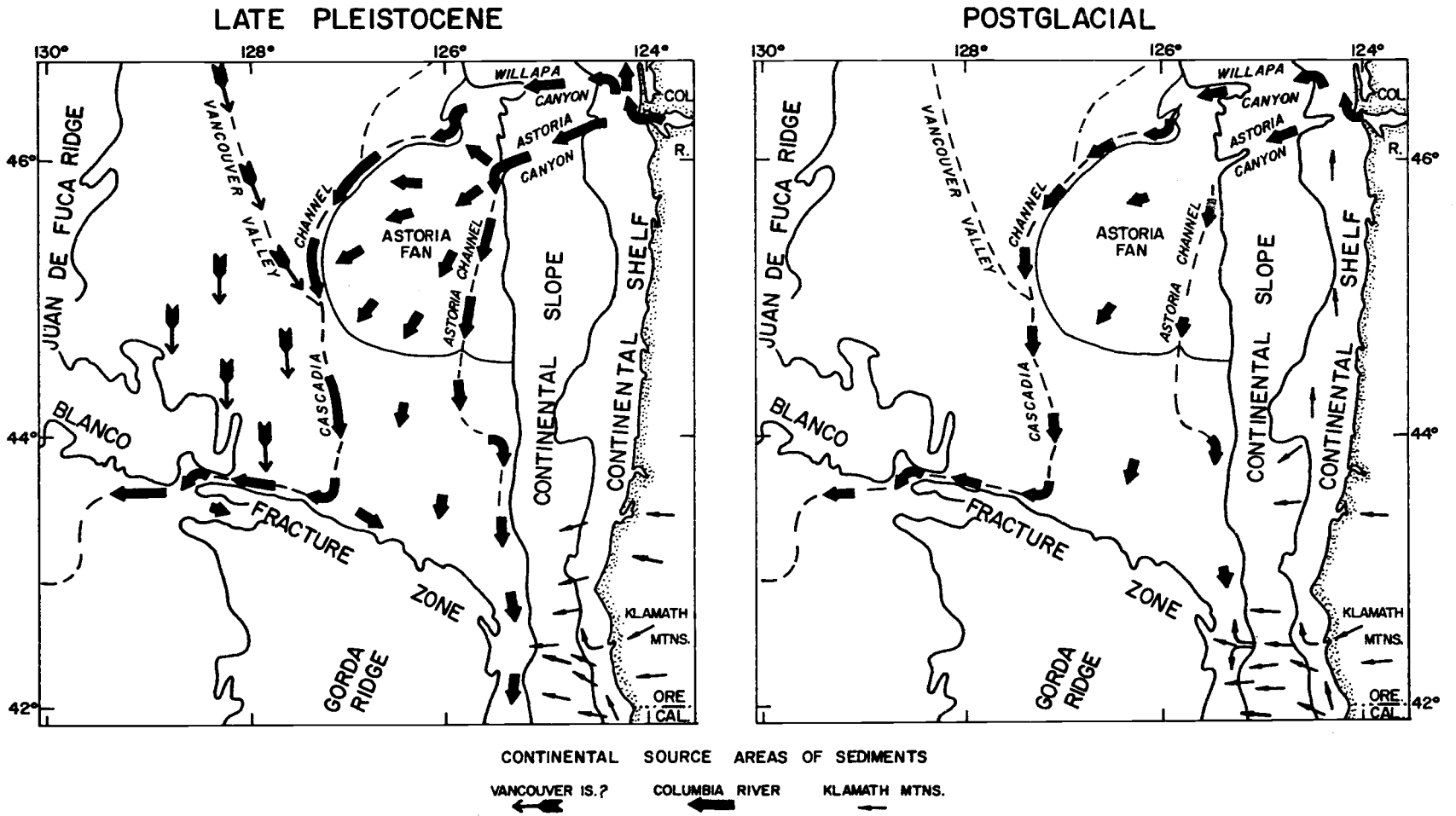

Figure 34. Late Pleistocene and postglacial terrigenous sediment sources and dispersal patterns for bottom-transported sediments in the marine environments off Oregon. The dispersal patterns are chiefly based on heavy mineral data and physiography. The lengths of the arrows for Columbia River sediments indicate the relative magnitude of sediment transport and deposition.

this is available since late Pleistocene sediments were not cored in the Channel). In contrast, the general lack of terrigenous sand-silt layers in the Blanco Fracture Zone troughs and the axial valley of Gorda Ridge indicate that the west-northwest trending ridges of the Blanco Fracture Zone, which form a considerable portion of the southern margin of Cascadia Basin, were (and are still) effective barriers to the bottom transport of coarse sediment to the south out of Cascadia Basin (except through Blanco Valley).

According to Curray (1960, 1961), sea level rose most rapidly from 15,000 to 7,000 years BP in response to the world-wide melting of continental glaciers at the end of the Pleistocene Epoch (Figure 33). Off Oregon, a combination of sea level rise (that resulted in a decrease of stream gradients, the drowning of river mouths, and the widening of the continental shelf area) and a general change in paleoclimatic conditions greatly affected deep-sea sedimentation starting about 12,500 years BP. The overall rate of sedimentation decreased by a factor of about six (Figure 33; Table 2). In addition, proportionately less coarse debris (terrigenous sand-silt layers) reached the deep-sea environments (Figures 13, 33); on the average only nine percent of the postglacial stratigraphic section consists of terrigenous sand-silt layers, while 32 percent of the late Pleistocene section consists of these layers. Apparently, during the present interval (postglacial time), less sediment is reaching the edge of the continental

shelf; this hinders the generation of turbidity currents capable of transporting the coarse-grained sediment to the deep-sea environments.

The postglacial decrease of coarse sediment influx is most striking in the Vancouver Valley-western Cascadia Abyssal Plain area where terrigenous sand-silt layers make up 12 to 93 percent of the late Pleistocene section but are absent in the postglacial section. With the change to postglacial environmental conditions, Vancouver Island sediments, which presumably compose most of the coarse-grained detritus found in the marine area described above, became trapped behind the sills of the long, narrow, glacially-scoured inlets of Vancouver Island, and thus, the seaward flow of coarse sediment from the Island was very effectively cut off (Figure 34).

The clay fractions (<2 microns) of the late Pleistocene lutites contain proportionately more illite (on a comparative basis with montmorillonite and chlorite) than those of the postglacial section (Figures 20, 22, 33); the stratigraphic change in clay composition is abrupt (Figure 23) and, therefore, not believed to be due to marine diagenesis. The difference in clay mineral composition probably reflects climatically controlled changes in the weathering and erosion processes in the Columbia River drainage area which apparently supplied most of the clays in the deep-sea environments off Oregon.

Much of the organic carbon in the deep-sea lutites is in the

form of terrigenous plant fibers. Since the influx of lithogenous material was much higher during the late Pleistocene than at present, it appears that this higher influx masks the organic carbon content in the late Pleistocene lutites. The lower influx of sediments during postglacial time has resulted in a considerably higher organic carbon content (up to five times higher) for lutites above the late Pleistocene-postglacial boundary, especially in eastern Cascadia Basin (Figures 27, 30, 33).

An abrupt change in color of the lutites occurs at the late Pleistocene-postglacial boundary in eastern Cascadia Basin (Figures 9, 33; Plate 1). The lutites of the postglacial interval are generally olive gray or light olive gray, while those in the late Pleistocene section are gray. The color difference appears to reflect mainly the organic carbon content; gray lutite has the lowest value, light olive gray lutite has an intermediate value, while olive gray lutite has the highest organic carbon content (Figure 27).

Although rather abrupt changes occurred in deep-sea sedimentation about 12,500 years BP, there is still some evidence for continued, gradual changes in sedimentation processes while the sea continued to rise and climatic conditions approached those of the present-day. Until at least 8500 years BP, turbidity currents carrying small amounts of coarse Columbia River clastics flowed southward along the base of the continental slope as far as Blanco

Valley (Figure 19). With the continued rise of sea level, the supply of coarse-grained detritus from the Columbia River diminished even more due to restricted offshore transport, and sediments derived more locally from the Klamath Mountains became dominant in the upper portion of the postglacial section in Blanco Valley (Figure 34).

The cataclysmic eruption of Mt. Mazama (6600 years BP) blanketed a very wide area of the northwestern United States with volcanic debris (Fryxell, 1965). No doubt, the land drainage basins were covered with ash, and the rivers began transporting it to the continental shelf almost immediately (Nelson et al., 1968). Turbidity currents began re-distributing the ash to the deep-sea environments (Astoria Canyon, Astoria Fan, Astoria Channel, Blanco Valley, Willapa Canyon, Willapa Channel, and Cascadia Channel), and the lowermost ash-rich horzon in the stratigraphic section can thus be used as an approximate time line of 6600 years BP (Figure 33). The Columbia River is believed to be the largest contributor of Mazama ash although rivers along the southern coast of Oregon most likely contributed the volcanic glass to the sediments in Blanco Valley.

Nelson (1968) has noted a general lack of terrigenous sand-silt layers above one or two ash-bearing layers deposited on Astoria Fan shortly after the Mt. Mazama eruption. This general lack of terrigenous sand-silt layers indicates that there have been few, if

any, turbidity currents on the Fan during the past few thousand years. Carlson (1968) has also reported a similar decrease of terrigenous sand-silt layers in the last few thousand years of sedimentation in Astoria Canyon. However, a somewhat different depositional history is evident for Cascadia Channel and its tributary, Willapa Channel. Numerous terrigenous sand-silt layers are present above the lowermost Mazama ash horizon in these channels (Plate 1). Apparently, even to the present-day, a substantial supply of Columbia River detritus is transported northward by continental shelf currents to Willapa Canyon and ultimately to Cascadia Channel by way of Willapa Channel (Figure 34).

Most of the postglacial sediments cored in Cascadia Channel were deposited by turbidity currents. The stratigraphic sequence consists of cyclic units of relatively thin basal terrigenous sand-silt layers grading up into thick olive gray lutite layers which are capped with thin gray lutites. The thin gray lutite layers are hemipelagic deposits, while both the terrigenous sand-silt layers and the overlying thick olive gray lutite layers were deposited by turbidity currents. Heavy minerals in the terrigenous sand-silt layers indicate that the sediments are of Columbia River origin. The olive gray lutites contain displaced benthic foraminiferans indigenous to continental shelf and slope environments. Several characteristics (clay mineralogy, grain size and coarse fraction compositions, organic carbon content,

and color) of these channel lutites are identical to those of the olive gray lutites in the vicinity of Astoria Canyon and presumably Willapa Canyon (Figures 20, 21, 24 and 27; Plate 1). It appears that the olive gray lutites in the Channel represent sediments that were originally deposited in a particle-by-particle fashion (hemipelagic sedimentation) in the shallower environments closer to the Columbia River. Subsequently, these materials slumped along with the coarser sediments and formed turbidity currents which entered Cascadia Channel through its tributary system and then generally remained within the confines of the Channel. The olive gray lutites in the Channel contrast greatly with those of hemipelagic origin on eastern and western Cascadia Abyssal Plain.

Sometime after the eruption of Mt. Mazama and the subsequent introduction of ash into the deep-sea environments, the flow of sediments along Cascadia Channel out onto Tufts Abyssal Plain was cut off when a structural depression developed in the axis of the Channel west of Cascadia Gap (Figure 5); this depression is now being rapidly filled with turbidity current deposits.

The lutites which comprise approximately 80 percent of the sediment in the deep-sea environments off Oregon generally show (except for Cascadia Channel) a decrease in coarse fraction terrigenous components and grain size composition with increased distance from continental sources (Figures 24, 26). This trend reflects the

nature of hemipelagic sedimentation by which the coarser components settle out of the water column more rapidly than the finer components and thereby are not transported as far laterally.

Variations in the clay mineral percentage compositions of the less than 2-micron fraction of the postglacial lutites show a lateral facies pattern radiating outward into southern Cascadia Basin and the adjoining Blanco Fracture Zone from the Columbia River (Figures 20, 21). The percent of montmorillonite generally decreases while the percent of chlorite, to a greater extent, and of illite to a lesser extent, increase with distance from the point source. The Columbia River appears to introduce clays with a higher percentage of montmorillonite than are introduced by adjacent source areas. Chlorite-rich clays appear to be derived from both far northern (coastal regions of Canada, Alaska, and the Aleutian Islands) and local southern (Klamath Mountains) sources. The higher montmorillonite content of the Columbia River sediments is probably the result of weathering of the vast exposures of volcanic rock in the Columbia River drainage area.

Debris from local submarine volcanic eruptions occurs in the sediments of the Blanco Fracture Zone-Gorda Ridge transition area. Most likely, the volcanic activity is associated with the growth and expansion (sea-floor spreading) of the young crestal zone of Gorda Ridge.

Evidence of crustal adjustments in the Blanco Fracture Zone, which probably result from sea-floor spreading along the Gorda and the Juan de Fuca Ridges, is present in some of the deep-sea deposits. The presence of unstratified angular sand- to pebble-size greenstone fragments in core 6604-6 from one of the Blanco Fracture Zone troughs (Figure 31) is evidence for both submarine regional metamorphism of basalt flows and subsequent vertical displacement which exposed the metamorphosed rocks on the wall of the trough. Fragments of the metamorphosed rocks are now accumulating in the bottom of the trough along with hemipelagic sediments. Uplift of as much as 250 fathoms (460 m) of the abyssal hilly area north of Cascadia Gap in the last 25,000 to 30,000 years BP is inferred from the stratigraphic sequence in core 6609-20 (Figure 32); turbidity current deposits are present at the base of the core, while the upper sections contain only hemipelagic lutites. Even more recent (post Mt. Mazama eruption) tectonic movements may be inferred where the axis of Cascadia Channel is depressed 70 fathoms (128 m) cutting off the flow of sediments to Tufts Abyssal Plain in the vicinity west of Cascadia Gap in the Blanco Fracture Zone.

BIBLIOGRAPHY

Allen, David W. 1966. Clay mineral distribution in Columbia River sediments. Corvallis. 9 numb. leaves. (Oregon State University. Department of Oceanography. Unpublished report in geology of the ocean basins)

Allen, John E. and Robert Van Atta. 1964. Geologic field guide to the northwest Oregon coast. Portland, Portland State College. 30 p.

Anderson, G. C. 1964. The seasonal and geographical distribution of primary productivity off the Washington and Oregon Coasts. Limnology and Oceanography 9:284-302.

Armstrong, J. E., Dwight R. Crandell, Donald J. Easterbrook and J. B. Noble. 1965. Late Pleistocene stratigraphy and chronology in southwestern British Columbia and northwestern Washington. Geological Society of America, Bulletin 76:321-330.

Arrhenius, G. O. S. 1952. Sediment cores from the east Pacific. Reports of the Swedish Deep-Sea Expedition, 1947-1948. 5: 1-227.

Arrhenius, G. O. S. 1963. Pelagic sediments. In: The sea, ed. by M. N. Hill. Vol. 3. New York Wiley. p. 655-727.

Bailey, E. H. and R. E. Stevens. 1960. Selective staining of K-feldspar and plagioclase on rock slabs and thin sections. American Mineralogist 45:1020-1025.

Baldwin, Ewart M. 1964. Geology of Oregon. 2d ed. Eugene, University of Oregon Cooperative Book Store. 165 p.

Bandy, Orville L. 1960. The geologic significance of coiling ratios in the foraminifer Globigerina pachyderma (Ehrenberg). Journal of Paleontology 34:671-681.

Bandy, Orville L. 1967. Foraminiferal definition of the boundaries of the Plesistocene in southern California, U. S. A. In: Progress in oceanography, ed. by M. Sears. Vol. 4. Oxford, Pergamon Press. p. 27-49.

Be, Allan, W. H. 1960. Some observations on Arctic planktonic foraminifers. Contributions from the Cushman Foundation for Foraminiferal Research 11:64-68.

Berger, Wolfgang H. 1967. Foraminiferal ooze: solution at depths. Science 156:383-385.

Biscaye, P. E. 1964a. Distinction between kaolinite and chlorite in Recent sediments by X-ray diffraction. American Mineralogist 49:1281-1289.

Biscaye, P. E. 1964b. Mineralogy and sedimentation of the deep-sea sediment fine fraction in the Atlantic Ocean and adjacent seas and oceans. New Haven. 86 numb. leaves. (Yale University. Geochemistry Technical Report 8)

Biscaye, P. E. 1965. Mineralogy and sedimentation of Recent deep-sea clay in the Atlantic Ocean and adjacent seas and oceans. Geological Society of America, Bulletin 74:803-832.

Bradshaw, John S. 1959. Ecology of living planktonic foraminifers in the North Equatorial Pacific Ocean. Contributions from the Cushman Foundation for Foraminiferal Research 10:25-64.

Bretz, J. Harlan, H. T. V. Smith and George E. Neff. 1956. Bretz's flood hypothesis. Geological Society of America, Bulletin 67:957-1050.

Broecker, W. S., K. K. Turekian and B. C. Heezen. 1958. The relation of deep sea sedimentation rates to variations in climate. American Journal of Science 256:503-517.

Bushnell, David C. 1964. Continental shelf sediments in the vicinity of Newport, Oregon. Master's thesis. Corvallis, Oregon State University. 107 numb. leaves.

Byrne, John V. 1962. Geomorphology of the continental terrace off the central coast of Oregon. Ore Bin 24:65-74.

Byrne, John V. 1963a. Geomorphology of the continental terrace off the northern coast of Oregon. Ore Bin 25:201-209.

Byrne, John V. 1963b. Geomorphology of the Oregon continental terrace south of Coos Bay. Ore Bin 25:149-157.

Byrne, John V. 1966. Effect of the East Pacific Rise on the geomorphology of the continental margin off Oregon. (Abstract) In: Program of the 79th Annual Meeting of the Geological Society of America. San Francisco, 1966. p. 33-34.

Cann, J. R. and F. J. Vine. 1966. An area on the crest of the Carlsberg Ridge; petrology and magnetic survey. Philosophical Transactions of the Royal Society of London, ser. A, 259: 198-217.

Carlson, Paul R. 1968. Marine geology of Astoria Submarine Canyon. Ph. D. thesis. Corvallis, Oregon State University. 259 numb. leaves.

Chambers, David M. 1967. Heavy mineral distribution on the continental shelf off the Rogue River, Oregon. Corvallis. 20 numb. leaves. (Oregon State University. Department of Oceanography. Unpublished report in marine sedimentation)

Conolly, J. R. and M. Ewing. 1967. Sedimentation in the Puerto Rico Trench. Journal of Sedimentary Pettology 37:44-59.

Curl, Herbert, Jr. 1962. Analysis of carbon in marine plankton organisms. Journal of Marine Research 20:181-188.

Curray, Joseph R. 1960. Sediments and history of Holocene transgression, continental shelf, northwest Gulf of Mexico. In: Recent sediments, northwest Gulf of Mexico, ed. by Francis P. Shepard, Fred B Phleger and Tjeerd H. van Andel. Tulsa, America Association of Petroleum Geologists. p. 221-266.

Curray, Joseph R. 1961. Late Quaternary sea level: a discussion. Geological Society of America, Bulletin 72:1707-1712.

Duncan, John R. 1966. Microfaunal evidence for differentiating pelagic and bottom-transported deposits in a piston core from Cascadia Channel. Corvallis. 12 numb. leaves. (Oregon State University. Department of Oceanography. Unpublished report in distribution of modern Foraminifera)

Emery, K. O. 1960. The sea off southern California. New York, Wiley. 366 p.

Emiliani, Cesare. 1966. Paleotemperature analysis of Caribbean cores P6304-8 and P6304-9 and a generalized temperature

curve for the past 425,000 years. Journal of Geology 74: 109-124.

Ericson, David B. 1959. Coiling direction of Globigerina pachyderma as a climatic index. Science 130:219-220.

Ericson, David B., Maurice Ewing, Goesta Wollin and Bruce C. Heezen. 1961. Atlantic deep-sea sediment cores. Geological Society of America, Bulletin 72:193-286.

Fenneman, N. M. 1931. Physiography of western United States. New York, McGraw-Hill. 534 p.

Flint, Richard F. 1957. Glacial and Pleistocene geology. New York, Wiley. 553 p.

Folk, R. L. 1956. The role of texture and composition in sandstone classification. Journal of Sedimentary Petrology 26:166-171.

Fowler, Gerald A. 1968. Assistant Professor, Oregon State University, Department of Oceanography. Personal communication. Corvallis, Oregon.

Fowler, Gerald A. and John R. Duncan. 1967. Late Pleistocene planktonic foraminiferal trends off Oregon. (Abstract) American Association of Petroleum Geologists, Bulletin 51:464.

Fowler, Gerald A. and L. D. Kulm. 1966. A multiple corer. Limnology and Oceanography 11:630-633.

Frerichs, William E. 1968. Pleistocene-Recent boundary in the Indian Ocean. (Submitted to Science)

Fryxell, Roald. 1965. Mazama and Glacier Peak volcanic ash layers: relative ages. Science 147:1288-1290.

Geological Society of America. 1963. Rock color chart. New York. 6 p.

George, W. O. 1924. The relation of physical properties of natural glasses to their chemical composition. Journal of Geology 32: 353-372.

Gibson, W. M. 1960. Submarine topography in the Gulf of Alaska. Geological Society of America, Bulletin 71:1087-1108.

Glenn, Jerry L. 1967. Hydrologist, United States Geological Survey. Water Resources Division. Personal communication. Portland, Oregon.

Goddard, Edwin N. et al. 1965. Geologic map of North America. United States Geological Survey, Washington, D. C.

Gorsline, D. S. and K. C. Emery. 1959. Turbidity-current deposits in San Pedro and Santa Monica Basins off southern California. Geological Society of America, Bulletin 70:279-290.

Griffin, J. J. and E. D. Goldberg. 1963. Clay-mineral distributions in the Pacific Ocean. In: The sea, ed. by M. N. Hill. Vol. 3. New York, Interscience. p. 728-741.

Griggs, Gary B. 1966. Foraminiferal trends in a recent turbidite. Corvallis, Oregon State University, Department of Oceanography. 10 numb. leaves.

Griggs, Gary B. 1968. (Oregon State University, Department of Oceanography. Unpublished research)

Griggs, Gary B., L. D. Kulm and A. G. Carey. 1968. Deep-sea sedimentation and sediment-fauna interaction. (Submitted to Deep-Sea Research)

Grim, Ralph E. 1953. Clay mineralogy. New York, McGraw-Hill. 384 p.

Gross, M. Grant. 1966. Distribution of radioactive marine sediments derived from the Columbia River. Journal of Geophysical Research 71:2017-2021.

Gross, M. Grant. 1967. Organic carbon in surface sediment from the Northeast Pacific Ocean. Oceanology and Limnology 1:46-54.

Gross, M. Grant, Dean A. McManus and Hsin-yi Ling. 1967. Continental shelf sediment, northwestern United States. Journal of Sedimentary Petrology 37:790-795.

Gross, M. Grant and Jack L. Nelson. 1966. Sediment movement on the continental shelf near Washington and Oregon. Science 154:879-881.

Hagenstein, W. D. et al. 1966. Sixth biennial report. Salem, Oregon, State Water Resources Board. 50 p.

Hamilton, Edwin L. 1967. Marine geology of abyssal plains in the Gulf of Alaska. Journal of Geophysical Research 72:4189-4213.

Heezen, Bruce C. and Charles Hollister. 1964. Turbidity currents and glaciation. In: Problems of paleoclimatology, ed. by A. E. M. Nairn. New York, Wiley. p. 99-111.

Heezen, Bruce C., Charles D. Hollister and William F. Ruddiman. 1966. Shaping of the continental rise by deep geostrophic contour currents. Science 152:502-508.

Hess, H. H. 1962. History of ocean basins. In: Petrologic studies: a volume in honor of A. F. Buddington, ed. by A. E. J. Engel, Harold L. James and B. F. Leonard. New York, Geological Society of America. p. 599-620.

Hubert, John F. 1964. Textural evidence for deposition of many western North Atlantic deep-sea sands by ocean-bottom currents rather than turbidity currents. Journal of Geology 72: 757-785.

Hurley, Robert J. 1960. The geomorphology of abyssal plains in the northeast Pacific Ocean. San Diego, California. Scripps Institute of Oceanography, Marine Physical Laboratory. 105 numb. leaves. (SIO Reference 60-7)

Krumbein, W. C. and F. J. Pettijohn. 1938. Manual of sedimentary petrography. New York, D. Appleton-Century. 549 p.

Kulm, L. D. and Gary B. Griggs. 1966. Sedimentation in Cascadia Deep-Sea Channel. (Abstract) Program of the 79th annual meeting of the Geological Society of America, San Francisco, 1966. p. 116.

Kulm, L. D. 1968. Preliminary investigation of the heavy minerals of Oregon and northern California coastal rivers. Corvallis, Oregon State University, Department of Oceanography. (Unpublished research)

Lockett, John B. 1965. Phenomena affecting improvement of the lower Columbia estuary and entrance. In: Proceedings of the Federal Inter-Agency Sedimentation Conference, Jackson, Mississippi, 1963. Symposium 3: Sedimentation in estuaries, harbors and coastal areas. Washington, D.C. p. 626-669. (United States Department of Agriculture. Miscellaneous publication 970)

Lowry, W. D. and E. Baldwin. 1952. Late Cenozic geology of the Lower Columbia River Valley, Oregon and Washington. Geological Society of America, Bulletin 63:1-24.

McManus, Dean A. 1964. Major bathymetric features near the coast of Oregon, Washington and Vancouver Island. Northwest Science 38:65-82.

McManus, Dean A. 1965. Blanco fracture zone, northeast Pacific Ocean. Marine Geology 3:429-455.

McManus, Dean A. 1967. Physiography of Cobb and Gorda rises, northeast Pacific Ocean. Geological Society of America, Bulletin 78:527-546.

Malde, Harold E. 1965. Snake River Plain. In: The Quaternary of the United States, ed. by H. E. Wright, Jr. and D. G. Frey. Princeton, New Jersey, Princeton University Press. p. 255-263.

Mathews, W. H. 1951. A useful method of determining approximate composition of fine-grained igneous rocks. American Mineralogist 36:1279-1294.

Melson, William G. 1967. Associate Curator, Smithsonian Institution, Division of Petrology. Personal communication. Washington, D.C.

Melson, William G., V. T. Bowin, T. H. van Andel and R. Siever. 1966. Greenstones from the central valley of the Mid-Atlantic Ridge. Nature 209:604-605.

Melson, William G. and Tjeerd H. van Andel. 1966. Metamorphism in the Mid-Atlantic Ridge, 22°N Latitude. Marine Geology 4: 165-186.

Menard, H. W. 1953. Pleistocene and Recent sediments from the northeast Pacific Ocean. Geological Society of America, Bulletin 64:1279-1294.

Menard, H. W. 1955. Deep-sea channels topography and sedimentation. American Association of Petroleum Geologists, Bulletin 39:236-255.

Menard, H. W. 1962. Correlation between length and offset on very large wrench faults. The Journal of Geophysical Research 67: 4096-4098.

Menard, H. W. 1964. Marine geology of the Pacific. New York, McGraw-Hill. 271 p.

Menard, H. W. and R. S. Dietz. 1951. Submarine geology of the Gulf of Alaska. Geological Society of America, Bulletin 62: 1263-1285.

Nayudu, Y. R. 1964a. Carbonate deposits and paleoclimatic implications in the northeast Pacific Ocean. Science 146:515-517.

Nayudu, Y. Rammohanroy. 1964b. Palagonite tuffs (hyaloclastites) and the products of post-eruptive processes. Bulletin Volcanologique 27:1-20.

Nayudu, Y. R. and B. J. Enbysk. 1964. Bio-lithology of northeast Pacific surface sediments. Marine Geology 2:310-342.

Nelson, C. Hans. 1968. Marine geology of Astoria Deep-Sea Fan. Ph. D. thesis. Corvallis, Oregon State University. 287 numb. leaves.

Nelson, C. Hans, et al. 1968. Mt. Mazama ash: recognition, distribution and use in northeastern Pacific Ocean. (Submitted to Science)

Olausson, Eric. 1960. Description of sediment cores from the Indian Ocean. Reports of the Swedish Deep-Sea Expedition, 1947-1948. 9:53-88.

Olausson, Eric. 1965. Evidence of climatic changes in North Atlantic deep-sea cores, with remarks on isotopic paleotemperature analysis. In: Progress in oceanography, ed. by M. Sears. Vol. 3. Oxford, Pergamon Press. p. 221-252.

Powers, Howard A. and Ray E. Wilcox. 1964. Volcanic ash from Mount Mazama (Crater Lake) and from Glacier Peak. Science 144:1334-1336.

Raff, A. D. and R. G. Mason. 1961. A magnetic survey off the west coast of North America, 40° N to 52½° N. Geological Society of America, Bulletin 72:1259-1265.

Richmond, Gerald M., et al. 1965. The Cordilleran ice sheet of the northern Rocky Plateau. In: The Quaternary of the United States, ed. by H. E. Wright, Jr. and David G. Frey. Princeton, New Jersey, Princeton University Press. p. 231-242.

Rittenhouse, Gordon. 1943. Transportation and deposition of heavy minerals. Geological Society of America, Bulletin 54:1725-1780.

Royse, Chester F. 1964. Sediments of Willapa Submarine Canyon. Seattle. 62 p. (Washington. University. Department of Oceanography. Technical report no. 111)

Royse, Chester F. 1967. Mazama ash from the continental slope off Washington. Northwest Science 41:103-109.

Rubin, M. and C. Alexander. 1960. Radiocarbon age determination W-858, Crater Lake, Oregon. American Journal of Science Radiocarbon Supplement 2:161.

Runge, Erwin J., Jr. 1966. Continental shelf sediments. Columbia River to Cape Blanco, Oregon. Ph. D. thesis. Corvallis, Oregon State University. 143 numb. leaves.

Russell, Kenneth L. 1967. Clay mineral origin and distribution on Astoria Fan. Master's thesis. Corvallis, Oregon State University. 47 numb. leaves.

Shepard, Francis P. 1954. Nomenclature based on sand-silt-clay ratios. Journal of Sedimentary Petrology 24:151-158.

Shepard, Francis P. 1963. Submarine geology. 2d ed. New York, Harper. 557 p.

Shepard, Francis P. and D. G. Moore. 1960. Bays of central Texas coast. In: Recent sediments, northwest Gulf of Mexico, ed.

by Francis P. Shepard, Fred B Phleger and Tjeerd H. van Andel. Tulsa, American Association of Petroleum Geologists. p. 117-152.

United States Geological Survey. Water Resources Division. 1964. Surface water records of California 1:1-498.

United States Geological Survey. Water Resources Division. 1966. Surface water records of Oregon 1:1-355.

van Andel, Tjeerd H. 1960. Sources and dispersion of Holocene sediments, northern Gulf of Mexico. In: Recent sediments, northwest Gulf of Mexico, ed. by Francis P. Shepard, Fred B Phleger and Tjeerd H. van Andel. Tulsa, American Association of Petroleum Geologists. p. 34-55.

van Andel, Tjeerd H. 1964. Recent marine sediments of the Gulf of California. In: Marine geology of the Gulf of California, ed. by Tjeerd H. van Andel and George C. Shor, Jr. Tulsa, Okłahoma. p. 216-310. (American Association of Petroleum Geologists. Memoir 3)

van Andel, Tjeerd H. and Carl O. Bowin. 1968. The Mid-Atlantic Ridge between 22° and 23° north latitude and the tectonics of mid-ocean rises. Journal of Geophysical Research 73: 1279-1298.

Vine, F. J. 1966. Spreading of the ocean floor: new evidence. Science 154:1405-1415.

Vine, F. J. and D. H. Matthews. 1963. Magnetic anomalies over oceanic ridges. Nature 199:947-949.

Vine, F. J. and J. Tuzo Wilson. 1965. Magnetic anomalies over a young oceanic ridge off Vancouver Island. Science 150:485-489.

Waters, A. C. 1955. Volcanic rocks and the tectonic cycle. In: Crust of the earth, ed. by Arie Poldervaart. New York, Geological Society of America. p. 703-722. (Special Paper 62)

White, William H. 1959. Cordilleran tectonics in British Columbia. American Association of Petroleum Geologists, Bulletin 43: 60-100.

Wilde, Pat. 1965. Recent sediments of the Monterey Deep-Sea Fan. Berkeley. 155 numb. leaves. (California. University. Hydraulic Engineering Laboratory. Technical report HEL-2-13)

Williams, H., F. J. Turner and C. M. Gilbert. 1958. Petrography. San Francisco, Freeman. 406 p.

Wilson, J. Tuzo. 1965. Transform faults, oceanic ridges and magnetic anomalies southwest of Vancouver Island. Science 150:482-485.

ZoBell, C. E. 1946. Studies on redox potential of marine sediments. American Association of Petroleum Geologists, Bulletin 30:477-513.

APPENDIX 1. STATION LOCATIONS AND SAMPLER TYPES

Station number	Latitude (north)	Longitude (west)	Water depth (fms)	Physiographic environment*	Type of sampler**	Core length (cm)
6208-K1	45°08.0'	126°10.0'	1458	AFl	PC	530
6408-A1	45°51.0'	125°39.5'	1180	AFu	PC	295
6408-C3	45°41.8'	126°07.0'	1393	AFm	PC	470
6412-PD6	46°03.5'	125°08.0'	780	ACNf	P	
6501-A3(2)	46°02.1'	126°06.4'	1460	AFm	PC	600
6501-C4(1)	45°30.0'	126°45.0'	1500	AFl	PC	600
6502-PC1	45°58.7'	125°17.0'	960	ACNf	PC	475
6502-PC6	46°14.3'	124°25.0'	225	ACNw	PC	412
6508-K1	46°14.9'	126°23.2'	1487	WCH	PC	630
6508-PC12	46°12.8'	124°42.8'	519	ACNf	PC	520
6508-PC13	46°13.8'	124°46.7'	460	ACNw	PC	190
6508-PC14	46°03.2'	124°45.7'	212	ACNw	PC	230
6508-PC18	46°06.4'	125°14.2'	845	ACNt	PC	305
6509-2	44°40.5'	125°40.0'	1537	AFl	PC	396
6509-4	44°57.0'	125°47.2'	1519	ACH	PC	495
6509-7	44°59.2'	126°31.2'	1520	AFl	PC	274
6509-18	44°39.0'	127°42.5'	1561	CAPw	PC	240
6509-19	44°39.0'	128°10.3'	1530	CAPw	PC	325
6509-20A	44°39.5'	128°50.2'	1528	CAPw	PC	1055
6509-21A	44°03.5'	129°56.2'	1736	TAP	PC	1020
6509-25A	43°35.0'	129°12.0'	1823	CCH	PC	390
6509-26	43°44.5'	127°12.0'	1721	CCH	PC	600
6509-27	44°27.8'	127°13.6'	1696	CCH	PC	580
6509-28	44°27.0'	127°19.8'	1552	CAPw	PC	515
6509-30	44°13.6'	126°16.0'	1584	CAPe	PC	150
6511-5	43°39.5'	125°28.6'	1647	BV	PC	460
6511-69	42°00.4'	125°19.5'	1661	BV	PC	560
6601-1	42°26.0'	125°14.6'	1495	GRm	PC	560
6604-1	43°34.0'	128°44.5'	1820	CCH	PC	70
6604-2	43°08.5'	128°08.0'	2070	BFZt	PC	380
6604-3	43°27.1'	128°11.1'	1741	BFZt	PC	345
6604-4	43°38.5'	127°58.2'	1774	CCH	PC	470
6604-5	43°33.6'	127°32.0'	1732	CCH	PC	30
6604-6	43°10.5'	127°30.0'	1815	BFZt	PC	60
6604-10	43°15.5'	126°23.6'	1595	CAPe	PC	840
6604-11	43°16.9'	125°31.3'	1650	BV	PC	520

*Physiographic environment--ACH = Astoria Channel, ACNf, w, t = Astoria Canyon floor, wall, tributary; AFu, m, l = Astoria Fan upper, middle, lower; BFZt, m, v = Blanco Fracture Zone trough, mountain, valley; BV = Blanco Valley; CAPe, w = Cascadia Abyssal Plain east of Cascadia Channel, west of Cascadia Channel; CCH = Cascadia Channel; CR = Columbia River; GRv, m = Gorda Ridge valley, mountain; RR = Rogue River; TAP = Tufts Abyssal Plain; VV = Vancouver Valley; WCH = Willapa Channel.

**Type of sampler--PC = piston corer; MC = multiple corer; P = pipe dredge; G = grab sampler.

APPENDIX 1. (Continued)

Station number	Latitude (north)	Longitude (west)	Water depth (fms)	Physiographic environment*	Type of sampler**	Core length (cm)
6604-12	42°50.0'	125°24.0'	1651	BV	PC	925
6609-1	42°26.0'	125°14.6'	1656	BV	PC	765
6609-2	42°35.1'	125°40.0'	1646	BV	PC	860
6609-3	42°47.9'	125°58.4'	1534	BFZv	PC	340
6609-4	43°00.8'	126°09.5'	1590	CAPe	PC	370
6609-5	43°33.8'	126°27.5'	1602	CAPe	PC	985
6609-6	42°37.3'	126°49.3'	1820	GRv	PC	40
6609-7	43°12.0'	126°43.5'	1566	CAPe	PC	985
6609-8	43°09.6'	127°02.8'	2343	BFZt	MC	65
6609-10	43°17.0'	127°02.7'	1570	CAPe	PC	355
6609-11	43°31.5'	127°26.0'	1725	CCH	PC	200
6609-13	43°07.2'	127°44.4'	2196	BFZt	PC	910
6609-14A	43°47.6'	127°52.8'	1610	CAPw	PC	835
6609-15	43°51.2'	128°11.2'	1598	CAPw	MC	35
6609-16	43°59.1'	128°22.0'	1515	CAPw	MC	30
6609-19	43°43.2'	128°40.9'	1880	CCH	PC	860
6609-20	43°43.3'	128°29.0'	1420	BFZm	PC	850
6609-21	44°13.2'	128°05.4'	1560	CAPw	MC	50
6609-22	44°11.5'	127°45.0'	1572	CAPw	MC	50
6610-2	46°24.8'	128°13.2'	1505	VV	PC	415
CR-1	46°14.5'	123°55.0'	5	CR	G	---
CR-2	46°13.0'	123°49.0'	6	CR	G	---
CR-3	46°16.0'	123°40.0'	6	CR	G	---
CR-4	46°14.0'	123°25.0'	5	CR	G	---
CR-5	45°54.0'	119°19.0'	10	CR	G	---
CR-6	46°16.0'	123°40.0'	1	CR	G	---
RR-1	42°25.5'	124°24.5'	0	RR	G	---

APPENDIX 2. PETROGRAPHY OF ROCK FRAGMENTS FROM CORE 6604-6: BLANCO FRACTURE ZONE (Analysis performed by William G. Melson, 1967)

Sample

A Greenstone

This rock is derived from medium-grained basalt. The main minerals are chlorite, actinolite, partially albitized plagioclase microlites and augite. The augite is characteristically replaced, in most cases completely, by actinolite. Epidote is restricted to veinlets, typically in euhedral crystals averaging about 0.2 mm long. Sphene and pyrite occur as accessory minerals. Widely spaced shear plains are the only evidence of deformation. This sample is mineralogically similar to samples 3-3 and 3-6 from the Mid-Atlantic Ridge at 22°N latitude (Melson and van Andel, 1966, Tables 5 and 6, Figure 2).

B Glassy basaltic tuff (hyaloclastite)

No clear cut metamorphic alteration is evident. Much of the basaltic glass is clear, light brown sideromelane. Such glass readily breaks down to chlorite, etc. when metamorphosed. The glass fragments are metasomatically rimmed by isotropic alteration products, which were probably formed by alteration of the tuff during or shortly after extrusion, although they may have been produced by submarine weathering. Hyaloclastites like this were also collected in the 22°N latitude area of the Mid-Atlantic Ridge, and have been reported previously from the Pacific Ocean (Nayudu, 1964b).

C Greenstone

This is an unusual specimen in that it consists of two rock types which are fused together along a plain and probably represent a dike contact. One portion of the specimen is a dense, extremely fine-grained metabasalt. The other portion is similar to sample A, the only exceptions being that this portion of sample C has no epidote and more accessory pyrite. After the intrustion of the dike, metamorphism probably did not set in for a long period of time.

D Greenstone

This greenstone sample is derived from porphyritic, medium-grained olivine basalt and contains small phenocrysts of plagioclase (now slightly albitized), augite (fresh) and olivine (now completely replaced by chlorite). Considerable fresh augite and intermediate plagioclase are present; that is, the basalt is only slightly mineralogically reconstituted. Plagioclase phenocrysts are veined by albite and chlorite, which is a common feature in the greenstones from the Mid-Atlantic Ridge (Melson and van Andel, 1966). Only traces of actinolite are present, and chlorite is the dominant neomineral. No epidote is evident.

E Greenstone

This fragment owes its green color to an abundant interstitial montmorillonite group mineral, probably saponite. Except for the saponite, this greenstone is derived from a basalt that has not been strongly altered. Chlorite and actinolite, if present at all, occur in trace amounts. Also, epidote was not noted. This type of alteration is common in some of the Mid-Atlantic Ridge basalts (unpublished research by Melson, 1967). This alteration probably occurs deuterically within thick, unpillowed lava flows, and may not be related to later, regional hydrothermal alterations.

APPENDIX 2. (Continued)

F Greenstone

This fragment is derived from a quenched pillow lava margin. The dominant neomineral is chlorite. Unaltered microlites and small phenocrysts of plagioclase are common.

APPENDIX 3. RADIOCARBON AGE DETERMINATIONS*

Sample number**	Depth in core (cm)	Material dated	Isotopic age (yrs. BP)
6508-PC18-1C14***	205-240	total carbon	18,900 ± 800
6509-20A-1C14	44-57	carbonate carbon	15,200 ± 460
6509-20A-2C14	1001-1016	carbonate carbon	20,400 +1400 -1600
6509-21A-1C14	224-236	carbonate carbon	15,900 ± 230
6509-21A-2C14	575-588	carbonate carbon	27,200 ± 700
6509-25A-1C14	255-290	total carbon	9670 ± 190
6509-27-1C14	485-505	total carbon	4645 ± 190
6601-1-1C14	42-80	carbonate carbon	37,850 +3300 -2300
6601-1-2C14	80-122	carbonate carbon	31,850 +1900 -1500
6601-1-3C14	216-257	carbonate carbon	23,000 ± 800
6601-1-4C14	436-480	carbonate carbon	26,900 +1000 - 900
6609-2-1C14	640-721	total carbon	11,840 ± 210
6609-5-1C14	795-850	organic carbon	28,150 +1500 -1300
6609-5-2C14	880-965	carbonate carbon	30,650 +1250 -1100
6609-7-1C14	520-560	organic carbon	29,300 +1350 -1150
6609-7-2C14	560-610	carbonate carbon	27,900 +1150 -1000
6609-7-3C14	854-934	carbonate carbon	31,050 +1700 -1400
6609-13-1C14	180-225	carbonate carbon	13,150 ± 160
6609-13-2C14	300-335	carbonate carbon	17,050 ± 260
6609-14A-1C14	401-450	carbonate carbon	23,900 +660 -610

*Radiocarbon analyses were made by Isotopes, Inc., Westwood, New Jersey. In most cases, several centimeters of core were required to obtain sufficient carbon for dating; the resulting ages are composites and are assumed to be centered at the midpoints of the samples.

**The sample number consists of three parts: the first two parts refer to the station location number (Appendix 1); the third part identifies the individual sample.

***Data obtained from Carlson (1968).

APPENDIX 3. (Continued)

Sample number**	Depth in core (cm)	Material dated	Isotopic age (yrs. BP)
6609-14A2C14	450-490	organic carbon	24,900 $^{+1150}_{-1000}$
6609-20-1C14	2-7	carbonate carbon	14,850 ± 200
6609-20-2C14	230-250	carbonate carbon	16,450 ± 710
6609-20-3C14	340-365	carbonate carbon	21,950 ± 950

APPENDIX 4. RATES OF TOTAL SEDIMENT ACCUMULATION DETERMINED BY RADIOCARBON DATES

Core number	Physiographic environment*	Depth to late Pleistocene-postglacial boundary (cm)	Sample interval (cm)	Radiocarbon age (years BP)		Rates of Sedimentation (cm/1000 years)			
						Between dated intervals	Average to surface	Postglacial	Late Pleistocene***
6508-PC18	ACNt	160	205-240	18,900	± 800		12		10
6509-20A	CAPw	40	44-57	15,200	± 460	} 184	3		4
			1001-1016	20,400	+1400 -1600		50		121
6509-21A	TAP	40	224-236	15,900	± 230	} 31	14		54
			575-588	27,200	± 700		21		37
6509-25A	CCH	390	255-290	9670	± 190		28	28	
6509-27	CCH	580	485-505	4645	± 190		106	106	
6609-2	BV	721	640-721	11,840	± 200		57	57	
6609-5	CAPe	135	795-850	28,150	+1500 -1300	} 40	29		44
			880-965	30,650	+1250 -1100		30		43
6609-7	CAPe	110	520-560	29,300	+1350 -1150		18		25
			560-610	27,900	+1150 -1000	} 98	21		31
			854-934	31,050	+1700 -1400		29		40
6609-13	BFZt	160	180-225	13,150	± 160	} 29	15		65
			300-335	17,050	± 260		19		34
6609-14A	CAPw	30	401-450	23,900	+ 660 - 610	} 40	18		34
			450-490	24,900	+1150 -1000		19		35
6609-20	BFZm	2	2-7	14,850	± 200	} 146	0.3		1
			230-250	16,450	± 710	} 20 } 49	16		59
			340-365	21,950	± 950		16		37

*Physiographic environment--ACNt = Astoria Canyon tributary; BFZt, m = Blanco Fracture Zone trough, mountain; BV = Blanco Valley; CAPe, w = Cascadia Abyssal Plain east of Cascadia Channel, west of Cascadia Channel; CCH = Cascadia Channel; TAP = Tufts Abyssal Plain.

**Age is assumed to be centered at the midpoint of the sample interval.

***Determined by extrapolation from the radiocarbon dated interval up to the late Pleistocene-postglacial boundary which is assumed to represent an age of 12,500 years BP.

APPENDIX 5. POSTGLACIAL RATES OF SEDIMENTATION*

Core number	Physiographic environment**	Sedimentation rate (cm/1000 yrs.) to core surface from: Lowermost Mazama ash horizon	Sedimentation rate (cm/1000 yrs.) to core surface from: Late Pleistocene-postglacial boundary
6208-K1	AFl	14	18
6408-A1	AFu	14	9
6408-C3	AFm	14	21
6501-A3(2)	AFm	9	8
6501-C4(1)	AFl	--	10
6502-PC1	ACNf	53	--
6502-PC6	ACNw	5	15
6508-K1	WCH	83	--
6508-PC12	ACNf	> 76	--
6508-PC13	ACNw	--	3
6508-PC14	ACNw	--	1
6508-PC18	ACNt	20	13
6509-2	AFl	--	20
6509-4	ACH	32	35
6509-7	AFl	--	8
6509-18	CAPw	--	1
6509-19	CAPw	--	3
6509-20A	CAPw	--	3
6509-21A	TAP	--	3
6509-25A	CCH	26	--
6509-26	CCH	>92	--
6509-27	CCH	> 77	--
6509-28	CAPw	--	3
6509-30	CAPe	--	> 12
6511-5	BV	27	--
6511-69	BV	44	--
6604-1	CCH	>11	--
6604-2	BFZt	--	7

*Rates were established by extrapolation to the surface from the lowermost horizon containing Mazama ash (assumed age is 6600 years BP) and the late Pleistocene-postglacial boundary (assumed age is 12,500 years BP). Where minimum rates (>) are presented, neither of the known time horizons were penetrated, and the indicated rate was determined by assuming that the base of the core represented either the lowermost Mazama ash horizon or the Late Pleistocene-postglacial boundary, depending upon which was most appropriate for the core in question.

**Physiographic environment--ACH = Astoria Channel; ACNf, w, t = Astoria Canyon floor, wall, tributary; AFu, m, l = Astoria Fan upper, middle, lower; BFZt, m, v = Blanco Fracture Zone trough, mountain, valley; BV = Blanco Valley; CAPe, w = Cascadia Abyssal Plain east of Cascadia Channel, west of Cascadia Channel; CCH = Cascadia Channel; GRv = Gorda Ridge valley; TAP = Tufts Abyssal Plain; VV = Vancouver Valley; WCH = Willapa Channel.

APPENDIX 5. (Continued)

Core number	Physiographic environment**	Sedimentation rate (cm/1000 yrs.) to core surface from: Lowermost Mazama ash horizon	Sedimentation rate (cm/1000 yrs.) to core surface from: Late Pleistocene-postglacial boundary
6604-3	BFZt	--	4
6604-4	CCH	> 71	--
6604-10	CAPe	--	10
6604-11	BV	33	32
6604-12	BV	100	--
6609-1	BV	65	52
6609-2	BV	62	57
6609-3	BFZv	27	--
6609-4	CAPe	--	7
6609-5	CAPe	--	11
6609-6	GRv	--	> 3
6609-7	CAPe	--	9
6609-8	BFZt	--	5
6609-10	CAPe	--	6
6609-11	CCH	> 30	--
6609-13	BFZt	--	13
6609-14A	CAPw	--	2
6609-15	CAPw	--	2
6609-16	CAPw	--	2
6609-19	CCH	>130	--
6609-20	BFZm	--	0.2
6610-2	VV	--	1

APPENDIX 6. PERCENTS OF THE TOTAL THICKNESS OF LATE PLEISTOCENE AND POSTGLACIAL CORE SECTIONS CONSISTING OF TERRIGENOUS SAND-SILT LAYERS

Core number	Physiographic environment*	Postglacial		Late Pleistocene	
		Total thickness of section (cm)	% terrigenous sand-silt layers in section	Total thickness of section (cm)	% terrigenous sand-silt layers in section
6208-K1	AFl	222	13.5	300	6.7
6408-A1	AFu	108	0.0	190	21.8
6408-C3	AFm	265	16.2	55	70.8
6501-A3(2)	AFm	100	58.0	200	27.0
6501-C4(1)	AFl	120	28.3	65	48.6
6502-PC1	ACNf	470	10.6	---	---
6502-PC6	ACNw	190	8.5	140	13.6
6508-K1	WCH	631	88.5	---	---
6508-PC12	ACNf	500	6.6	---	---
6508-PC13	ACNw	40	2.5	180	14.4
6508-PC14	ACNw	12	0.0	213	32.0
6508-PC18	ACNt	175	4.6	125	4.0
6509-2	AFl	250	4.8	80	43.7
6509-4	ACH	430	25.6	65	83.0
6509-7	AFl	100	11.0	170	31.2
6509-18	CAPw	15	0.0	220	75.0
6509-19	CAPw	43	0.0	280	58.6
6509-20A	CAPw	40	0.0	1000	14.6
6509-21A	TAP	40	0.0	975	18.4
6509-25A	CCH	397	15.8	---	---
6509-26	CCH	605	7.8	---	---
6509-27	CCH	580	22.9	---	---
6509-28	CAPw	40	0.0	470	12.0
6509-30	CAPe	150	23.8	---	---
6511-5	BV	463	1.7	---	---
6511-69	BV	560	1.8	---	---
6604-1	CCH	70	51.3	---	---
6604-2	BFZt	90	0.0	285	0.0
6604-3	BFZt	50	8.0	295	5.8
6604-4	CCH	470	6.6	---	---
6604-5	CCH	29	10.4	---	---
6604-6	BFZt	60	0.0	---	---
6604-10	CAPe	120	0.2	710	5.1
6604-11	BV	401	0.2	120	33.3
6604-12	BV	928	3.1	---	---

*Physiographic environment--ACH = Astoria Channel; ACNf, w, t = Astoria Canyon floor, wall, tributary; AFu, m, l = Astoria Fan upper, middle, lower; BFZt, m, v = Blanco Fracture Zone trough, mountain, valley; BV = Blanco Valley; CAPe, w = Cascadia Abyssal Plain east of Cascadia Channel, west of Cascadia Channel; CCH = Cascadia Channel; GRv, m = Gorda Ridge valley, mountain TAP = Tufts Abyssal Plain; VV = Vancouver Valley; WCH = Willapa Channel.

APPENDIX 6. (Continued)

Core number	Physiographic environment*	Postglacial		Late Pleistocene	
		Total thickness of section (cm)	% terrigenous sand-silt layers in section	Total thickness of section (cm)	% terrigenous sand-silt layers in section
6609-1	BV	630	7.9	140	60.0
6609-2	BV	720	3.2	140	23.8
6609-3	BFZv	340	0.1	---	---
6609-4	CAPe	90	1.1	282	1.5
6609-5	CAPe	135	6.7	997	12.5
6609-6	GRv	40	0.0	---	---
6609-7	CAPe	111	0.9	885	33.6
6609-8	BFZt	65	0.0	---	---
6609-10	CAPe	70	77.0	285	80.1
6609-11	CCH	200	0.0	---	---
6609-13	BFZt	160	0.0	750	0.0
6609-14A	CAPw	30	0.0	800	16.0
6609-15	CAPw	20	0.0	15	40.0
6609-16	CAPw	30	0.0	---	---
6609-19	CCH	860	2.0	---	---
6609-20	BFZm	2	0.0	843	32.7
6610-2	VV	12	0.0	400	93.0

APPENDIX 7. PERCENT BY WEIGHT OF TOTAL CARBON, ORGANIC CARBON AND CALCIUM CARBONATE IN SELECTED SAMPLES

Sample number*	Depth in core (cm)**	Water depth (fms)	Physiographic environment***	Age+	Sediment type++	% total carbon	% organic carbon	% $CaCO_3$
6509-20A-7	318	1528	CAPw	LP	GL	0.62	0.55	0.58
-27	634	1528	CAPw	LP	GL	2.03	0.35	13.99
-37	784	1528	CAPw	LP	Gl	0.63	0.23	3.33
-43	824	1528	CAPw	LP	GL	0.52	0.23	2.42
-48	891	1528	CAPw	LP	GL	1.59	0.37	10.16
-50	963	1528	CAPw	LP	GL	0.60	0.46	1.17
-52	1001	1528	CAPw	LP	GL	2.94	0.55	19.91
6509-25A-18	0	1823	CCH	PG	BL	0.87	0.85	0.17
-11	255	1823	CCH	PG	OL	1.35	1.21	1.17
6509-26- 36	0	1721	CCH	PG	OL	2.91	2.89	0.17
-32	210	1721	CCH	PG	OL	2.81	2.81	---
-14	485	1721	CCH	PG	OL	2.26	2.16	0.83
6509-28-8	253	1552	CAPw	LP	TS	0.60	0.39	1.75
5	442	1552	CAPw	LP	TS	0.57	0.34	1.92
6	515	1552	CAPw	LP	GL	1.15	0.40	6.52
6511-5-1	0	1647	BV	PG	LOL	1.78	1.43	0.35
6511-69-9	0	1661	BV	PG	LOL	1.79	1.45	0.34
6601-1-20	0	1495	GRm	PG	VL	0.64	0.64	---
-6	140	1495	GRm	LP	VL	1.50	0.53	8.08
-10	252	1495	GRm	LP	VL	0.82	0.76	0.50
-12	316	1495	GRm	LP	VL	0.57	0.54	0.25
-19	540	1495	GRm	LP	VL	2.63	0.66	16.41
6604-3-15	0	1741	BFZt	PG	BL	0.81	0.81	---
-18	58	1741	BFZt	LP	GL	0.73	0.44	2.42
-6	168	1741	BFZt	LP	GL	0.59	0.11	4.00
-19	226	1741	BFZt	LP	GL	0.70	0.45	2.08
6604-11-2	37	1595	BV	PG	LOL	1.64	1.64	---
-4	167	1595	BV	PG	LOL	1.43	1.43	---
-6	272	1595	BV	PG	LOL	1.43	1.07	3.00
-9	367	1595	BV	PG	LOL	1.50	1.39	0.91

*The sample number consists of three parts: the first two parts refer to the station location number (Appendix 1); the third part identifies the individual sample.

**Depth indicated refers to top of sample interval.

***Physiographic environment--BFZt, m = Blanco Fracture Zone trough, mountain; BV = Blanco Valley; CAPe, w = Cascadia Abyssal Plain east of Cascadia Channel, west of Cascadia Channel; CCH = Cascadia Channel; GRm = Gorda Ridge mountain.

+Age--LP = late Pleistocene; PG = postglacial.

++Sediment type--BL = brown lutite; FL = foraminiferal lutite; GL = gray lutite; LOL = light olive gray lutite; OL = olive gray lutite; VL = basaltic glass lutite; TS = terrigenous sand-silt layer.

APPENDIX 7. (Continued)

Sample number*	Depth in core (cm) **	Water depth (fms)	Physiographic environment ***	Age +	Sediment ++ type	% total carbon	% organic carbon	% $CaCO_3$
6604-11-12	413	1595	BV	LP	GL	0.68	0.40	2.33
-17	481	1595	BV	LP	GL	0.73	0.41	2.67
6609-1-1	0	1656	BV	PG	LOL	1.48	1.39	0.75
-2	184	1656	BV	PG	LOL	1.37	1.34	0.25
-4	322	1656	BV	PG	LOL	1.28	1.23	0.42
-7	595	1656	BV	PG	LOL	1.23	1.11	1.00
-9	643	1656	BV	LP	GL	0.85	0.51	2.83
6609-2-1	0	1646	BV	PG	LOL	1.60	1.60	---
-3	203	1646	BV	PG	LOL	1.36	1.26	0.83
-8	560	1646	BV	PG	LOL	1.24	1.15	0.75
-10	753	1646	BV	LP	GL	0.80	0.46	2.83
6609-3-1	0	1534	BFZv	PG	LOL	1.89	1.39	0.75
6609-4-1	0	1590	CAPe	PG	LOL	1.52	1.52	---
6609-5-1	0	1602	CAPe	PG	LOL	1.58	1.53	0.42
-4	220	1602	CAPe	LP	GL	0.87	0.41	3.83
-7	430	1602	CAPe	LP	GL	1.06	0.51	4.58
-14	954	1602	CAPe	LP	GL	0.94	0.58	3.00
6609-6-1	0	1820	GRv	PG	VL	1.26	1.26	---
6609-7-1	0	1566	CAPe	PG	LOL	1.39	1.34	0.42
6609-8-1	0	2343	BFZt	PG	VL	1.26	1.21	0.42
6609-11-1	0	1725	CCH	PG	OL	1.93	1.84	0.75
-2	98	1725	CCH	PG	OL	2.47	2.31	1.33
6609-13-1	0	2196	BFZt	PG	BL	1.20	0.95	2.08
-3	249	2196	BFZt	LP	GL	2.50	0.81	14.08
-5	410	2196	BFZt	LP	GL	1.16	0.87	2.42
-6	510	2196	BFZt	LP	GL	1.19	0.68	4.25
-7	623	2196	BFZt	LP	GL	1.35	0.80	4.58
6609-14A-1	0	1610	CAPw	PG	BL	0.98	0.82	1.33
-3	185	1610	CAPw	LP	GL	0.71	0.36	2.92
-7	520	1610	CAPw	LP	GL	1.44	0.56	7.33
6609-16-1	0	1515	CAPw	PG	BL	1.46	1.04	3.50
6609-19-1	0	1880	CCH	PG	BL	0.86	0.73	1.08
-9	107	1880	CCH	PG	OL	2.50	2.40	0.83
-11	345	1880	CCH	PG	OL	2.42	2.30	1.00
-16	855	1880	CCH	PG	OL	2.52	2.43	0.75
6609-20-1	0	1420	BFZm	PG	BL	4.45	0.64	31.74
-2	33	1420	BFZm	LP	FL	5.33	0.26	42.23
-13	180	1420	BFZm	LP	GL	0.63	0.51	1.00
-4	322	1420	BFZm	LP	FL	5.08	0.06	41.82
-5	407	1420	BFZm	LP	GL	0.61	0.55	0.50
-6	507	1420	BFZm	LP	GL	2.65	0.48	18.08
-11	670	1420	BFZm	LP	GL	1.09	0.51	4.83
6609-21-1	0	1560	CAPw	PG	BL	1.27	1.02	2.08
6609-22-1	0	1572	CAPw	PG	BL	1.19	1.11	0.67

APPENDIX 8. LIGHT MINERAL DATA FOR TOTAL SAND FRACTION OF SELECTED SAMPLES

Sample number*	Depth in core (cm)**	% sand in sample	Age***	Physiographic environment+	Total grains counted	Percent of light minerals by number: Quartz	K-feldspar	Plagioclase feldspar	Rock fragments	Mica	Colorless volcanic glass	Dark brown volcanic glass	Other++
6508-K1-42	419	28	PG	WCH	495	40	4	11	12	2	31	--	T
6509-4-N345	274	7	PG	ACH	328	37	8	17	30	2	4	--	2
-N352	438	40	PG	ACH	300	38	14	23	24	--	1	--	--
-N355	464	83	PG	ACH	304	23	13	22	41	1	T	--	1
6509-18-5	42	84	LP	CAPw	302	33	11	27	27	1	T	--	1
6509-25A-7	95	2	PG	CCH	304	14	5	13	10	5	52	--	--
-9	232	2	PG	CCH	301	27	10	18	19	14	12	--	--
-17	377	5	PG	CCH	305	19	7	22	25	24	3	--	T
6509-26-21	49	3	PG	CCH	304	25	4	27	31	4	30	--	1
-38	256	25	PG	CCH	309	37	6	14	39	1	3	--	1
-12	463	15	PG	CCH	302	15	3	15	16	6	45	--	T
6509-27-32	202	19	PG	CCH	307	26	7	18	23	1	24	--	1
-33	580	29	PG	CCH	304	26	9	14	26	2	23	--	T
6509-30-9	87		PG	CAPe	309	46	12	17	19	6	T	--	T
-6	125	93	PG	CAPe	312	37	8	31	23	--	--	--	1
6511-5-6	178	T	PG	BV	305	18	3	15	27	1	37	--	--
6511-69-8	524	7	PG	BV	310	35	10	9	43	2	--	--	1
6601-1-20	0	15	PG	GRm	333	--	--	5	5	--	1	88	1
-6	140	23	LP	GRm	300	--	--	29	--	--	--	71	--
6604-1-2	12	3	PG	CCH	305	27	6	14	31	1	21	--	--
-7	45		PG	CCH	304	44	3	20	32	--	1	--	--
6604-3-8	193	1	LP	BFZt	306	2	1	4	3	90	T	T	--
-20	330	T	LP	BFZt	101	26	7	14	48	5	--	--	--
6604-4-3	182	5	PG	CCH	294	11	4	11	14	30	30	--	T
-10	465	9	PG	CCH	307	16	2	16	5	2	59	--	--
6604-5-3	22	2	PG	CCH	366	34	7	20	21	1	17	--	--
6604-10-5	195	1	LP	CAPe	314	30	12	26	31	T	--	--	T
-9	323	2	LP	CAPe	326	25	7	19	18	29	2	--	--

*The sample number consists of three parts: the first two parts refer to the station location number (Appendix 1); the third part identifies the individual sample.

**Depth indicated refers to top of sample interval.

***Age--LP = late Pleistocene; PG = postglacial.

+Physiographic environment--ACH = Astoria Channel; BFZt, m, v = Blanco Fracture Zone trough, mountain, valley; BV = Blanco Valley; CAPe, w = Cascadia Abyssal Plain east of Cascadia Channel, west of Cascadia Channel; CCH = Cascadia Channel; GRv, m = Gorda Ridge valley, mountain; VV = Vancouver Valley; WCH = Willapa Channel.

++Other--diatoms, glauconite, radiolarians and unidentified grains.

"T" denotes less than one percent.

APPENDIX 8. (Continued)

Sample number*	Depth in core (cm)**	% sand in sample	Age***	Physiographic environment+	Total grains counted	Percent of light minerals by number							
						Quartz	K-feldspar	Plagioclase feldspar	Rock fragments	Mica	Colorless volcanic glass	Dark brown volcanic glass	Other++
6604-10-19	745	1	LP	CAPe	371	44	10	19	22	4	1	--	--
6604-11-16	469	1	LP	BV	328	35	9	19	34	1	T	--	--
-18	487	30	LP	BV	325	25	10	29	26	8	2	--	--
6604-12-2	30	6	PG	BV	342	53	3	15	28	--	1	--	T
-12	496	18	PG	BV	316	39	1	13	41	2	3	T	1
-22	879		PG	BV	304	25	5	36	34	1	T	--	--
6609-1-3	267	38	PG	BV	315	32	4	11	46	--	2	--	5
-6	484	32	PG	BV	334	16	6	30	46	1	T	--	T
-10	744	52	LP	BV	305	24	14	21	39	1	--	--	1
6609-2-4	266	14	PG	BV	306	16	7	24	50	1	1	--	1
-14	811	11	LP	BV	314	17	6	30	40	3	5	--	1
6609-3-3	210	T	PG	BFZv	223	22	2	20	39	10	5	--	2
6609-4-3	94	5	PG	CAPe	306	13	9	38	21	18	T	--	1
6609-5-3	120	23	PG	CAPe	307	33	14	25	22	5	1	--	--
-6	420	1	LP	CAPe	304	7	6	9	10	68	--	--	1
-9	636	2	LP	CAPe	300	7	5	10	9	67	--	--	--
-13	910	1	LP	CAPe	335	28	5	18	17	26	5	T	1
6609-6-1	0	45	PG	GRv	304	1	--	9	7	--	--	83	--
6609-7-2	114	1	LP	CAPe	304	14	5	21	27	32	--	--	--
-7	478	T	LP	CAPe	312	2	T	1	1	96	--	--	--
6609-8-2	25	7	PG	BFZt	272	5	2	20	56	3	--	1	13
-3	51	65	LP	BFZt	225	6	--	40	47	T	--	7	--
6609-10-10	105	7	LP	CAPe	325	26	10	25	25	11	1	--	2
-11	276	5	LP	CAPe	311	20	11	25	28	14	1	--	1
6609-11-3	198	1	PG	CCH	302	8	6	20	9	40	16	--	T
6609-14A-2	74	6	LP	CAPw	381	19	13	38	25	4	--	--	1
-12	779	1	LP	CAPw	304	3	1	2	1	90	3	--	--
6609-15-4	29	5	LP	CAPw	327	25	9	23	31	11	1	--	1
6609-19-4	48	3	PG	CCH	403	22	6	28	28	8	5	--	3
-12	444	15	PG	CCH	359	29	6	23	38	3	1	--	T
6609-20-3	170	5	LP	BFZm	330	32	2	16	30	19	--	--	1
-9	585	3	LP	BFZm	304	32	9	22	35	2	--	--	--
-12	835	10	LP	BFZm	415	37	10	20	22	8	2	--	1
6610-2-16	405		LP	VV	315	20	15	24	24	15	1	--	1

APPENDIX 9. HEAVY MINERAL DATA FOR THE SAND FRACTION (62-125 MICRONS) OF SELECTED SAMPLES (Mineral quantities given as percents of total count.)

Mineral data / Sample Number *	6502-PC1-20+++	6502-PC1-22+++	6502-PC1-27+++	6502-PC1-30+++	6508-K1-42	6508-PC12-11+++	6508-PC13-9+++	6508-PC14-8+++	6508-PC18-12+++	6508-4-N345
Depth in core (cm)**	323	347	400	466	419	462	157	93	298	274
Age***	PG	PG	PG	PG	PG	PG	LP	LP	LP	PG
Physiographic environment****	ACNf	ACNf	ACNf	ACNf	WCH	ACNf	ACNw	ACNw	ACNt	ACH
% sand in sample	49	31	56	64	28	22	11	50	38	7
% heavies of sd. frac.	3.3	3.1	6.4	6.1	2.8	3.2	6.3	3.7	3.2	1.1
Total grains counted	196	186	170	151	354	182	288	385	177	65
CP/H ratio+	0.88	0.92	1.14	0.97	1.47	0.68	1.60	1.14	0.51	0.97
Actinolite-Tremolite	1.7	0.5	1.2	1.3	1.4	0.5	1.0	---	---	
Aegirineaugite	---	---	---	---	0.8	---	---	---	---	
Andalusite	---	---	---	---	0.3	---	---	---	---	
Apatite	1.7	0.5	2.4	2.6	---	1.6	---	---	---	
Basaltic Hornblende	2.0	1.6	1.2	2.6	1.7	1.6	0.7	0.5	---	
Biotite	1.7	4.3	3.5	1.3	4.5	5.5	0.7	0.5	6.8	
Chlorite	1.0	0.5	1.8	0.7	2.8	1.6	0.7	0.7	3.4	
Clinopyroxene++	15.3	17.7	19.5	16.6	33.5	14.4	13.9	5.6	14.7	
Clinozoisite-Zoisite	0.5	---	1.2	1.3	2.0	1.6	0.7	0.7	2.8	
Enstatite	6.1	3.8	1.2	1.3	0.9	1.6	1.8	1.2	4.0	
Epidote	1.0	---	3.0	2.0	1.4	3.9	0.3	0.2	1.1	
Garnet	1.0	0.5	2.4	2.6	1.4	3.3	1.8	1.9	6.0	
Glaucophane	---	---	---	---	---	---	---	---	---	
Hematite	1.7	1.6	2.4	2.6	---	---	---	---	---	
Hornblende										
Blue-green	2.6	1.6	1.8	3.3	2.6	2.2	0.7	0.2	3.4	
Brown	3.3	4.3	4.1	5.3	0.6	2.8	1.4	0.2	2.8	
Common	11.7	13.4	11.2	8.6	20.3	16.0	6.6	5.0	22.6	
Hypersthene	6.6	5.9	6.5	7.3	12.8	5.5	7.6	6.6	4.5	
Ilmenite-Magnetite-Chromite	7.1	4.3	8.8	10.3	2.3	5.5	3.8	2.1	4.5	
Kyanite	---	---	---	---	---	---	---	---	---	
Leucoxene	---	---	---	---	0.3	---	---	---	---	
Muscovite	---	---	---	---	0.3	---	---	---	---	
Olivine	1.0	0.5	2.4	2.0	1.1	1.1	---	---	0.6	
Rutile	---	---	---	---	0.6	---	---	---	---	
Sillimanite	---	---	0.6	1.3	0.3	1.1	0.3	---	---	
Sphene	0.5	0.5	1.2	2.0	---	---	1.0	1.2	2.3	
Tourmaline	---	---	---	---	---	---	---	---	---	
Zircon	1.0	0.5	---	0.7	---	---	---	---	0.6	
Other+++	2.2	1.1	1.2	3.3	0.8	3.7	36.7	63.9	2.9	
Rock fragments	12.3	19.4	10.6	10.0	3.1	10.5	14.2	2.8	7.9	
Weathered grains	18.4	17.2	11.8	11.0	4.2	16.0	6.1	6.8	9.0	

APPENDIX 9. (Continued)

Mineral data / Sample Number*	6509-4-N352	6509-4-N355	6509-18-5	6509-18-24	6509-18-25	6509-19-8	6509-25A-7	6509-25A-17	6509-26-21
Depth in core (cm)**	438	464	42	64	198	156	95	377	49
Age***	PG	PG	LP	LP	LP	LP	PG	PG	PG
Physiographic environment****	ACH	ACH	CAPw	CAPw	CAPw	CAPw	CCH	CCH	CCH
% sand in sample	40	83	84	63	49	38	2	5	3
% heavies of sd. frac.	4.2	5.6	11.6	9.1	6.3	6.2	0.9	5.2	1.1
Total grains counted	324	316	346	273	101	247	365	343	55
CP/H ratio+	1.13	1.15	1.70	1.79	1.58	1.6	0.41	0.88	1.12
Actinolite-Tremolite	2.1	2.9	0.9	1.5		0.8	1.4	1.2	
Aegirineaugite	1.2	0.7	---	---		---	---	1.5	
Andalusite	0.3	---	---	---		---	---	0.3	
Apatite	---	---	1.2	---		0.8	---	---	
Basaltic Hornblende	1.2	1.3	0.9	1.5		1.6	0.8	0.9	
Biotite	---	0.7	0.3	2.6		8.9	3.3	3.2	
Chlorite	---	---	0.6	1.5		2.8	0.8	---	
Clinopyroxene ++	33.9	23.0	35.7	43.7		37.0	15.4	21.0	
Clinozoisite-Zoisite	0.9	0.3	0.6	0.4		1.2	0.8	2.3	
Enstatite	1.5	0.7	---	---		0.4	0.8	0.3	
Epidote	3.4	3.9	3.2	2.9		1.2	1.2	1.2	
Garnet	1.5	3.2	2.0	1.5		0.4	1.4	2.0	
Glaucophane	---	---	---	P	P	0.4	---	---	
Hematite	---	1.3	0.9	0.4		0.4	0.3	---	
Hornblende									
Blue-green	5.3	5.1	3.2	2.2		2.0	6.8	4.4	
Brown	3.1	0.7	1.2	1.1		0.4	1.1	0.6	
Common	23.8	14.6	16.6	21.1		20.6	29.6	21.0	
Hypersthene	8.4	8.5	7.2	6.3		4.1	3.6	8.4	
Ilmenite-Magnetite-Chromite	1.8	6.6	10.4	4.0		3.7	1.7	0.6	
Kyanite	---	---	---	---		---	---	0.3	
Leucoxene	---	0.3	0.3	---		---	0.3	---	
Muscovite	---	0.7	---	1.1		0.4	23.1	14.2	
Olivine	0.3	---	2.0	0.4		0.4	0.3	0.3	
Rutile	0.3	0.7	0.9	0.4		1.6	---	---	
Sillimanite	---	0.3	---	---		---	---	---	
Sphene	0.9	1.0	0.6	0.4		1.2	0.6	1.5	
Tourmaline	0.9	---	---	---		---	---	0.6	
Zircon	---	---	0.3	---		0.8	---	---	
Other +++	1.5	0.3	0.9	0.7		2.8	1.4	1.7	
Rock fragments	1.5	9.2	5.8	2.2		3.7	1.4	0.6	
Weathered grains	6.2	14.0	4.3	4.0		2.4	3.8	11.9	

APPENDIX 9. (Continued)

Mineral Data / Sample Number*	6509-26-38	6509-26-12	6509-27-32	6509-27-33	6509-30-9	6509-30-6	6511-5-6	6511-69-8	6601-1-6
Depth in core (cm)**	256	463	202	580	87	125	178	524	140
Age***	PG	PG	PG	PG	PG	PG	PG	PG	LP
Physiographic environment****	CCH	CCH	CCH	CCH	CAPe	CAPe	BV	BV	GRm
% sand in sample	25	1	19	29		93	T	7	23
% heavies of sd. frac.	4.8	1.3	3.0	3.9	4.9	12.2	12.5	5.2	1.3
Total grains counted	321	330	310	301	318	288	114	317	303
CP/H ratio+	1.20	0.89	1.25	1.32	0.94	1.19	0.40	0.30	87.50
Actinolite-Tremolite	1.2	3.9	2.0	3.4	3.4	1.0	4.4	8.8	---
Aegirineaugite	0.3	0.3	1.0	0.3	0.7	0.7	---	0.3	---
Andalusite	0.6	---	---	---	---	---	0.9	---	---
Apatite	---	---	---	---	---	---	---	---	---
Basaltic Hornblende	1.6	0.9	1.9	0.7	---	1.0	---	---	---
Biotite	1.6	3.6	0.3	0.3	0.7	0.7	---	0.3	---
Chlorite	---	---	---	---	---	---	---	0.3	---
Clinopyroxene++	30.6	19.3	26.5	31.3	27.0	34.2	5.3	15.2	57.7
Clinozoisite-Zoisite	1.6	2.1	1.3	2.7	3.1	1.0	0.9	1.9	---
Enstatite	---	0.9	---	1.0	0.3	0.4	---	2.2	---
Epidote	1.9	0.6	1.9	1.7	3.4	3.5	0.9	1.9	---
Garnet	3.4	0.6	1.0	1.3	4.1	7.3	---	1.0	---
Glaucophane	---	---	---	---	---	---	0.9	1.0	---
Hematite	---	---	0.6	---	---	---	---	---	---
Hornblende									
Blue-green	5.0	3.3	4.2	5.3	5.7	4.2	3.5	7.6	0.3
Brown	0.9	2.1	0.3	1.7	2.5	0.4	---	1.9	---
Common	19.9	16.5	17.4	20.1	21.1	25.0	9.6	41.5	0.3
Hypersthene	10.6	4.9	11.0	8.3	3.1	8.3	1.7	1.6	---
Ilmenite-Magnetite-Chromite	2.5	0.9	1.0	0.3	2.2	2.4	3.5	0.3	---
Kyanite	0.3	---	---	---	---	---	---	---	---
Leucoxene	0.9	0.3	0.6	0.3	0.7	0.4	---	---	0.3
Muscovite	---	16.1	1.0	---	---	---	0.9	7.6	---
Olivine	---	---	0.3	0.3	1.0	---	---	---	---
Rutile	---	---	---	---	---	---	---	---	---
Sillimanite	0.3	---	---	0.7	0.3	---	---	---	---
Sphene	1.2	0.3	0.3	1.0	2.5	1.4	---	---	---
Tourmaline	---	---	---	---	0.3	---	---	---	---
Zircon	0.3	---	---	---	0.7	0.4	---	---	---
Other +++	2.5	0.9	1.0	1.0	2.0	0.7	2.6	2.5	---
Rock fragments	---	6.7	7.4	6.0	6.1	3.5	1.7	0.6	36.8
Weathered grains	12.8	15.8	19.0	12.3	9.1	3.5	63.2	3.5	4.6

APPENDIX 9. (Continued)

Mineral data	Sample Number* 6601-1-20	6604-1-1	6604-1-2	6604-3-8	6604-3-20	6604-4-3	6604-4-10	6604-5-3
Depth in core (cm)**	0	0	12	193	330	182	465	22
Age***	PG	PG	PG	LP	LP	PG	PG	PG
Physiographic environment****	GRm	CCH	CCH	BFZt	BFZt	CCH	CCH	CCH
% sand in sample	15	9	3	1	T	5	9	2
% heavies of sd. frac.	5.2	5.2	8.2	1.6	17.8	1.3	1.8	6.4
Total grains counted	234	106	302	244	160	319	312	311
CP/H ratio	66.00	0.63	0.69	0.64	0.96	0.15	0.96	0.90
Actinolite-Tremolite	---		1.6	2.5	1.3	0.3	1.3	2.3
Aegirineaugite	---		0.7	---	---	---	---	0.3
Andalusite	---		0.7	---	---	---	---	0.3
Apatite	---		---	---	---	---	---	---
Basaltic Hornblende	---		0.3	0.4	---	---	1.0	0.3
Biotite	0.3		1.0	2.1	0.6	50.0	---	1.6
Chlorite	---		1.3	---	---	0.3	---	---
Clinopyroxene ++	21.9		27.2	12.3	15.0	1.3	25.7	19.5
Clinozoisite-Zoisite	---		1.3	0.8	0.6	0.3	1.6	0.6
Enstatite	0.3		0.7	0.8	1.3	---	1.0	---
Epidote	---		1.7	0.8	0.6	---	1.3	1.2
Garnet	---		2.0	1.6	3.7	---	0.6	0.6
Glaucophane	---		0.3	0.4	---	0.3	---	---
Hematite	---		0.3	---	2.5	---	---	---
Hornblende								
Blue-green	---		7.7	3.7	5.0	4.1	1.9	3.2
Brown	---		1.3	1.2	1.3	---	1.9	0.3
Common	0.3		31.0	14.3	9.4	4.1	23.5	18.5
Hypersthene	---		9.7	2.5	3.8	---	5.8	4.5
Ilmenite-Magnetite-Chromite	---		0.7	2.0	13.1	1.0	0.6	0.6
Kyanite	---		0.3	---	---	---	---	---
Luecoxene	---		---	0.8	---	---	0.6	---
Muscovite	---		0.3	42.4	---	28.5	2.2	12.9
Olivine	6.9		---	---	0.6	---	---	0.3
Rutile	0.3		---	---	5.6	---	---	---
Sillimanite	---		---	---	---	---	---	---
Sphene	---		0.3	0.4	---	---	1.0	1.0
Tourmaline	---		---	---	---	---	---	0.3
Zircon	---		0.3	0.4	---	---	---	---
Other +++	---		0.3	---	3.1	---	0.6	0.3
Rock fragments	56.5		2.3	0.4	10.0	2.3	5.4	7.7
Weathered grains	13.5		6.7	10.2	22.5	7.5	24.0	23.7

APPENDIX 9. (Continued)

Mineral data	Sample Number* 6604-10-5	6604-10-9	6604-10-19	6604-11-16	6604-11-18	6604-12-2	6604-12-5	6604-12-12	6604-12-22
Depth in core (cm)**	195	323	745	469	487	30	237	496	879
Age***	LP	LP	LP	LP	LP	PG	PG	PG	PG
Physiographic environment****	CAPe	CAPe	CAPe	BV	BV	BV	BV	BV	BV
% sand in sample	1	2	1	1	30	6	5	18	
% heavies of sd. frac.	8.6	3.4	3.2	3.0	1.9	3.9	7.1	3.8	3.9
Total grains counted	335	351	312	319	308	308	343	313	301
CP/H ratio	0.95	0.75	0.67	0.94	0.78	0.32	0.50	0.20	0.34
Actinolite-Tremolite	2.7	2.3	5.1	1.2	4.9	8.1	7.6	8.6	6.3
Aegirineaugite	0.9	0.6	0.6	3.1	1.0	---	---	---	---
Andalusite	---	0.3	---	---	---	---	0.3	0.3	---
Apatite	---	---	---	---	---	---	---	---	---
Basaltic Hornblende	0.6	0.3	8.6	0.6	1.6	0.3	0.6	0.3	0.3
Biotite	0.6	6.6	5.5	1.2	1.3	---	0.6	0.3	0.3
Chlorite	---	---	---	0.3	0.3	---	---	---	0.3
Clinopyroxene ++	30.6	7.7	21.8	27.5	28.0	11.4	21.3	8.0	14.1
Clinozoisite-Zoisite	1.8	0.9	1.0	0.9	2.0	2.9	3.5	3.5	5.0
Enstatite	0.6	---	1.0	0.9	0.7	1.6	2.3	1.6	0.7
Epidote	4.5	---	2.2	2.8	3.6	3.6	1.5	3.5	2.0
Garnet	3.6	---	2.2	3.1	1.0	1.0	0.9	---	---
Glaucophane	---	0.3	---	---	---	0.3	0.3	0.6	---
Hematite	---	---	---	---	---	0.3	---	---	---
Hornblende									
Blue-green	3.6	1.1	5.5	3.1	7.7	9.1	8.2	7.7	11.6
Brown	2.1	1.1	1.0	0.9	2.6	2.3	1.5	2.9	1.3
Common	27.7	8.9	26.9	28.5	26.0	24.7	32.4	29.1	27.9
Hypersthene	2.4	2.6	4.8	7.2	7.2	4.2	1.5	4.8	3.3
Ilmenite-Magnetite-Chromite	2.4	---	1.0	2.8	---	0.7	0.6	1.3	1.0
Kyanite	0.3	---	---	---	0.7	---	---	0.3	---
Leucoxene	0.3	---	---	0.3	0.3	---	---	0.6	0.3
Muscovite	0.9	60.4	12.8	0.6	0.7	1.6	8.7	0.3	---
Olivine	---	---	0.3	0.3	0.3	0.3	---	1.3	---
Rutile	---	---	---	---	---	---	---	---	---
Sillimanite	---	---	---	---	0.3	---	---	---	---
Sphene	1.2	---	1.3	3.5	0.7	---	---	0.6	0.7
Tourmaline	---	---	0.6	0.3	---	---	---	---	---
Zircon	---	---	0.3	0.3	---	---	---	---	0.3
Other +++	1.2	0.9	1.6	1.5	1.3	2.6	0.3	0.3	1.0
Rock fragments	4.5	2.9	2.9	0.9	3.9	7.8	1.2	2.5	7.3
Weathered grains	7.5	3.1	1.6	8.2	3.9	17.2	6.7	21.6	16.3

APPENDIX 9. (Continued)

Mineral data	Sample Number* 6609-1-3	6609-1-6	6609-1-10	6609-2-4	6609-2-7	6609-2-9	6609-2-14	6609-3-3	6609-4-3
Depth in core (cm)**	267	484	744	266	510	670	811	210	94
Age***	PG	PG	LP	PG	PG	PG	LP	PG	PG
Physiographic environment****	BV	BV	BV	BV	BV	BV	BV	BFZv	CAPe
% sand in sample	38	32	52	14			11	T	5
% heavies of sd. frac.	10.2	11.1	4.8	5.9	6.5	7.6	6.8	8.1	2.1
Total grains counted	302	312	408	351	137	76	339	167	307
CP/H ratio	0.44	1.27	1.02	0.43	0.40	0.36	0.63	0.91	0.89
Actinolite-Tremolite	5.5	6.1	1.9	6.8			4.8	4.2	4.5
Aegirineaugite	---	0.3	1.0	0.3			0.3	---	---
Andalusite	1.0	---	0.3	0.3			---	---	---
Apatite	0.3	0.3	1.2	---			---	---	---
Basaltic Hornblende	0.3	---	1.2	0.3			0.3	---	1.0
Biotite	0.6	0.3	1.5	0.6			3.3	7.2	15.7
Chlorite	1.0	0.6	0.7	0.9			0.9	1.2	1.0
Clinopyroxene ++	13.4	34.0	32.9	22.2			26.6	10.8	15.9
Clinozoisite-Zoisite	5.8	0.6	1.5	2.6			1.8	1.8	1.3
Enstatite	0.3	1.0	0.7	0.3			0.3	---	1.0
Epidote	1.2	0.3	1.5	1.7			3.0	1.2	---
Garnet	0.4	0.3	2.2	---			0.6	---	0.7
Glaucophane	1.3	---	---	0.3	P	P	---	---	P
Hematite	0.3	0.3	---	0.3			0.3	---	1.9
Hornblende									
Blue-green	13.5	5.1	6.4	5.7			6.8	1.2	3.6
Brown	1.6	2.3	1.2	0.9			1.2	1.8	0.7
Common	16.3	19.6	25.4	40.1			34.0	9.8	14.0
Hypersthene	3.3	6.4	3.9	3.1			2.1	---	1.6
Ilmenite-Magnetite-Chromite	4.9	3.2	6.1	0.6			2.1	1.2	4.3
Kyanite	1.2	---	---	---			---	---	---
Leucoxene	1.0	0.6	---	---			---	---	0.3
Muscovite	---	---	---	0.3			1.5	5.4	1.0
Olivine	1.3	1.3	0.5	2.6			1.5	---	1.9
Rutile	0.3	0.3	---	---			---	---	1.3
Sillimanite	---	---	---	---			---	---	---
Sphene	---	---	2.5	0.6			0.3	---	---
Tourmaline	---	---	0.5	0.3			---	---	---
Zircon	0.6	---	---	---			---	---	---
Other +++	4.2	1.0	0.7	1.1			1.5	2.4	0.7
Rock fragments	1.0	6.1	2.5	1.4			1.5	12.8	13.6
Weathered grains	19.4	10.0	3.7	6.7			5.3	39.0	14.0

APPENDIX 9. (Continued)

Mineral data	Sample Number* 6609-5-3	6609-5-6	6609-5-13	6609-6-1	6609-7-2	6609-8-2	6609-8-3	6609-10-10	6609-10-11
Depth in core (cm)**	120	420	910	0	114	25	51	105	276
Age***	PG	LP	LP	PG	LP	PG	LP	LP	LP
Physiographic environment****	CAPe	CAPe	CAPe	GRv	CAPe	BFZt	BFZt	CAPe	CAPe
% sand in sample	23	1	1	45	1	7	65	7	5
% heavies of sd. frac.	4.0	3.9	1.9	4.8	2.8	6.2	18.0	3.5	2.7
Total grains counted	317	312	315	301	331	321	301	322	316
CP/H ratio	0.97	0.29	0.89	68.00	1.45	17.80	20.90	1.28	0.96
Actinolite-Tremolite	2.6	1.7	1.6	---	1.2	---	---	2.1	1.3
Aegirineaugite	2.2	0.3	0.3	---	---	---	---	---	0.3
Andalusite	---	---	---	---	0.3	---	---	---	---
Apatite	1.3	---	---	---	---	---	---	0.6	0.3
Basaltic Hornblende	0.3	---	0.3	---	1.2	---	0.3	---	1.0
Biotite	3.5	61.7	53.7	---	9.1	---	---	8.0	12.0
Chlorite	1.3	---	0.3	---	2.7	0.6	---	0.3	2.2
Clinopyroxene ++	29.7	0.7	7.6	22.7	31.3	55.9	62.5	26.1	27.5
Clinozoisite-Zoisite	0.6	---	---	---	0.6	0.3	---	1.2	1.6
Enstatite	0.6	---	0.3	---	0.3	0.9	0.3	0.3	0.6
Epidote	3.1	---	0.3	---	1.5	---	---	0.9	3.2
Garnet	2.2	---	---	---	0.6	---	---	---	1.3
Glaucophane	---	---	---	---	---	---	---	0.3	---
Hematite	---	---	---	---	1.2	---	---	---	1.0
Hornblende									
Blue-green	3.5	---	2.2	0.3	0.9	0.9	1.0	5.9	2.2
Brown	1.9	---	---	---	0.9	1.2	1.7	0.3	0.6
Common	27.6	2.3	6.6	---	19.6	0.9	0.3	14.6	27.3
Hypersthene	2.5	---	---	---	4.8	---	---	5.0	4.5
Ilmenite-Magnetite-Chromite	3.2	---	0.9	---	2.1	0.3	4.7	2.5	2.2
Kyanite	0.3	0.3	---	---	0.3	---	---	---	---
Leucoxene	0.6	---	---	---	0.3	---	---	0.3	---
Muscovite	---	32.0	16.9	---	0.3	---	---	0.3	---
Olivine	0.6	0.7	0.3	9.6	0.9	4.4	4.0	0.6	1.3
Rutile	1.6	0.3	0.6	---	1.5	---	---	3.1	1.3
Sillimanite	0.3	---	---	---	---	---	---	---	---
Sphene	1.0	---	---	---	---	---	---	0.6	---
Tourmaline	---	---	---	---	---	---	---	---	---
Zircon	0.3	---	---	---	---	---	---	---	---
Other +++	4.7	---	0.5	---	1.2	1.3	0.3	1.5	1.3
Rock fragments	3.5	0.3	1.6	44.1	12.1	7.8	10.6	13.4	2.3
Weathered grains	1.0	---	6.0	23.3	5.1	25.5	14.3	12.1	4.7

APPENDIX 9. (Continued)

Mineral data	Sample Number* 6609-11-3	6609-14A-2	6609-14A-12	6609-15-4	6609-19-4	6609-19-12	6609-20-3	6609-20-9
Depth in core (cm)**	198	74	779	29	48	444	170	585
Age***	PG	LP	LP	LP	PG	PG	LP	LP
Physiographic environment****	CCH	CAPw	CAPw	CAPw	CCH	CCH	BFZm	BFZm
% sand in sample	1	6	1	5	3	15	3	3
% heavies of sd. frac.	0.1	3.5	16.2	4.7	5.4	5.8	4.8	5.7
Total grains counted	316	284	321	358	326	327	305	311
CP/H ratio	1.00	1.61	---	1.86	0.83	0.94	0.31	0.68
Actinolite-Tremolite	1.3	1.8	---	---	1.5	1.5	2.0	1.6
Aegirineaugite	---	---	---	---	---	0.6	---	---
Andalusite	---	---	---	---	0.6	0.3	0.3	---
Apatite	---	0.7	---	0.3	---	---	---	0.6
Basaltic Hornblende	---	0.7	---	0.3	1.2	0.6	---	0.6
Biotite	61.3	1.4	41.7	2.8	6.6	0.9	35.4	9.0
Chlorite	---	2.8	0.3	0.6	0.6	0.6	1.6	1.9
Clinopyroxene ++	1.3	35.6	---	40.6	24.9	29.3	2.6	20.2
Clinozoisite-Zoisite	---	1.1	---	0.9	1.5	0.3	0.7	0.6
Enstatite	---	0.4	---	0.6	0.6	0.3	---	---
Epidote	---	2.1	---	2.0	2.1	4.3	1.3	7.1
Garnet	---	1.4	---	0.6	2.1	5.2	---	5.8
Glaucophane	---	---	---	---	---	---	---	---
Hematite	---	1.4	---	0.6	0.6	0.9	0.3	---
Hornblende								
Blue-green	0.6	1.4	---	4.2	3.1	4.6	2.6	4.2
Brown	---	---	---	1.1	0.3	1.5	---	0.3
Common	0.6	20.6	---	16.8	26.6	25.8	5.6	24.9
Hypersthene	0.3	5.3	---	5.3	5.8	9.2	0.3	6.1
Ilmenite-Magnetite-Chromite	---	2.8	---	6.7	2.8	3.7	---	5.5
Kyanite	---	---	0.3	---	---	---	---	---
Leucoxene	---	---	---	0.6	0.6	0.3	---	---
Muscovite	25.6	1.1	56.8	---	1.5	0.3	32.5	2.9
Olivine	0.3	0.7	---	0.6	1.2	0.6	---	1.0
Rutile	0.6	---	---	---	0.3	---	0.3	1.3
Sillimanite	---	---	---	---	0.6	0.3	---	---
Sphene	---	0.7	---	0.9	0.6	0.9	---	---
Tourmaline	---	---	---	---	---	---	---	---
Zircon	---	0.4	---	---	---	---	---	---
Other +++	1.0	2.8	---	1.7	1.8	0.9	0.7	0.6
Rock fragments	1.0	9.5	---	7.5	7.0	2.8	2.0	2.6
Weathered grains	6.1	5.3	0.9	5.3	5.5	4.3	11.8	3.2

APPENDIX 9. (Continued)

Mineral data	Sample Number* 6609-20-12	6610-2-16	CR-1-1	CR-2-1	CR-3-1	CR-4-1
Depth in core (cm)**	835	405	0	0	0	0
Age***	LP	LP	PG	PG	PG	PG
Physiographic environment****	BFZm	VV	CR	CR	CR	CR
% sand in sample	10		100	100	100	100
% heavies of sd. frac.	2.3	3.9				
Total grains counted	317	359	117	116	167	105
CP/H ratio	0.70	1.68	1.16	1.28	1.38	1.18
Actinolite-Tremolite	2.2	1.1				
Aegirineaugite	2.2	---				
Andalusite	---	0.3				
Apatite	---	---				
Basaltic Hornblende	1.6	2.0				
Biotite	13.6	20.7				
Chlorite	1.2	2.8				
Clinopyroxene ++	16.7	31.5				
Clinozoisite-Zoisite	1.6	0.9				
Enstatite	0.3	0.9				
Epidote	1.8	0.9				
Garnet	2.2	0.9				
Glaucophane	---	0.3				
Hematite	1.2	0.3				
Hornblende						
Blue-green	6.6	1.7				
Brown	0.6	0.9				
Common	19.9	16.3				
Hypersthene	2.5	3.8				
Ilmenite-Magnetite-Chromite	0.6	0.6				
Kyanite	---	---				
Leucoxene	---	---				
Muscovite	2.2	2.5				
Olivine	1.0	0.9				
Rutile	0.6	0.3				
Sillimanite	0.3	0.6				
Sphene	0.6	0.6				
Tourmaline	---	---				
Zircon	0.3	---				
Other+++	2.2	0.6				
Rock fragments	1.2	4.1				
Weathered grains	16.8	4.2				

APPENDIX 10. QUANTITATIVE ANALYSES OF CHLORITE, ILLITE AND MONTMORILLONITE FROM X-RAY DIFFRACTION TRACES OF SELECTED SAMPLES*

Sample number****	Depth in core (cm) +	Physiographic environment ++	Age +++	Sediment type ++++	% chlorite	% illite	% Montmorillonite
6208-K1-1***	0	AFl	PG	OL	27	28	45
-45***	0	AFl	PG	OL	29	25	46
-3***	71	AFl	PG	OL	31	21	48
-4***	74	AFl	PG	OL	26	27	47
-5***	135	AFl	PG	OL	27	25	48
-6***	201	AFl	PG	OL	30	32	38
-7***	207	AFl	PG	OL	27	29	44
-8***	275	AFl	LP	GL	25	40	35
-9***	411	AFl	LP	GL	30	39	31
-10***	416	AFl	LP	GL	28	40	32
-11***	455	AFl	LP	GL	24	41	35
6408-C3-43***	0	AFm	PG	OL	24	28	48
6412-PD6-17***	0	ACNf	PG	OL	25	29	46
6501-A3(2)-26***	0	AFm	PG	BL	25	25	50
-27***	95	AFm	LP	GL	29	40	31
6501-C4(1)-40***	0	AFl	PG	OL	29	28	43
6502-PC6-18	3	ACNw	PG	OL	23	18	59
-28***	181	ACNw	PG	TS	25	25	50
-29***	245	ACNw	LP	TS	23	44	33
-30***	322	ACNw	LP	GL	29	38	33
6508-K1-4	170	WCH	PG	OL	28	21	51
-17	278	WCH	PG	TS	26	21	53
6508-PC12-32***	0	ACNf	PG	OL	28	22	50
6509-2-59***	5	AFl	PG	OL	30	34	36

*Quantitative results are based on weighted peak-areas (Biscaye, 1965) adjusted to 100 percent for chlorite, illite and montmorillonite of the 2-micron or less size fraction.

**Values calculated from X-ray traces presented by Allen (1966).

***Values calculated from X-ray traces presented by Russell (1967).

****The sample number consists of three parts: the first two parts refer to the station location number (Appendix 1); the third part identifies the individual sample.

++Physiographic environment--ACH = Astoria Channel; ACNf, w = Astoria Canyon floor, wall; AFu, m, l = Astoria Fan upper, middle, lower; BFZt = Blanco Fracture Zone trough; BV = Blanco Valley; CAPe, w = Cascadia Abyssal Plain east of Cascadia Channel, west of Cascadia Channel; CCH = Cascadia Channel; CR = Columbia River; GRm = Gorda Ridge mountain; RR = Rogue River; WCH = Willapa Channel.

+++Age--LP = late Pleistocene; PG = postglacial.

++++Sediment type--BL = brown lutite; GL = gray lutite; L = lutite; LOL = light olive gray lutite; OL = olive gray lutite; TS = terrigenous sand-silt layer; VL = basaltic glass lutite.

APPENDIX 10. (Continued)

Sample number****	Depth in core (cm) +	Physiographic environment ++	Age +++	Sediment type ++++	% chlorite	% illite	% Montmorillonite
6509-2-60***	53	AFl	PG	OL	33	31	36
-61***	150	AFl	PG	OL	32	33	35
-62***	210	AFl	PG	OL	29	34	37
6509-4-N344	264	ACH	PG	OL	32	24	44
6509-7-51***	10	AFl	PG	OL	33	29	38
-52***	52	AFl	PG	LOL	31	32	37
-53***	77	AFl	PG	OL	29	28	43
-54***	108	AFl	LP	GL	26	42	32
-55***	147	AFl	LP	GL	26	45	29
-56***	196	AFl	LP	GL	36	48	16
-57***	226	AFl	LP	GL	31	48	21
-58***	260	AFl	LP	GL	30	50	20
6509-25A-6	85	CCH	PG	OL	28	22	50
6509-26-24	115	CCH	PG	OL	24	22	54
6509-27-27**	7	CCH	PG	OL	30	22	48
-26**	211	CCH	PG	GL	32	22	46
-25**	370	CCH	PG	OL	25	17	58
-24**	529	CCH	PG	OL	31	22	47
6509-28-18**	3	CAPw	PG	BL	42	29	29
-19**	17	CAPw	PG	GL	39	26	35
-20**	219	CAPw	LP	GL	40	31	29
-21**	512	CAPw	LP	GL	31	48	21
6511-5-1	0	BV	PG	LOL	41	33	26
6511-69-5	287	BV	PG	LOL	48	29	23
6601-1-20	0	GRm	PG	VL	39	33	28
-7	165	GRm	LP	VL	29	38	33
-19	540	GRm	LP	VL	32	36	32
6604-2-15	0	BFZt	PG	BL	39	34	27
-2	38	BFZt	PG	GL	32	31	37
6604-3-5	100	BFZt	LP	GL	28	51	21
6604-4-5	214	CCH	PG	OL	27	24	49
6604-10-22	0	CAPe	PG	LOL	36	31	33
-21	826	CAPe	LP	GL	33	35	32
6604-11-2	37	BV	PG	LOL	37	29	34
-4	167	BV	PG	LOL	41	30	29
-6	271	BV	PG	LOL	39	33	28
-9	367	BV	PG	LOL	37	31	32
-10	409	BV	LP	GL	30	44	26
-17	481	BV	LP	GL	30	42	28

APPENDIX 10. (Continued)

Sample number****	Depth in core (cm) +	Physiographic environment ++	Age +++	Sediment type ++++	% chlorite	% illite	% Montmorillonite
6604-12-23	881	BV	PG	LOL	41	28	31
6609-1-1	0	BV	PG	LOL	40	31	30
-2	184	BV	PG	LOL	41	32	27
-4	323	BV	PG	LOL	41	32	27
-5	424	BV	PG	LOL	43	30	27
-7	595	BV	PG	LOL	45	32	23
-9	644	BV	LP	GL	30	39	31
-11	756	BV	LP	GL	32	40	28
6609-15-1	0	CAPw	PG	BL	37	32	31
CR-5-33***	0	CR	PG	L	16	24	60
CR-6-68***	0	CR	PG	L	15	13	72
RR-1-1	0	RR	PG	L	52	27	21
-2	0	RR	PG	L	50	26	24

APPENDIX 11. GRAIN SIZE AND COARSE FRACTION COMPOSITIONS OF SELECTED SAMPLES

Sample number*	Depth in core (cm)**	% sand % silt % clay	Sediment type***	Age+	Physiographic environment++	Total grains counted	Percent of coarse fraction by number: Benthic foraminiferans	Planktonic foraminiferans	Radiolarians	Diatoms	Plant fibers	Mica	Colorless volcanic glass	Dark brown volcanic glass	Other minerals & rock frags.	Pyrite	Other+++
6509-18-1MC	0	2-23-75	BL	PG	CAPw	320	1	1	74	5	--	1	1	--	17	--	--
-2MC	8	3-26-71	GL	PG	CAPw												
-1	15	62-36-02	TS	LP	CAPw	356	--	T	--	--	--	5	1	--	93	1	--
-5	42	84-14-02	TS	LP	CAPw	351	--	T	--	--	--	3	T	--	97	--	--
-6	46	1-24-75	GL	LP	CAPw	367	T	49	T	--	T	2	T	--	48	--	--
-8	63	43-45-12	TS	LP	CAPw	483	T	3	--	--	--	2	--	--	95	--	--
-11	83	82-15-03	TS	LP	CAPw	430	--	1	--	--	--	1	--	--	98	--	--
-18	135	59-31-10	TS	LP	CAPw	384	T	3	--	--	--	11	--	--	86	--	--
-20	174	1-24-75	GL	LP	CAPw	345	T	61	1	T	--	4	--	--	33	--	--
-21	200	53-40-07	TS	LP	CAPw	451	--	5	--	--	T	2	--	--	93	--	--
-23	229	3-28-69	GL	LP	CAPw												
6509-19-1MC	0	2-24-74	BL	PG	CAPw	312	1	--	91	7	--	--	--	--	--	--	1

*The sample number consists of three parts: the first two parts refer to the station location number (Appendix 1); the third part identifies the individual sample.

**Depth indicated refers to top of sample interval.

***Sediment type--BL = brown lutite; BS = basaltic sand layer; FL = foraminiferal lutite; GL = gray lutite; GRL = greenstone lutite; LOL = light olive gray lutite; OL = olive gray lutite; TS = terrigenous sand-silt layer; VL = basaltic glass lutite.

+Age--LP = late Pleistocene; PG = postglacial.

++Physiographic environment--BFZt, m, v = Blanco Fracture Zone trough, mountain, valley; BV = Blanco Valley; CAPe, w = Cascadia Abyssal Plain east of Cascadia Channel, west of Cascadia Channel; CCH = Cascadia Channel; GRv, m = Gorda Ridge valley, mountain; TAP = Tufts Abyssal Plain.

+++Other--fecal pellets, glauconite, pollen, spone spicules, and unidentified grains.

"T" denotes less than one percent.

Continued on next page

APPENDIX 11. (Continued)

Sample number*	Depth in core (cm)**	% sand % silt % clay	Sediment type ***	Age+	Physiographic environment++	Total grains counted	Percent of coarse fraction by number										
							Benthic foraminiferans	Planktonic foraminiferans	Radiolarians	Diatoms	Plant fibers	Mica	Colorless volcanic glass	Dark brown volcanic glass	Other minerals & rock frags.	Pyrite	Other+++
6509-19-8	156	38-55-07	TS	LP	CAPw	313	--	98	--	--	--	2	T	--	--	T	--
-12	262	4-32-64	GL	LP	CAPw	302	3	94	2	--	--	T	--	--	T	--	T
6509-20A-1MC	0	2-24-74	BL	PG	CAPw	326	1	2	89	5	--	--	--	--	1	--	2
-1	31	T-20-80	GL	LP	CAPw												
-9	334	T-77-23	TS	LP	CAPw	622	T	23	T	T	7	6	1	--	61	1	T
-15	452	T-75-25	TS	LP	CAPw	280	1	11	T	1	14	25	--	--	39	7	2
-17	466	T-38-62	GL	LP	CAPw												
-22	527	6-85-09	TS	LP	CAPw	676	--	1	T	--	1	18	--	--	80	--	--
6509-21A-1MC	0	1-30-69	BL	PG	TAP	338	1	4	90	2	T	T	--	--	1	--	2
-16	230	6-38-56	GL	LP	TAP	300	1	98	--	--	--	--	--	--	1	--	--
-19	257	T-64-36	GL	LP	TAP	394	--	98	--	--	--	1	--	--	1	--	--
6509-25A-18	0	3-44-53	BL	PG	CCH	436	T	--	57	8	11	14	3	1	6	--	--
-2	39	2------	OL	PG	CCH	585	1	T	4	3	33	22	24	--	11	T	T
-4	45	1------	GL	PG	CCH	275	2	1	84	T	1	5	1	--	4	--	1
-5	80	3------	OL	PG	CCH	693	1	1	2	1	25	6	39	--	22	T	2
-7	95	2-85-13	TS	PG	CCH	383	1	--	13	1	12	15	42	--	15	1	--
-8	102	1------	GL	PG	CCH	283	3	--	83	1	2	5	1	--	3	1	1
-20	171	2------	TS	PG	CCH	300	1	--	4	1	10	5	64	--	15	--	--
-9	232	2-80-18	TS	PG	CCH	357	1	--	5	1	28	31	3	T	30	T	--
-11	255	2------	OL	PG	CCH	604	2	T	2	5	40	24	2	--	23	1	--
-12	307	4------	TS	PG	CCH	623	2	2	7	5	24	24	3	--	29	1	3
-14	317	2------	GL	PG	CCH	260	5	10	74	1	3	3	--	--	3	T	2
-15	348	1------	TS	PG	CCH	560	3	3	3	2	28	41	2	--	16	1	1
-16	355	2------	GL	PG	CCH	358	6	10	55	1	6	7	1	--	6	6	2
-17	377	5-73-22	TS	PG	CCH	327	1	T	4	T	22	29	1	--	42	--	--
6509-26-36	0	1-41-58	OL	PG	CCH	494	1	--	9	21	60	6	T	--	3	--	T
-20	40	1-54-45	OL	PG	CCH	481	1	--	2	5	27	7	9	--	47	T	1

Continued on next page

APPENDIX 11. (Continued)

Sample number*	Depth in core (cm)**	% sand % silt % clay	Sediment type***	Age+	Physiographic environment++	Total grains counted	Percent of coarse fraction by number										
							Benthic foraminiferans	Planktonic foraminiferans	Radiolarians	Diatoms	Plant fibers	Mica	Colorless volcanic glass	Dark brown volcanic glass	Other minerals & rock frags.	Pyrite	Other+++
6509-26-21	49	3-77-20	TS	PG	CCH												
-22	54	--------	GL	PG	CCH	241	8	T	51	9	12	4	1	--	12	1	2
-26	140	T -37-63	OL	PG	CCH												
-31	188	T -32-68	GL	PG	CCH	317	4	4	48	8	10	2	2	--	12	10	--
-38	256	25-68-07	TS	PG	CCH	439	--	T	1	--	T	17	1	--	80	--	--
-34	267	1-26-73	GL	PG	CCH	760	3	10	41	2	2	2	4	--	23	9	4
-3	322	T -35-65	GL	PG	CCH	274	4	1	64	3	7	5	7	--	8	1	--
-8	389	T -31-69	GL	PG	CCH	268	6	1	62	1	13	7	2	--	3	2	3
-11	459	T -47-53	OL	PG	CCH	300	1	T	3	7	36	13	18	--	18	2	1
-12	463	1-89-10	TS	PG	CCH												
-13	470	T -32-68	GL	PG	CCH	259	5	2	60	1	11	6	4	--	7	2	2
-14	485	T -37-63	OL	PG	CCH	468	1	T	3	9	63	3	5	--	9	3	3
-17	544	10-79-11	TS	PG	CCH	695	T	--	T	T	T	21	22	--	56	--	--
6509-27-1	0	1-40-59	OL	PG	CCH												
-31	37	22-55-23	TS	PG	CCH	537	1	--	2	2	9	13	2	--	72	1	--
-4	54	T -28-72	GL	PG	CCH												
-5	102	3-67-30	TS	PG	CCH												
-8	127	1-37-62	OL	PG	CCH												
-9	156	24-53-23	TS	PG	CCH												
-10	174	1-42-57	OL	PG	CCH												
-32	202	19-52-29	TS	PG	CCH	366	1	T	--	1	6	7	1	--	84	T	--
-11	261	6-58-37	TS	PG	CCH	694	1	T	6	6	18	22	14	--	31	T	1
-12	281	6-72-22	TS	PG	CCH	434	2	1	5	2	4	9	30	--	44	1	2
-13	283	T -34-66	GL	PG	CCH	300	1	--	52	1	8	3	3	--	29	3	--
-14	290	0-41-59	OL	PG	CCH												
-15	331	2-51-46	OL	PG	CCH												
-16	358	12-46-42	OL	PG	CCH	428	1	--	2	2	8	14	20	--	49	--	4

Continued on next page

APPENDIX 11. (Continued)

Sample number*	Depth in core (cm)**	% sand % silt % clay	Sediment type***	Age+	Physiographic environment++	Total grains counted	Percent of coarse fraction by number										
							Benthic foraminiferans	Planktonic foraminiferans	Radiolarians	Diatoms	Plant fibers	Mica	Colorless volcanic glass	Dark brown volcanic glass	Other minerals & rock frags.	Pyrite	Other+++
6509-27-17	365	15-62-23	TS	PG	CCH	567	1	T	1	--	3	5	18	--	72	--	--
-18	459	22-51-27	TS	PG	CCH	507	1	T	2	1	4	11	20	--	59	--	T
-19	468	29-50-21	TS	PG	CCH	649	T	T	--	T	1	4	19	--	76	--	--
-20	470	0-34-66	GL	PG	CCH												
-21	480	0-42-58	OL	PG	CCH	485	1	--	2	2	56	8	16	--	10	5	--
-22	520	1-45-54	OL	PG	CCH	188	2	T	2	5	15	7	17	--	46	2	4
-23	574	23-42-35	TS	PG	CCH	620	2	--	3	19	32	20	10	--	4	--	--
-33	580	29-44-27	TS	PG	CCH	300	T	--	2	T	7	11	10	--	69	T	--
6509-28-11	0	1-20-79	BL	PG	CAPw	578	2	--	87	1	1	1	1	--	4	T	3
-7	380	1-47-52	GL	LP	CAPw	318	2	91	--	--	--	2	--	--	3	T	1
6509-30-8	0	2-24-74	LOL	PG	CAPe	344	2	2	70	17	3	1	--	--	4	T	T
-3	100	60-36-04	TS	PG	CAPe	330	--	--	T	--	T	8	--	--	91	--	--
-6	125	93-07-00	TS	PG	CAPe	340	--	--	--	--	1	1	--	--	98	--	--
6511-5-1	0	1-36-63	LOL	PG	BV	668	2	2	39	36	8	3	--	T	6	1	2
-2	27	T-47-53	LOL	PG	BV	314	T	T	19	35	17	6	T	--	19	--	3
-6	178	T-42-58	LOL	PG	BV	321	T	2	31	1	14	16	14	T	15	6	--
-10	372	--------	TS	PG	BV	337	6	2	11	4	10	24	T	--	42	1	--
6511-69-9	0	T-43-57	LOL	PG	BV	351	1	--	44	24	7	3	--	--	20	1	--
-5	287	T-36-64	LOL	PG	BV	343	2	4	41	15	--	7	1	--	22	6	2
-6	421	1-72-27	TS	PG	BV	321	3	1	3	3	--	32	--	1	49	2	6
-8	524	7-68-25	TS	PG	BV	353	3	2	3	1	8	20	1	T	57	3	1
6601-1-20	0	15-28-57	VL	PG	GRm	366	2	2	28	T	--	1	1	40	26	--	--
-6	140	23-28-49	VL	LP	GRm	313	T	24	1	--	--	--	--	49	26	--	--
-9	219	-------	VL	LP	GRm	316	1	14	1	--	1	--	T	29	52	--	1
-12	316	8-34-58	VL	LP	GRm	311	--	--	17	--	--	T	--	58	24	T	1
-19	540	2-27-71	VL	LP	GRm	362	15	62	1	--	--	1	--	4	13	T	4
6604-1-1	0	9-53-38	BL	PG	CCH	422	T	--	21	4	1	19	3	--	51	--	T

Continued on next page

APPENDIX 11. (Continued)

Sample number *	Depth in core (cm)**	% sand % silt % clay	Sediment type***	Age+	Physiographic environment++	Total grains counted	Percent of coarse fraction by number										
							Benthic foraminiferans	Planktonic foraminiferans	Radiolarians	Diatoms	Plant fibers	Mica	Colorless volcanic glass	Dark brown volcanic glass	Other minerals & rock frags.	Pyrite	Other+++
6604-1-2	12	3-78-19	TS	PG	CCH	311	T	--	13	4	11	15	10	--	45	--	2
-3	20	3-74-23	TS	PG	CCH	350	T	T	16	4	18	18	7	--	33	--	3
-4	25	3-47-50	GL	PG	CCH	300	--	--	38	3	1	3	2	--	53	T	--
6604-2-15	0	1-21-78	BL	PG	BFZt	423	1	--	74	7	1	--	T	--	2	15	--
-16	32	1-19-80	GL	PG	BFZt	351	--	--	92	6	T	--	--	--	--	2	--
-2	38	1-22-77	GL	PG	BFZt	386	--	--	93	2	1	1	T	--	1	1	T
-5	160	2-21-77	GL	LP	BFZt	289	15	53	10	T	2	3	1	T	4	4	7
-13	359	T -34-66	GL	LP	BFZt												
6604-3-15	0	1-45-54	BL	PG	BFZt	454	T	--	87	4	T	5	--	--	3	--	--
-4	46	0-73-27	TS	PG	BFZt	328	1	1	4	--	--	4	1	8	81	--	--
-5	100	0-35-65	GL	LP	BFZt	139	1	8	17	3	9	8	1	1	51	1	--
-8	193	1-68-31	TS	LF	BFZt	339	T	T	1	T	16	65	1	1	15	--	--
-12	276	0-80-20	TS	LP	BFZt	344	--	T	T	1	31	37	1	T	5	24	--
-14	313	T -30-70	GL	LP	BFZt												
-20	330	T -24-76	GL	LP	BFZt												
6604-4-9	0	1-28-71	OL	PG	CCH	344	1	T	18	12	35	15	2	--	16	--	--
-3	182	5-50-45	TS	PG	CCH	332	1	T	8	12	20	15	2	--	40	--	1
-4	195	3-50-47	GL	PG	CCH	297	1	2	22	8	2	18	2	--	45	--	T
-5	214	1-41-58	OL	PG	CCH	406	1	1	6	22	49	7	T	--	12	1	T
-6	368	7-59-34	TS	PG	CCH	380	1	--	3	2	11	15	4	--	62	--	--
-10	465	9-82-09	TS	PG	CCH	342	--	--	T	T	2	58	12	--	27	--	--
6604-5-1	0	1-43-56	OL	PG	CCH	478	1	--	31	12	11	9	--	--	8	22	6
-3	22	2-55-43	OL	PG	CCH	573	T	1	15	7	25	24	2	--	26	--	--
6604-6-2	0	2-21-77	BL	PG	BFZt	507	2	--	81	6	1	1	T	T	7	T	1
-5	34	54-24-22	GRL	PG	BFZt	322	--	--	1	T	--	1	T	--	97	--	--
6604-10-22	371	1-25-74	LOL	PG	CAPe	371	1	11	76	6	1	1	--	--	2	1	1

Continued on next page

APPENDIX 11. (Continued)

Sample number*	Depth in core (cm)**	% sand % silt % clay	Sediment type***	Age+	Physiographic environment++	Total grains counted	Percent of coarse fraction by number										
							Benthic foraminiferans	Planktonic foraminiferans	Radiolarians	Diatoms	Plant fibers	Mica	Colorless volcanic glass	Dark brown volcanic glass	Other minerals & rock frags.	Pyrite	Other+++
6604-10-5	195	1-86-13	TS	LP	CAPe	447	T	12	6	1	T	9	1	--	69	T	T
-9	323	2-59-39	TS	LP	CAPe	462	1	7	3	--	2	46	1	1	38	1	--
-19	745	1-66-33	TS	LP	CAPe	378	1	1	7	--	1	28	--	1	60	1	--
-21	826	1-29-70	GL	LP	CAPe	333	4	22	46	2	§	3	T	1	8	9	2
6604-11-19	0	T-33-67	LOL	PG	BV	614	4	1	44	31	5	3	T	--	9	1	1
-2	37	1-34-65	LOL	PG	BV	379	1	--	49	16	8	2	--	T	23	--	T
-6	272	1-31-68	LOL	PG	BV	322	3	12	61	8	8	2	--	--	5	1	T
-10	409	T-31-69	GL	LP	BV	320	--	--	2	2	71	15	T	--	1	9	--
-16	469	1-81-18	TS	LP	BV	556	--	--	1	--	1	5	T	--	93	--	T
-18	487	30-60-10	TS	LP	BV	401	--	--	--	--	2	12	--	--	86	--	--
6604-12-24	0	1-50-49	LOL	PG	BV	323	1	T	19	12	23	20	--	--	20	1	3
-2	30	6-52-42	TS	PG	BV	326	1	--	12	4	6	13	1	1	60	1	1
-5	237	5-65-30	TS	PG	BV	335	2	2	6	2	5	23	3	1	54	1	1
-12	496	18-48-34	TS	PG	BV	322	2	1	2	--	5	14	1	1	69	2	2
-15	602	--------	TS	PG	BV	330	2	1	1	1	2	7	1	1	80	3	1
-22	879	--------	TS	PG	BV	327	7	3	T	T	2	6	T	1	76	2	1
-23	881	T-35-65	LOL	PG	BV	325	2	7	23	16	4	6	--	--	22	19	T
6609-1-1	0	1-43-56	LOL	PG	BV	378	3	1	34	4	6	3	T	--	46	1	1
-3	267	38-47-15	TS	PG	BV	321	1	--	1	--	--	5	2	--	90	--	1
-5	424	1-44-55	LOL	PG	BV	335	1	3	9	T	4	3	67	--	12	T	1
-6	484	32-41-27	TS	PG	BV	370	1	T	T	--	1	2	T	--	94	--	T
-10	744	52-38-10	TS	LP	BV	320	--	T	--	--	1	5	--	--	92	2	T
-11	756	7-45-48	GL	LP	BV	356	--	--	--	--	--	11	--	--	89	--	--
6609-2-1	0	T-47-53	LOL	PG	BV	320	1	--	40	17	23	4	T	--	14	--	T
-4	266	14-51-35	TS	PG	BV	327	1	1	5	T	1	4	5	--	81	--	1
-6	414	1-35-64	LOL	PG	BV	300	3	9	70	1	1	2	4	--	4	3	1

Continued on next page

APPENDIX 11. (Continued)

Sample number*	Depth in core (cm)**	% sand % silt % clay	Sediment type ***	Age+	Physiographic environment++	Total grains counted	Percent of coarse fraction by number										
							Benthic foraminiferans	Planktonic foraminiferans	Radiolarians	Diatoms	Plant fibers	Mica	Colorless volacanic glass	Dark brown volcanic glass	Other minerals & rock frags.	Pyrite	Other+++
6609-2-10	753	T-37-63	GL	LP	BV												
-14	811	11-68-21	TS	LP	BV	305	T	--	2	T	3	18	2	T	73	--	T
6609-3-1	0	1-30-69	LOL	PG	BFZv	360	--	T	72	7	3	1	T	T	15	--	1
-3	210	T-28-72	LOL	PG	BFZv	315	2	17	62	3	4	2	3	--	5	1	1
-4	325	1-35-64	LOL	PG	BFZv	362	2	27	18	T	6	7	T	--	38	T	1
6609-4-1	0	1-30-69	LOL	PG	CAPe	353	1	--	78	1	3	T	--	--	16	--	T
-5	176	2-29-69	GL	LP	CAPe	311	2	77	13	--	--	1	--	--	5	T	3
-7	347	2-34-64	GL	LP	CAPe												
6609-5-1	0	1-26-73	LOL	PG	CAPe	327	2	2	84	1	1	--	--	--	3	--	7
-2	90	1-30-69	LOL	PG	CAPe	372	11	36	45	--	1	1	--	--	2	--	4
-3	120	23-47-30	TS	PG	CAPe	309	1	--	2	T	1	17	--	--	79	--	--
-4	220	1-44-55	GL	LP	CAPe	313	3	72	T	--	--	1	--	--	22	1	T
-6	420	1-95-04	TS	LP	CAPe	352	--	1	2	--	1	75	9	--	12	--	--
-7	430	1-41-58	GL	LP	CAPe	300	3	59	28	--	2	3	--	T	3	1	1
-9	636	2-82-16	TS	LP	CAPe	308	2	33	17	--	15	30	1	--	2	--	T
-10	691	1-43-56	GL	LP	CAPe	323	4	68	24	T	1	1	--	--	1	T	T
-13	910	1-83-16	TS	LP	CAPe	327	T	1	3	--	4	29	8	--	54	1	--
-14	954	1-36-63	GL	LP	CAPe	357	8	55	28	T	--	2	--	--	5	1	T
6609-6-1	0	45-16-39	VL	PG	GRv	673	--	T	18	T	--	--	--	72	9	--	1
6609-7-1	0	1-26-73	LOL	PG	CAPe	316	2	2	89	1	1	T	--	--	2	--	3
-2	114	1-92-07	TS	LP	CAPe	329	1	4	T	T	2	42	5	--	44	--	1
-3	181	1-39-60	GL	LP	CAPe	308	11	85	1	T	--	1	--	T	T	1	--
-7	478	T-73-27	TS	LP	CAPe	342	1	23	11	T	16	46	--	--	2	1	--

Continued on next page

APPENDIX 11. (Continued)

Sample number*	Depth in core (cm)**	% sand % silt % clay	Sediment type ***	Age+	Physiographic environment++	Total grains counted	Percent of coarse fraction by number										
							Benthic foraminiferans	Planktonic foraminiferans	Radiolarians	Diatoms	Plant fibers	Mica	Colorless volcanic glass	Dark brown volcanic glass	Other minerals & rock frags.	Pyrite	Other+++
6609-7-8	575	3-30-67	GL	LP	CAPe	300	8	64	21	T	--	--	2	--	2	2	1
-9	704	T-43-57	GL	LP	CAPe	313	5	47	43	--	T	--	T	1	2	1	--
-12	848	3-25-72	GL	LP	CAPe	323	4	24	38	--	1	--	--	T	29	2	2
-13	934	T-77-23	TS	LP	CAPe	308	4	7	12	3	3	4	--	--	2	64	1
6609-8-1	0	3-35-62	VL	PG	BFZt	332	1	T	46	1	T	T	T	1	47	2	1
-2	25	7-32-61	VL	PG	BFZt	301	--	--	45	--	T	--	--	4	50	--	T
-3	51	65-21-14	BS	LP	BFZt	305	--	1	--	--	--	T	T	2	96	--	T
6609-10-1	0	2-76-22	TS	PG	CAPe	304	1	--	30	--	T	3	T	--	65	--	--
-3	35	2-64-34	TS	LP	CAPe	306	7	44	10	T	T	18	--	--	20	--	1
-10	105	7-86-07	TS	LP	CAPe	316	1	T	T	--	9	40	2	--	47	--	--
-6	269	1-37-62	GL	LP	CAPe	300	2	75	1	--	2	9	--	--	11	--	--
-11	276	5-88-07	TS	LP	CAPe	345	--	1	--	1	2	41	1	--	54	--	--
6609-11-1	0	1-46-53	OL	PG	CCH	300	2	T	36	6	21	3	1	--	4	--	27
-3	198	1-45-54	OL	PG	CCH	319	--	T	13	1	72	8	2	--	4	--	T
6609-13-1	0	1-27-72	BL	PG	BFZt	333	1	--	82	5	2	T	T	--	1	--	8
-3	249	7-27-66	GL	LP	BFZt	310	14	71	1	--	T	1	1	--	9	T	2
-5	410	2-26-72	GL	LP	BFZt	333	10	7	76	--	--	2	1	--	3	--	1
-6	510	1-23-76	GL	LP	BFZt	321	46	26	8	T	2	5	2	--	9	--	2
-7	623	2-08-90	GL	LP	BFZt	329	22	7	64	--	T	1	1	--	4	--	1
-11	901	1-22-77	GL	LP	BFZt	374	15	27	9	--	1	15	1	--	10	11	11
6609-14A-1	0	2-31-67	BL	PG	CAPw	308	3	--	90	1	--	2	T	--	2	2	T
-2	74	6-80-14	TS	LP	CAPw	411	--	T	--	--	--	8	1	--	91	--	--
-3	185	1-19-80	GL	LP	CAPw	308	3	81	--	--	--	1	--	--	2	--	13
-5	362	T-47-53	GL	LP	CAPw	318	5	83	--	--	T	4	--	T	6	--	1

Continued on next page

APPENDIX 11. (Continued)

Sample number*	Depth in core (cm)**	% sand % silt % clay	Sediment type***	Age+	Physiographic environment++	Total grains counted	Percent of coarse fraction by number										
							Benthonic foraminiferans	Planktonic foraminiferans	Radiolarians	Diatoms	Plant fibers	Mica	Colorless volcanic glass	Dark brown volcanic glass	Other minerals & rock frags.	Pyrite	Other+++
6609-14A-7	520	T -56-44	GL	LP	CAPw	300	8	79	2	--	2	4	--	--	2	1	2
-8	571	T -87-13	TS	LP	CAPw	306	--	1	1	--	18	78	--	--	1	1	T
-12	668	1-80-19	TS	LP	CAPw	323	--	T	1	T	23	67	3	--	3	1	1
-13	842	2-42-56	GL	LP	CAPw	300	4	77	15	--	1	3	--	--	T	T	--
6609-15-1	0	2-38-60	BL	PG	CAPw	302	1	2	78	--	--	3	1	--	15	--	--
-4	29	5-81-14	TS	LP	CAPw	361	T	3	T	--	4	28	1	--	64	T	--
6609-16-1	0	1-24-75	BL	PG	CAPw	311	1	--	94	1	T	T	--	--	4	--	--
-2	20	1-31-69	GL	LP	CAPw	303	7	53	39	--	T	T	--	--	T	--	1
6609-19-1	0	5-57-38	BL	PG	CCH	300	3	--	5	--	T	8	--	--	83	--	1
-4	48	3-59-38	TS	PG	CCH	394	--	T	3	1	28	6	T	--	61	--	--
-5	55	1-66-33	TS	PG	CCH	303	T	1	4	--	4	20	3	--	64	--	4
-9	107	T -44-56	OL	PG	CCH	305	--	--	10	8	55	11	T	--	16	--	--
-11	345	2-46-52	OL	PG	CCH	300	--	--	7	3	45	7	T	--	38	--	--
-12	444	15-58-27	TS	PG	CCH	343	--	--	1	T	8	3	1	--	86	1	--
-13	449	3-51-46	GL	PG	CCH												
6609-20-1	0	--------	BL	PG	BFZm	312	1	2	18	--	--	3	--	--	75	--	1
-2	33	21-40-39	FL	LP	BFZm	312	3	80	--	--	--	2	--	--	15	--	T
-3	170	3-52-45	TS	LP	BFZm	300	--	--	T	--	--	51	--	--	48	--	T
-4	322	8-31-61	FL	LP	BFZm	322	3	89	T	--	1	4	--	1	2	--	T
-5	407	T -57-43	GL	LP	BFZm	313	--	--	--	--	--	4	--	--	96	--	--
-6	507	4-33-63	GL	LP	BFZm	308	19	51	1	--	T	11	3	1	14	--	T
-9	585	3-92-05	TS	LP	BFZm	331	--	--	--	--	1	22	3	--	74	--	--
-11	670	1-51-48	GL	LP	BFZm	312	15	10	--	--	1	10	T	1	62	--	T
-12	835	10-87-03	TS	LP	BFZm	331	--	--	--	--	1	22	3	--	74	--	--